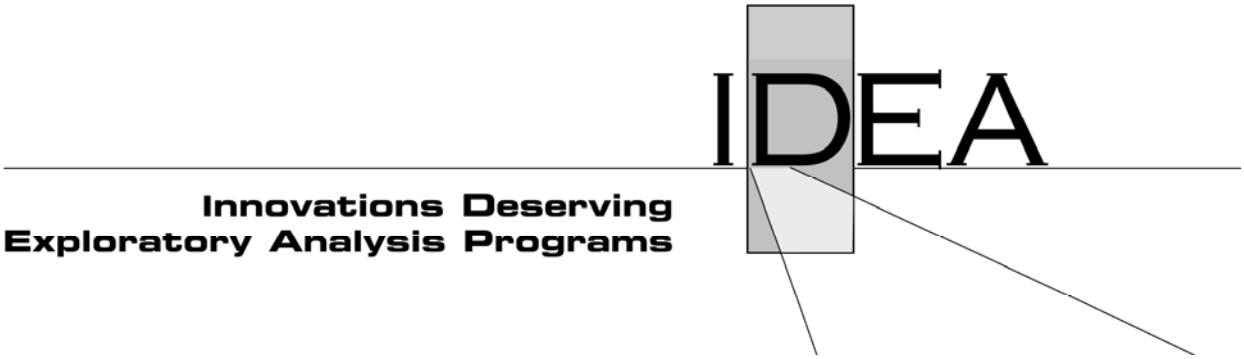

Highway IDEA Program

A Shape Memory Polymer Based Self-Healing Sealant for Expansion Joint

Final Report for
Highway IDEA Project 142

Prepared by:
Guoqiang Li
Louisiana State University
Baton Rouge, LA

April 2012

TRANSPORTATION RESEARCH BOARD
OF THE NATIONAL ACADEMIES

Innovations Deserving Exploratory Analysis (IDEA) Programs Managed by the Transportation Research Board

This IDEA project was funded by the NCHRP IDEA Program.

The TRB currently manages the following three IDEA programs:

- The NCHRP IDEA Program, which focuses on advances in the design, construction, and maintenance of highway systems, is funded by American Association of State Highway and Transportation Officials (AASHTO) as part of the National Cooperative Highway Research Program (NCHRP).
- The Safety IDEA Program currently focuses on innovative approaches for improving railroad safety or performance. The program is currently funded by the Federal Railroad Administration (FRA). The program was previously jointly funded by the Federal Motor Carrier Safety Administration (FMCSA) and the FRA.
- The Transit IDEA Program, which supports development and testing of innovative concepts and methods for advancing transit practice, is funded by the Federal Transit Administration (FTA) as part of the Transit Cooperative Research Program (TCRP).

Management of the three IDEA programs is coordinated to promote the development and testing of innovative concepts, methods, and technologies.

For information on the IDEA programs, check the IDEA website (www.trb.org/idea). For questions, contact the IDEA programs office by telephone at (202) 334-3310.

IDEA Programs
Transportation Research Board
500 Fifth Street, NW
Washington, DC 20001

A Shape Memory Polymer Based Self-Healing Sealant for Expansion Joint

by

Guoqiang Li

Department of Mechanical Engineering
Louisiana State University
Baton Rouge, LA 70803

NCHRP IDEA142

conducted for

NCHRP IDEA Program

April 2012

ABSTRACT

Failure of expansion joints is a leading cause of damage to bridge superstructures and concrete pavements. Failure of sealant material facilitates decay of the structure beneath it. The objective of this study is to develop a novel shape memory polymer (SMP) based smart sealant to solve a couple of critical problems facing compression-sealed joint: building-up of compressive stress and sealant squeezing out of the channel. By programming SMP in 2-D stress condition (compression in horizontal or traffic direction and tension in vertical direction) and by controlling the transition temperature of the SMP below the highest temperature of the environment to be experienced, the accumulated compressive stress can be significantly released due to the two orders of drop in the stiffness of the SMP at temperature above its transition temperature; consequently, the concrete and the sealant may not be crushed. Simultaneously, the squeezing-out problem may also be eliminated due to shrinkage of the sealant in the vertical direction when the sealant recovers (shape memory effect), which is seemingly against the physics because it contracts when temperature rises. In this study, a two-dimensional programming device was designed and fabricated, and shape fixity and shape recovery ratios of SMP and its syntactic foam were determined. Laboratory-scale performance evaluation of the developed syntactic foam as a smart sealant for bridge deck and concrete pavement joints was conducted, including uniaxial compression, tension and shear tests, cyclic loading tests, water immersion tests, and functional stability tests under ultraviolent radiation. The feasibility of using two-step 1-D programming to replace one-step 2-D programming was established. Shape memory polymer based sealant was fabricated, programmed, and installed in two expansion joints at the Louisiana State University campus in January 2012.

ACKNOWLEDGMENTS

This research project was funded by the Transportation Research Board (TRB)/Innovations Deserving Exploratory Analysis (IDEA) and the Louisiana Transportation Research Center (LTRC). The investigator would like to thank TRB and LTRC for sponsoring this project. The investigator would also like to thank Dr. Gefu Ji, Dr. Harper Meng, Dr. Tao Xu, Dr. Zhenyu Ouyang, and Mr. Abe King in the Department of Mechanical Engineering at Louisiana State University (LSU) for their assistance in conducting this research and the Office of Facility Service at LSU for helping in installing two expansion joints at LSU campus. Dr. Inam Jawed at TRB and Dr. Walid Alaywan at LTRC, managers of this project, shared their experience and knowledge with the investigator. My sincere thanks also go to the anonymous reviewers of this report for their in-depth comments and suggestions.

IMPLEMENTATION STATEMENT

This project aims at developing a new smart sealant for small span bridges or concrete pavements. Because this is an innovative concept, there is no similar study in the open literature. This study has answered several key questions: (1) The shape memory polymer (SMP) based sealant can lower the compressive stress significantly in the summer when the concrete wall expands so that crushing of concrete in the edge would be avoided. (2) This SMP based sealant can contract in the vertical direction in the summer so that sealant squeezing-out problem can be solved. (3) It is validated in the lab experiments that the smart sealant is resilient when subjected to environmental attacks and cyclic loadings. (4) This sealant can be programmed (or trained) by hybrid two-step 1-D programming. (5) This sealant can be easily installed in expansion joint.

However, it must be indicated that this study is not ready to be used in practice because large-scale installation and long-term field-level performance data are not available.

TABLE OF CONTENTS

LIST OF TABLES

LIST OF FIGURES

INTRODUCTION

Expansion joints are weak links in a bridge or concrete pavement system. Expansion joint failure is a leading cause for structural damage to bridge superstructures and concrete pavements [1-3]. Various types of sealants have been utilized to seal expansion joints in small-span bridge decks and concrete pavements. These sealants are typically hot-poured, cold-poured, or preformed. A comprehensive review of the existing sealants used in concrete pavements and bridge decks has shown that the failure of these sealants is dominated by adhesive failure and cohesive failure besides aging [4-11]. The need for a joint sealant that does not suffer from this weakness becomes obvious.

Recently, a new silicone foam based sealant was developed for field-poured sealant [12,13]. One advantage of this new material is its high ductility. Since the accommodation of movement by field-poured sealant is realized through the high ductility of the sealant under both tension and compression, adhesion to the concrete edge and cohesion in sealant itself are critical. However, one problem of the normal foam sealant used for compression sealed joint is the loss of compression over time. It was reported that large sustained compressive movements force air out of the seal material (gas leakage) [13], which may not recover when the joint expands, and thus causes compression loss in the compression sealed joint under cyclic loading. Another problem of foam sealant is the filling of the open cells (void) with water after long-term service. This problem can accelerate and magnify due to micro-cracking and damage caused by thermal stress and traffic loading.

Shape memory polymer (SMP) is a new member of the family of shape memory materials. It has been found that, while most SMPs can be deformed and fixed into a temporary shape and recover their original permanent shape by heating to above their transition temperature (glass transition temperature for amorphous SMPs and melting temperature for crystalline SMPs), shape recovery can also be triggered by light if the SMP molecules consist of photo sensitive functional groups or by magnetic field if magnetic particles are dispersed in heat-activating SMP matrix [14-18]. The driving force for heat-activated shape recovery is the conformational entropy of the molecular segments in terms of micro-Brownian thermal motion. Thermodynamically, the molecular segments experience a change from a temporary and ordered configuration to its random and coiled configuration

during the shape recovery process. Since this process is accompanied by an increase in entropy, it is an autonomous process. However, it is noted that, while the motion of the molecules during the shape recovery process can be described by micro-Brownian thermal motion, the micro-Brownian thermal motion itself cannot trigger shape recovery. The shape recovers only when the temperature is above the transition temperature. Therefore, external heating not only affects the shape recovery rate, but also determines if the shape recovery occurs or not for heat-activated SMPs.

A recent development in SMPs is the use of confined shape recovery for the purpose of self-healing structural-length scale damage. Li and John investigated the concept for SMP based syntactic foam to repeatedly heal impact damage [19]. Later, it has been proved that SMP based syntactic foam can be used in grid stiffened SMP based syntactic foam cored sandwich and 3-D woven fabric reinforced SMP based syntactic foam panel for repeatedly and efficiently heal impact damage [20,21]. Most recently, a biomimetic two-step close-then-heal self-healing scheme has been proposed by Li and Nettles [22] and Xu and Li [23], and elucidated by Li and Uppu [24]. This is a scheme by mimicking self-healing of biological systems such as human skin. This concept has been experimentally validated by Nji and Li [25], which shows that this system can heal structural-length scale damage repeatedly, efficiently, timely, molecularly, and almost autonomously (the only human intervention is by heating the material above its transition temperature).

An important scientific implication is that SMP may be used as sealant in expansion joints. It is known that an ideal sealant should be able to apply a consistent compressive stress to the concrete wall so that adhesive failure can be avoided. Also, the sealant needs to maintain in the groove when the joint narrows due to thermal expansion of the structural elements. Additionally, the sealant should prevent water from seeping into it and also have self-healing capabilities so that cohesive failure can be healed. To this end, we propose to use SMP based syntactic foam as a sealant for expansion joint. First, the foam sealant can be programmed or trained by a 2-D stress condition: compression in longitudinal (horizontal or traffic direction) and tension in transverse or vertical direction; see Figure 1 (a) for a three-step programming process. When the foam sealant is installed at the lowest temperature that the sealant will experience, the sealant will always apply a compressive stress to the concrete wall due to thermal expansion and shape recovery; see Figure 1 (b). When the environmental

temperature rises, the compressive stress applied to the sealant will increase, which further ensures that the sealant apply a compressive stress to the concrete wall and adhesive failure can be avoided. Also, because the stiffness of the SMP based sealant reduces as temperature rises, the compressive stress will not become excessive such that compressive failure of the concrete occurs. Usually, the squeezing out problem dominates due to Poisson's ratio effect. With SMP based sealant and the special 2-D training, this problem can be solved because the rising temperature will trigger the shape recovery process of the sealant, which makes the sealant contract in vertical direction. If properly trained, the Poisson's effect (squeezing out) and shape recovery effect (shrinking) can be balanced and the sealant may maintain at the same level; see Figure 1 (c). When temperature drops, the shape recovery stops and the sealant returns to Figure 1 (b). As discussed by Li and Uppu [24], each compressively constrained shape recovery completes a new cycle of programming. It is thus believed that this sealant will be able to experience many such cycles without failure. In order to solve the problem of water damage, we propose to use close-celled foam instead of open-celled foam. Therefore, we believe that a SMP based syntactic foam trained by 2-D programming (compression in one direction and tension in the transverse direction) would be a viable alternative as a sealant for expansion joint.

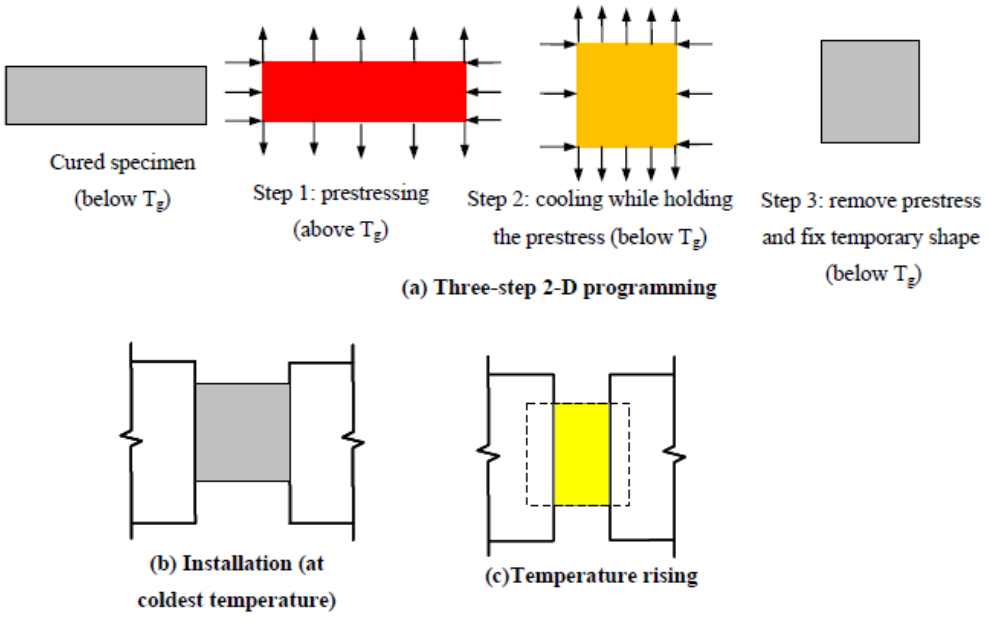

Figure **1**. Schematic of (a) three-step 2-D programming, (b) installation, and (c) working as temperature rises for the proposed syntactic foam sealant

OBJECTIVE

The objective of this study is to investigate the feasibility of using SMP based composite as sealant in expansion joints through both lab-scale experiments and field-level installation.

SCOPE

The scope of this project focused on lab-scale testing and field-level installation. This was a systematic experimental study. First, an extensive literature survey was conducted. Following this, the focus was on the materials selections, thermomechanical characterization, functional stability, programming method, and manufacturing and installation in concrete pavement.

METHODOLOGY

Literature Survey

The discovery of shape memory effect by Chang and Read in 1932 [26] is one of the revolutionary steps in the field of active materials research. Materials are said to show shape memory effect if they can be deformed and fixed into a temporary shape and recover their original permanent shape only on exposure of external stimuli like heat, light, magnetic, etc. [16, 18, 27, 28]. Technological uses include durable, shape-recovery eye-glass frames, packaging, temperature-sensitive switches, generation of stress to induce mechanical motion, heat-shrink tubing, deployable structures, microdevices, biomedical devices, etc. [26, 29-34].

Among the various shape memory materials such as shape memory alloy (SMA, for instance Ni–Ti alloy), shape memory ceramic, and shape memory polymer (SMP), SMPs have drawn increasing attention because of their scientific and technological significance [17, 26]. SMP was first developed by CDF Chimie Company (France) in 1984 under the trade name of Polynorbornene [26]. It was found that SMP offers deformation to a much higher degree and a wider scope of varying mechanical properties compared to SMAs or ceramics. In addition to their inherent advantages of being cheap, light weight, and easy process-ability, SMPs offer extra advantages due to the fact that they may be biocompatible, nontoxic, and biodegradable [26]. The driving force for shape recovery is the conformational entropy of the molecular segments in terms of micro-Brownian thermal motion. Thermodynamically, the molecular segments experience a change from a temporary and ordered configuration to its random and coiled configuration during the shape recovery process. Since this process is accompanied by an increase in entropy, it is an autonomous process. It is the recovery in strain and in stress that makes SMP a viable choice as sensors and actuators. In order to make the polymer smart, it usually experiences a typical four-step thermomechanical cycle called programming; see Fig. 2 for a 1-D tensile stress (σ), tensile strain (ε), and temperature (T) relationship during the programming cycle. The programming starts at a temperature above the glass transition temperature (T_g) of the SMP. It involves a high-strain deformation in the rubbery state, which is called ‘‘pre-deformation’’ or ‘‘pre-strain”. Step 2 is a ‘‘strain storage’’ process by maintaining the pre-strain constant while cooling down to below T_g. Because of the thermal contraction of the SMP during cooling, the tensile stress needed to

maintain the pre-deformed shape increases as the temperature drops. The third step is a ‘‘low temperature unloading’’ process, which is defined as the removal of the stress in the glassy state. The low temperature unloading process may be accompanied by ‘‘springback”, i.e., some pre-strain may be rebounded. In step 4, which involves reheating to its starting temperature (above T_g) without applying any constraint, sometimes called ‘‘free strain recovery’’ or ‘‘unconstrained recovery’’, brings the pre-strain back to zero (if the recovery ratio is 100%).

This strain-controlled programming is schematically shown in Fig. 3 for a polymer with glass transition temperature (T_g) as its transition temperature (T_{trans}) and the molecular mechanisms are schematically shown in Fig. 4. The efficiency of a shape-memory polymer is empirically controlled by its composition, as defined by the polymer’s chemical structure, molecular weight, degree of cross-linking, and fraction of amorphous and crystalline domains [17, 26]. The energy that is restored with shape recovery is a growing function of the energy supplied during the deformation at a high temperature [33,34]. A critical science and technological implication of SMP is that we can utilize its shape memory functionality for sealant in expansion joints.

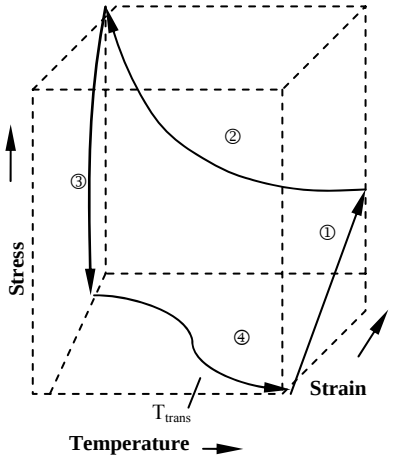

Figure **2**. Schematic of four-step strain controlled programming and recovery

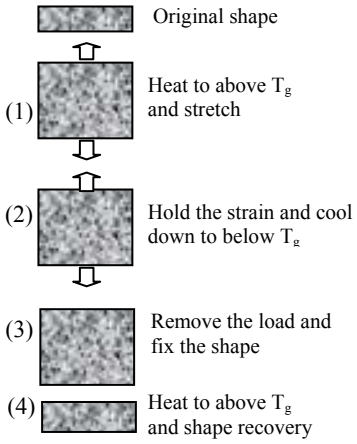

Figure **3**. Experimental procedure of programming

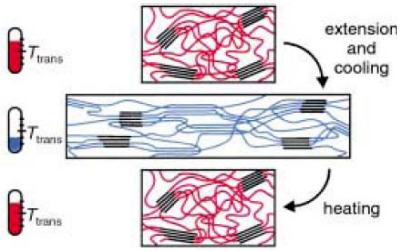

Figure **4**. Molecular mechanism of the thermally induced shape-memory effect for a multilock copolymer [17]

The Idea

Usually, compression-sealed sealant suffers from a couple of critical problems when the concrete wall expands at high temperature: building-up of compressive stress and sealant

squeezing out of the channel. By programming SMP based syntactic foam in 2-D stress condition (compression in horizontal or traffic direction and tension in vertical direction) and by controlling the transition temperature of the foam below the highest temperature of the environment to be experienced, the accumulated compressive stress can be significantly released due to the two orders of drop in the stiffness of the foam at temperature above its transition temperature; consequently, the concrete and the sealant will not be crushed. Simultaneously, the squeezing-out problem can also be eliminated due to the shrinkage of the foam in the vertical direction when the foam recovers (shape memory effect), which is seemingly against the physics because it contracts when temperature rises. Also, this 2-D programmed sealant can solve the problem of loss of interfacial contact when temperature drops. For conventional polymeric sealant, the plastic deformation accumulated at high temperature cannot be recovered. As a result, the sealant may gradually lose contact with the concrete wall as temperature drops, leading to leaking and gradual failure of the sealant. However, with the 2-D programmed smart sealant, the compression programming in the traffic direction ensures that the plastic deformation recovers at high temperature (sealant tends to become wider in the traffic direction), maintaining contact with the concrete wall and minimizing the leaking problem. Based on the above discussion, the special 2-D stress programmed SMP based syntactic foam has a potential to be used as sealant in expansion joints. The working principle for the smart sealant is schematically shown in Fig. 1.

Thermomechanical Characterization of Shape Memory Polymer Based Self-healing Syntactic Foam Sealant for Expansion Joint

Raw materials

The syntactic foam consisted of hollow glass microspheres dispersed temperature (T_g) = 62^{o}C) by CRG Industries under the name of Veriflex®. The hollow glass microspheres were from Potters Industries (Q-CEL6014: average outer diameter of 85μm, effective density of 0.14 g/cm^3, maximum working pressure of 1.73MPa, and wall thickness of 0.8μm). These raw materials have been used previously for the smart syntactic foam [21, in a shape memory polymer matrix. The polymer was a styrene based thermoset SMP (glass transition 22].

Biaxial specimen fabrication

The SMP based syntactic foam sealant consisted of hollow glass microspheres and SMP matrix, which was fabricated by dispersing 40% by volume of microspheres into the SMP resin [22, 24]. The microspheres were added to the resin while slowly stirring the mixture to minimize air bubbles in the resin. The microspheres were added in multiple steps to avoid agglomeration. After dispersion, a hardening agent was added and the mixture was mixed for 10 min. The mixture was poured into a 229×229×12.7 mm steel mold and placed in a vacuum chamber at 40kPa for 20 min in order to remove any air pockets introduced during the mixing process. Based on our previous study [22], the curing cycle was 79^{o}C for 24h, 107^{o}C for 3h, and 121^{o}C for 9h. After curing, the foam panel was de-molded and was machined into biaxial cruciform specimens for programming and further testing. The cruciform specimen dimensions were given in Figure 5 (a). With such a dimension, the central square is roughly under a 2-D stress condition as validated by a finite element analysis; see Figure 5 (b).

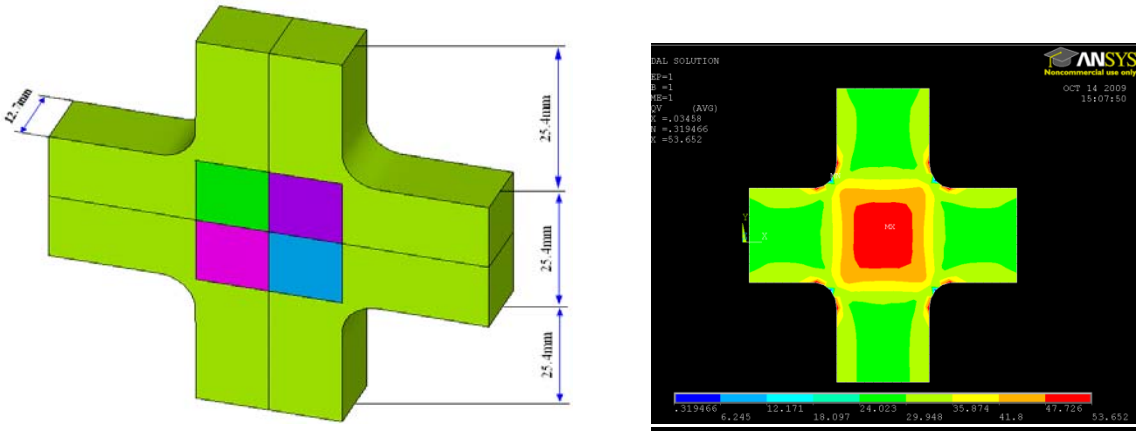

(a) (b)

Figure **5**. Cruciform specimens for 2-D programming (a) a schematic of biaxial specimen dimensions and (b) von Mises stress distribution in the specimen (there is a piece of square material (red color) at the center of the specimen (about 25.4mm by 25.4mm) that is subjected to a uniform 2-D stress condition.)

2-D programming of biaxial specimen

In order to make the polymer smart, it usually subjects to a typical three-step thermomechanical cycle called programming [19]. The energy that is restored with shape recovery is a growing function of the energy supplied during the deformation at a high temperature [35]. The SMP based foam sealant can be programmed to consistently and

autonomously apply a compressive stress to the edges of the concrete deck/pavement regardless of the environmental conditions (expansion or contraction) of the expansion joint. This feature ensures that the debonding problem be avoided by preventing tensile stress from occurring at the interface.

After machining the cruciform foam sealant specimen, two small steel tabs were fixed by using strong glue along the edge of the central square (uniform 2-D stress condition as shown in Figure 5 (b)) on to one side surface of the specimen (one in the vertical and the other in the horizontal direction) to measure the displacement of the two directions (see Figure 6(a)). Then the cruciform specimen was introduced into the truss-form fixture and the bolts were tightened to grip the four arms of the specimen, with each arm by 12.7mm (as shown in Figure 6(b)). The truss fixture can transform 1-D compression into 2-D loading (vertical compression and horizontal tension) by directly applying a compressive load to the top and bottom nodes. The ratio of the vertical load and horizontal load can be adjusted by changing the length of the members of the truss fixture. Finally the temperature was monitored with the help of thermocouples connected to a Yokagawa DC100 data acquisition system.

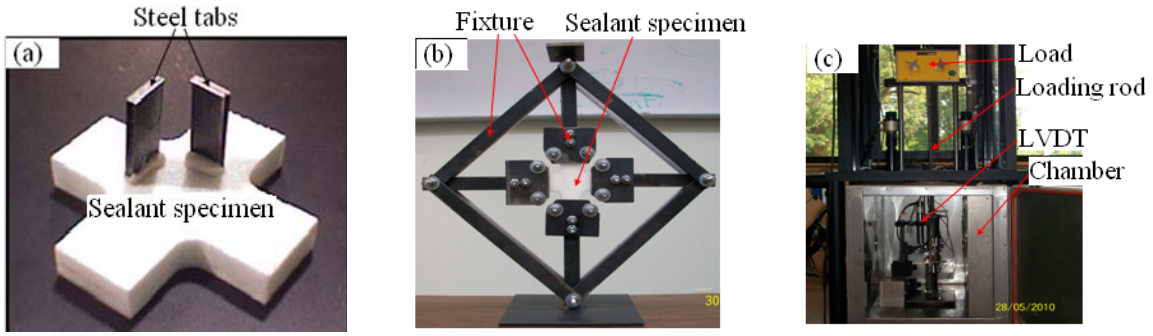

Figure **6**. (a) Specimen, (b) fixture, and (c) test set-up for 2-D programming of the cruciform foam sealant specimen

According to the previous study [22], the glass transition region of the foam is 63.69–76.19^{o}C with a glass transition temperature of T_g = 70.50^{o}C. In order to perform efficient programming and shape recovery tests, 79^{o}C was chosen as a testing temperature since it was just above the upper limit of the T_g region of the foam.

The device was put into a chamber, heated to 79^{o}C, held at 79^{o}C for about 25 minutes, and then the bolts were re-tightened to clamp the sample tighter because the specimen became soft at this temperature. After re-tightening, the set-up was placed back

into the chamber and two linear differential transducers (LVDT) were installed in conjunction with the two pre-attached tabs in the vertical and horizontal directions, respectively (see Figure 6(c)). Also, the weight-bearing rod was installed on the top node of the truss fixture and the system was reheated to 79^{o}C for another 20 minutes to equilibrate the temperature. Immediately afterwards a weight was put on to the rod by hand. This compressive load led the specimen to compression in the vertical direction and tension in the horizontal direction. Approximately 20 min were allowed for the deformation to stabilize. This completed the first step (pre-strain) of the programming. In the next step (cooling), the heating was first stopped, and the chamber was kept closed and the system was allowed to naturally cool for 8-10h to room temperature while maintaining the applied load constant. The LVDTs tracked the deformation of the specimen during this cooling step. Because of creep and contraction during cooling, the strain was continuously increasing until the temperature reached room temperature. This completed step 2 of the programming. Then the specimen was unloaded (step 3). The entire process completed the 3-step 2-D thermo-mechanical programming or shape fixity of the cruciform foam specimen (see Figure 4(a)). After completing the programming, the central square in some of the specimens was machined to four smaller cube specimens with a side length of 12.7mm (see Figure 7) for further mechanical testing. In Figure 7, Orientation-1 is subjected to compressive prestress; Orientation-2 is subjected to tensile prestress; and Orientation-3 is free of prestress.

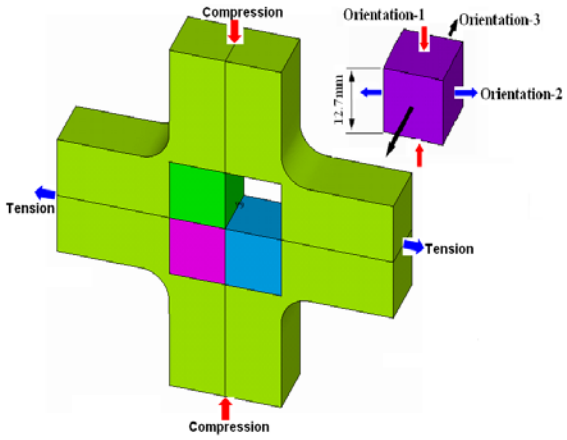

Figure **7**. A schematic of the preparation for programmed sealant specimens

In order to evaluate the effect of prestress level on the thermomechanical behavior, four compressive prestress levels in the vertical direction were used. They were 168.3kPa, 207.7kPa, 247.6kPa, and 300.7kPa, respectively. Because of the symmetry of the truss

fixture and the specimen, the tensile prestress in the horizontal direction was the same as the corresponding vertical compressive prestress. In addition, some specimens with 300.7kPa prestress experienced 10 thermomechanical cycles to evaluate the functional stability of the foam sealant.

XRD examination

An X-ray diffractometer (MiniFlex model, Rigaku Corporation, Japan) with Ni-filtered Cu-Kα radiation (λ =1.54178Å) was used to investigate the microstructure change of the original, programmed, and recovered foam specimens, original pure SMP specimens, and hollow glass microspheres. For all samples, XRD spectra were obtained by scanning over 2θ angles from 1° to 30° at a scanning speed of 2°/min and step width of 0.5°.

Experimental

2-D shape recovery of programmed biaxial specimens

For some specimens, 2-D free-shape recovery started immediately after the completion of the programming by using the same heating chamber and LVDT system. According to our previous study [22], the chamber was heated up quickly from room temperature to 49^{o}C and allowed to soak for 20 min. Then the heating was continued again at an average heating rate of 0.3^{o}C/min until 77^{o}C. Soaking for 7 minutes, the heating was ramped quickly to 79^{o}C and the temperature was held for 30 minutes. It is noted that, while the heating profile affects the recovery rate, it does not affect the final recovery strain or recovery stress because the recovery is driven by entropy (depending on temperature only).

Compression test

To evaluate the performance of the smart sealant when the deck/pavement is experiencing expansion during temperature rising, uniaxial compression tests along the Orientation-1 were conducted as shown schematically in Figure 7. The maximum movement that the joint may experience needs to be first established. Assuming the span-length of the bridge is 10m, the coefficient of thermal expansion (CTE) of concrete is $10\times10^{-6}/^{o}$C, and the

maximum temperature rise is 50^{o}C, then the maximum joint movement can be estimated to be 5mm. Because the specimen width was 12.7mm, this translated to a maximum compressive strain of 39.4%. Therefore, the purpose was to evaluate if the programmed foam sealant could survive this compressive strain or not. Sandwich specimens formed by sandwiching the foam sealant in between two concrete blocks along the Orientation-1 were prepared by using a conventional adhesive for the compression test (as shown in Figure 7 and Figure 8). The dimensions of the sealant and concrete blocks were both 12.7 mm long, 12.7mm wide and 12.7mm deep.

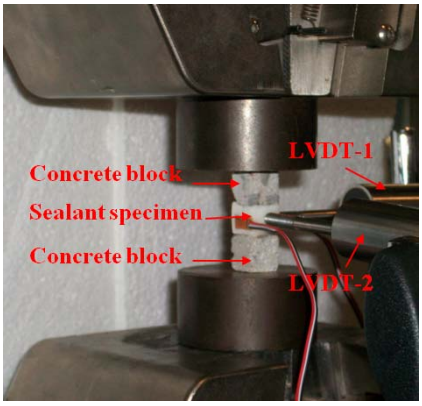

Figure **8**. Compression test setup

However, they cannot create a compressive strain of 39.4% by temperature rise due to their small size. In order to impose the joint movement in the specimen, a MTS 810 machine was used to apply this strain (39.4%) on the joint in the specimen. In practice, the temperature rise occurs slowly. To reflect this slow heating process, the rate of the hydraulic ram displacement was controlled to simulate the strain occurring due to the temperature rise. Assuming the temperature rise is uniform and the 5mm joint displacement occurs in 2-hours, the ram displacement rate during testing would be 6.94×10^{-4}mm/s (or 41.64μm/min). The tests were conducted at room temperature. Three effective specimens were tested for each group of samples. Two Teflon sheets were interposed between the specimen and loading platens to reduce friction, leading to free transverse expansion. Each test was stopped when the compressive strain was 40%, regardless of specimen failure or not.

In order to evaluate the effects of the programming on the strain/deformation of the smart sealant, the lateral strains of the tension programmed face (along Orientation-2 by utilizing LVDT-2) and nonprogrammed face (along Orientation-3 by utilizing LVDT-1) were

measured during compression test, respectively. And the two LVDT rods were adhered at the center of the two lateral faces of the specimen by using glue, respectively. The picture of the compression test is shown in Figure 8.

Tension test

In order to evaluate the tensile performance of the foam sealant when the joint experiences elongation as temperature drops, tension tests were conducted. The dimensions of the sealant specimens were the same as the compression test, but the dimensions of the concrete blocks were 50.8mm long, 12.7mm wide and 12.7mm deep (as shown in Figure 9). The foam sealant specimens were bonded to the two concrete blocks with a strong epoxy adhesive. The sandwich specimen was placed in the grips of the MTS 810 machine, using care to adjust the specimen symmetrically to distribute tension uniformly over the sealant cross section (see Figure 9). The tests were conducted at room temperature. Three effective specimens were tested for each group of samples. The same ram displacement rate as the compression tests was used for tension tests.

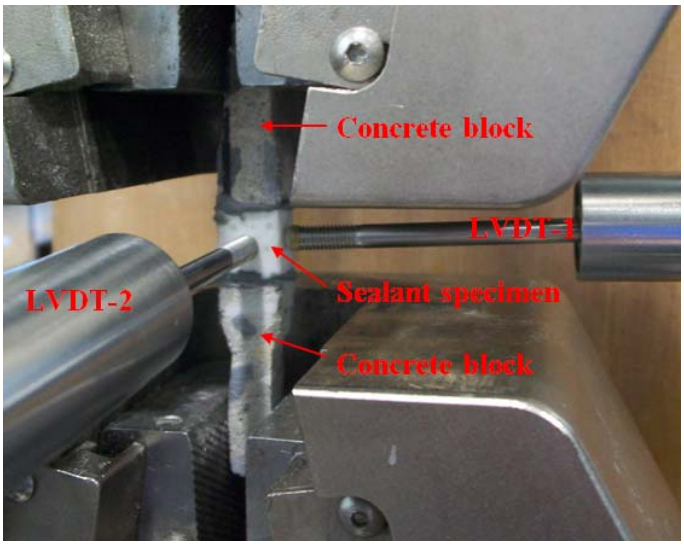

Figure **9**. Tension test set-up

Shear test

Shear performance of the sealant was investigated by using a double-lap joint configuration which consisted of three concrete blocks separated by two gaps that were filled

in with two pieces of programmed foam sealant. Shear tests were conducted on the double lap joint by applying a compressive load to the central concrete block. Due to the special configuration, the compressive load was actually a shear force. For some specimens, transverse compressive load was also applied to the substrate concrete blocks by a C-clamp to simulate the traverse compressive stress applied to the sealant at various temperatures. The shear test specimen in the double lap joint configuration used in this study is shown in Figure 7. The sealant layer dimensions were as follows: thickness of 6.3 mm, height of 12.7mm, and width of 12.7mm. The dimensions of the middle concrete block were 12.7mm wide, 12.7mm deep, and 12.7 mm long. The dimensions of the substrate concrete blocks were 12.7mm wide, 12.7mm deep, and 25.4mm long.

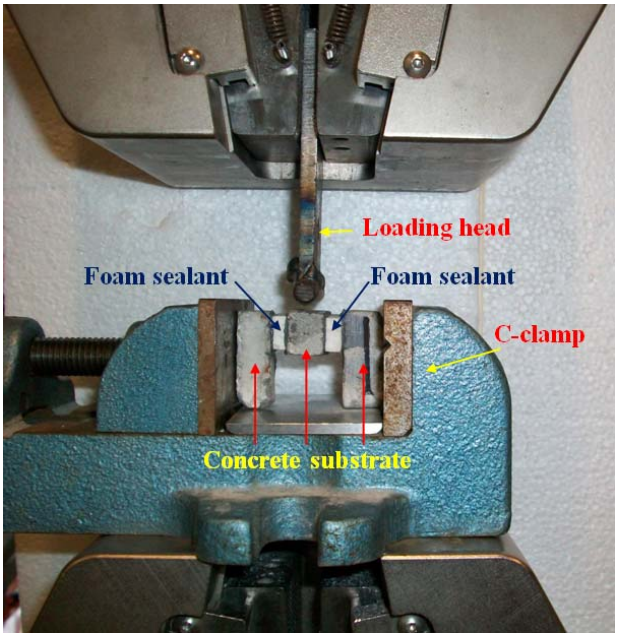

Figure **10**. Shear test set-up

Three groups of specimens were prepared. Each group consisted of at least three effective specimens. According to the compression test result, the first group was subjected to a larger sustained transverse compressive stress to simulate the compressive stress in the sealant at higher service temperature. The second group of specimens was subjected to a smaller sustained transverse compression stress to simulate the stress in the sealant at lower service temperature. The third group was a control group, and did not have any transverse stress. For this purpose, a C-clamp fixture was employed to apply various transverse compressive stresses on the shear sandwich specimens (as shown in Figure 10). All shear

tests were conducted at room temperature. To simulate the actual working condition of the foam sealant in expansion joints, shear tests were conducted along Orientation-2.

From Figure 10, the shear sandwich was placed symmetrically below the movable loading head. The middle concrete block was pushed downward at 20 mm/min until the specimen failed. The shear stress (τ) and strain (γ) of the sealant were determined by using the following relationships:

$$\tau = \frac{F}{2A},$$

$$\gamma = \frac{\delta}{T},$$

where F − applied load; A − sealant cross-sectional area in contact with each substrate; T − sealant thickness; and δ − vertical displacement.

Functional Stability under Environmental Attacks

Accelerated ultraviolet (UV) ageing

To investigate the effect of UV ageing on the programmed foam, two groups of the programmed cube specimens were exposed to UV for compression and shape recovery tests, respectively. Another group of the programmed cuboid specimens was exposed to UV for tension test. Each group contains three effective specimens. UV lamp was placed 33cm above the foam's top surface for 90 days. Heat effects from the light source were measured. The temperature on the exposed specimen surface is about 20~23^{o}C higher than that without UV exposure. Even with the increased temperature, the temperature of the foam is still lower than its T_g. Therefore, shape recovery is impossible during the ageing process. Then these prepared samples were used to conduct some tests proposed in this study, such as compression and tension tests.

Additionally, in order to investigate synergistic effects of UV and moisture on the degradation and mechanical properties, four additional groups of the programmed cube specimens were immersed in saturated salt water and rainwater at room temperature for 90 days, respectively. They were prepared for compression and shape recovery test. Meanwhile, two groups of the programmed cuboid specimens were also immersed in the salt water and rainwater for tension test, respectively. All these immersed specimens were synchronously exposed to UV. After this immersion and exposure, mechanical and shape recovery tests

were conducted on these aged specimens. Correspondingly, the original foams were also prepared as control specimens for each group of programmed foams. And the test results were compared to the performance of control specimens without radiation and immersion to determine the aging resistance of the SMP foam.

Accelerated hydrolytic ageing

Once the block specimens were prepared, accelerated hydrolytic ageing experiments were conducted. Four groups of original and programmed foam specimens were immersed in saturated saltwater and rainwater for further testing, respectively. Each group had three effective specimens numbered individually. Synthetic sea salt named *Instant ocean*® was used to prepare the saturated saltwater. The rainwater was collected in the open air when it was raining. Specimens were kept in a closed container to minimize the evaporation losses, maintaining the salt concentration approximately constant in the saltwater.

After the specimens were immersed in the saltwater and rainwater for 90 days, equilibrium state was reached [15]. The immersed foam specimens were quickly taken out of the container for moisture absorption testing. Before weighing the specimens, excess surface water was wiped off and specimens were left in air for about 5 min. The moisture content can be calculated as follow:

$$m_s = \frac{w' - w_0}{w_0} \times 100\%$$

where m_s−moisture content; w_0−mass before immersion; w'−mass after immersion.

Then mechanical tests were conducted on the immersed specimens at room temperature, including compression, tension, and shape recovery test. As-fabricated foam specimens, referred as dry specimens, were also tested as controls.

Compression test after environmental attacks

To evaluate the effects of hydrolytic ageing and/or UV exposure on compressive properties of the programmed foam, compression tests were conducted along the compression direction during programming. The dimensions of the foam specimen were 12.7 mm long, 12.7mm wide and 12.7mm deep. A MTS 810 machine with a 100KN load cell was used to apply a compressive strain of 40% onto the foam. The tests were conducted at room

temperature at a loading rate of 41.64μm/min. And two Teflon sheets were interposed between the specimen and loading platens to reduce contact surface friction, leading to free transverse expansion. Three effective specimens were tested for each environmental conditioning and control.

Tension test after environmental attacks

In order to estimate the influence of hydrolytic and/or UV ageing on tensile properties of the foam, tension tests were conducted on the programmed specimens along the compression direction during programming. The specimen was placed in the grips of the MTS 810 machine with a 50kN load cell, using care to adjust the specimen symmetrically to distribute tension uniformly over the foam cross section. The middle 1/3 of the programmed specimen was tested as the gauge length, and the other two 1/3 lengths at the two ends were clamped. The tests were conducted at room temperature and the same rate of ram displacement as the compression test was adopted during tension testing. Again, three effective specimens were tested for each environmental conditioning and control.

Shape recovery test after environmental attacks

To investigate the effects of hydrolytic and/or UV ageing on the shape memory functionality of the programmed foam, full confinements were used to test the recovery stress. Fully confined recovery test was performed using the MTS machine with a temperature-controlled furnace. After the specimens were conditioned, as described above, they were placed in the fixture shown in Fig. 11 such that the strain was fixed and the stress was initially zero. The fixture provided full confinement and the furnace were used to trigger the shape memory effect by heating the specimen above its T_g. During heating, the sample attempts to expand against the fixed strain boundary condition, resulting in the generation of recovery stress. The MTS machine was used to record the resulting recovery stress. Heating was performed at an average rate of 0.3^oC/min from room temperature until 79^oC and then the temperature was maintained constant for approximately 20 min. The MTS machine's load cell was used to record the recovered force as a function of time and temperature. Similarly, three effective specimens were tested for each environmental conditioning and control.

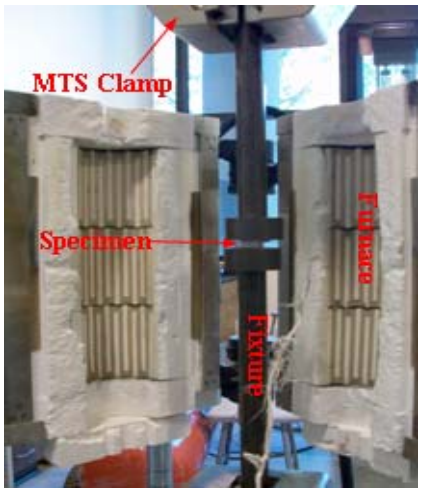

Figure **11**. MTS machine with furnace and fixture used for fully-confined recovery

Cyclic Loading Test

Cyclic loading tests at room temperature

To evaluate the fatigue properties of the syntactic foam and pure SMP, cyclic loading tests were conducted under strain controlled mode at room temperature. The specimens were tested under fully reversed compression-tension uniaxial cyclic stress. A triangular wave form and a constant loading rate were used for all tests. The tests were conducted on MTS 810 machine (see Fig. 12), using care to adjust the specimen symmetrically to distribute compression and tension force uniformly over the specimen cross section. The middle 1/3 central length of the programmed specimen was tested, and the other two 1/3 lengths along the two ends were tightly clamped to avoid buckling under high compressive loads needed to impose the deformation desired. However, cyclic testing of specimens under fully reversed uniaxial loading condition is currently not covered by any specific standard [36]. In this test, each specimen was compressed to a 5% strain and then reversed to zero strain by tension. This compression-tension cycle continued until failure. The loading rate was 0.5 mm/min. The loading frequency was approximately 1/305 Hz. Also, some characteristic parameters can be automatically obtained from the testing results in the MTS system, for example, peak stress, dynamic modulus (the ratio of stress to strain under dynamic conditions), and stiffness (the frequency dependant ratio of the dynamic force over the resulting displacement).

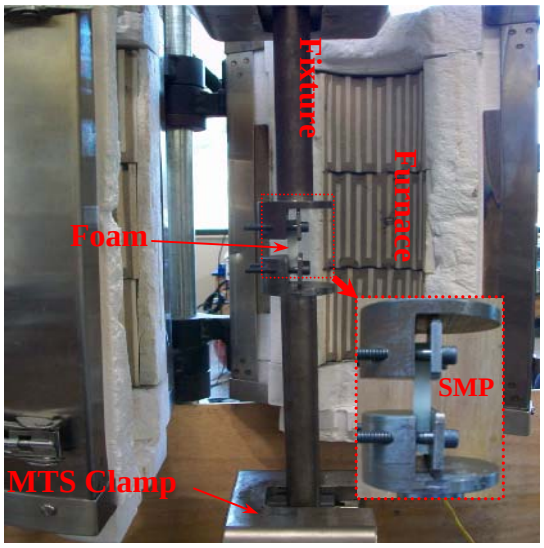

Figure **12**. MTS machine with furnace and fixture used for cyclic tests (The SMP specimen is shown in the subplot)

Mechanical response under one thermo-mechanical cyclic loading

To evaluate the combined effects of cyclic loading and temperature changing on the stress-strain responses of the foam, each specimen was first compressed to 40% strain endpoint in the fixture and then immediately reversed to tension until zero strain. The loading rate during compression and tension stage was 41.64μm/min, which was used to better simulate the condition when the foam is used as a sealant in bridge deck with daily temperature change. At the same time, the chamber was heated from room temperature to 79^{o}C at an average heating rate of 0.3^{o}C/min (Fig. 12) during the compression process. When the temperature reaches 79^{o}C, the heating was first stopped, the chamber was kept closed and the system was allowed to naturally cool to room temperature. Meanwhile, the compression was reversed to tension at the same loading rate. This cyclic loading test was only subjected to one cycle due to the excessive testing time incurred.

Mechanical response under one-cyclic loading at room temperature

To evaluate the effects of the temperature on the cyclic stress-strain behavior of the

foam, one-cyclic loading tests at constant room temperature were conducted for nonprogrammed and programmed foams. The testing setup and loading method were the same as that of thermo-mechanical test (Fig. 12), but without the furnace. In this case, each specimen was also first compressed to a 40% strain endpoint and then immediately reversed to tension until zero strain at a loading rate of 41.64μm/min during both compression and tension.

Feasibility of Replacing One Step 2-D Programming by Two-Step 1-D Programming

Raw Materials

The syntactic foam sealant consists of hollow glass microspheres dispersed in a shape memory polymer matrix. The polymer is a styrene based thermoset SMP resin system sold commercially by CRG Industries under the name Veriflex® (glass transition temperature: 62^{o}C, tensile strength: 23 MPa, density: 920 kg/m^{3}, and elastic modulus: 1.24 GPa at room temperature.). The glass microballoons were purchased from Potters Industries (Q-CEL6014: average outer diameter: 85μm, bulk density: 0.08 g/cm^{3}, effective density: 0.14 g/cm^{3}, maximum working pressure: 1.73MPa, and wall thickness: 0.8μm). No special surface treatment was conducted. These raw materials have been used previously for the smart syntactic foam [37, 38].

Syntactic foam fabrication and specimen preparation

The SMP based syntactic foam was fabricated by dispersing 40% by volume of the hollow glass microspheres into the SMP resin. The microspheres were added to the resin while slowly stirring the mixture to minimize air bubbles in the resin. The microspheres were added in multiple steps to avoid agglomeration. After dispersion, a hardening agent was added and the solution mixed for 10 min.

The mixture was then poured into a 229×229×12.7 mm steel mold and placed in a vacuum chamber at 40kPa for 20 min in order to remove any air pockets introduced during the mixing process. Based on our previous study [19,22,24], the curing cycle was 79^{o}C for 24h, 107^{o}C for 3h, and 121^{o}C for 9h. After curing, the foam panel was de-molded and was ready to be machined into required specimens for programming.

Our strategy for preparing test specimens is to first prepare tension specimens for programming at temperature above T_g, and after programming, the tensile specimens be machined into compression specimens for second programming at temperatures below T_g. The reason is that the foam has a maximum tensile strain of about 5% at temperatures below T_g and cannot be programmed because it fractures without yielding under tension [37]. Also, if the foam is programmed first at temperature below T_g, the second programming at temperatures above T_g will lead to recovery of the first programming.

By referencing ASTM D638M-89 standard, dog-bone specimen was used for tension programming. The only revision was to increase the specimen thickness from 2 mm to 10 mm, in order to avoid buckling in the subsequent compression programming. A finite element analysis was conducted which validated the uniform tensile stress distribution in the gage length of the dog-bone specimen; see Fig. 13 (a) – (d). During the FEM analysis, only half of the specimen was modeled due to symmetry. Because a section with a length of 25mm at each end (Fig. 13 (a)) was gripped during tension programming, the 25mm long section at each end was not meshed; instead, boundary conditions were applied to simulate the gripped loading condition. In this study, the left hand boundary was fixed and the right hand boundary was allowed to move in the x direction (loading direction) only. At the centerline of the dog bone specimen, symmetry boundary condition was enforced. The

analysis was conducted using ANSYS10.0 software package and the element type was PLANE82. After convergence analysis, a total of 12,544 elements with 38,401 nodes were used to model the specimen. After tension programming, block specimens with a length of 10 mm in the tension direction were machined from the dog-bone specimen for compression programming.

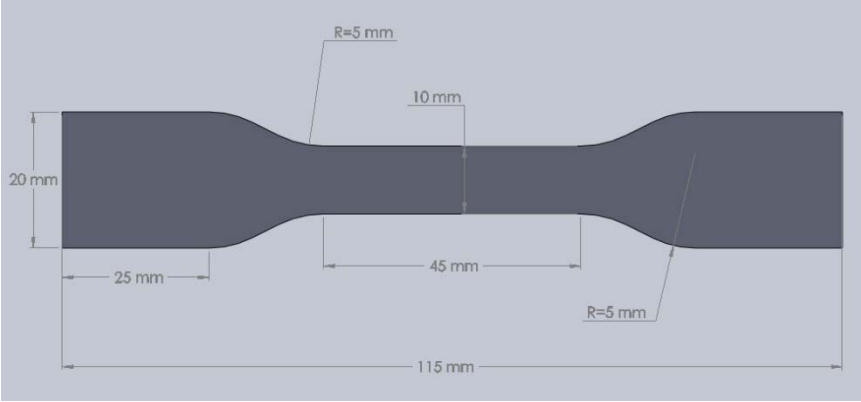

(a)

(b)

(c)

(d)

Figure **13**. (a) Schematic of the dog-bone specimen, (b) Normal stress distribution in the longitudinal direction (σ_x), (c) Normal stress distribution in the transverse direction (σ_y), (d) In-plane shear stress distribution (τ_{xy}). Note the uniform stress distribution in the gage length. Due to symmetry, only half of the specimen is analyzed.

Programming

The two-stage, hybrid, and biaxial programming process is schematically shown in Fig. 14. Four groups of specimens were programmed with various combinations of "nominal" prestrain levels: T25C5, T5C25, T40C5, and T25C25, here T represents tension and C stands for compression. The numbers represent "nominal" prestrain levels. For example, T25C5 stands for 25% "nominal" pretension at temperature above T_g followed by 5% "nominal" precompression in the transverse direction below T_g. The word "nominal" is used because this is the strain applied without considering the Poisson's ratio effect. The "actual" strain in each direction is the sum of the "nominal" strain and the strain due to Poisson's ratio effect. At least three effective specimens were tested for each group.

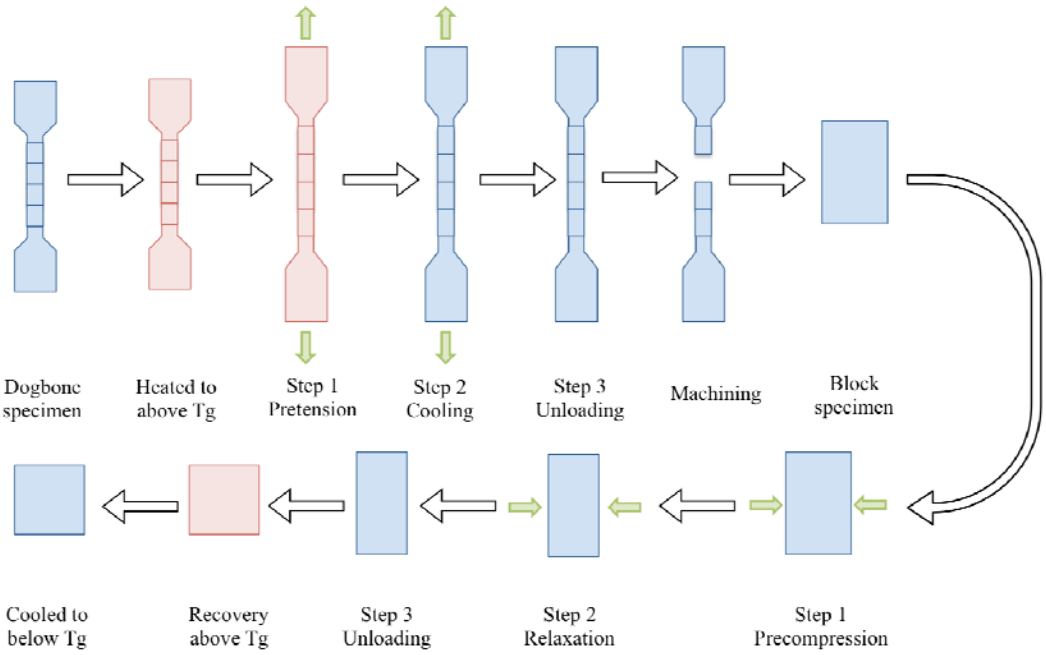

Figure **14**. Schematic of the entire thermomechanical cycle (two-stage programming and one step free shape recovery)

The stage 1 programming was similar to the traditional one-stage uniaxial programming [17, 22]. The heating chamber was first brought to a temperature of 79°C and held for 45 minutes. After this, the dog-bone specimen was placed in the chamber to soak for 20 minutes. At this point the specimen was mounted in the tensile fixtures and the heating chamber was closed. The specimen was allowed to dwell for 10 more minutes to achieve uniform temperature. Then, the MTS machine applied a tensile stress at a constant rate of 1.3 mm/min until the desired tensile strain level was reached (step 1-pretesnion). The displacement in the gage length was measured by an LVDT system (Cooper Instruments LDT 200 series) and the strain was calculated based on the definition of engineering strain (change of the gage length over the original gage length). Once the desired strain level was achieved, the strain was maintained and the specimen was allowed to slowly cool to room temperature, which took about 10 hours (step 2-cooling). Once the specimen reached room temperature, the load was removed by releasing the grips, causing a small springback of the specimen (step 3-unloading). This completed the tensile programming. The temperature, stress, and strain were recorded throughout this process using thermocouples and the MTS

machine load cell, similar to Li and Nettles [22]. Once the specimen was tension programmed, it was machined into four block specimens for compression programming. Figure 15 (a) shows the test chamber and Figure 15 (b) shows the tension-programmed specimens under various prestrain levels.

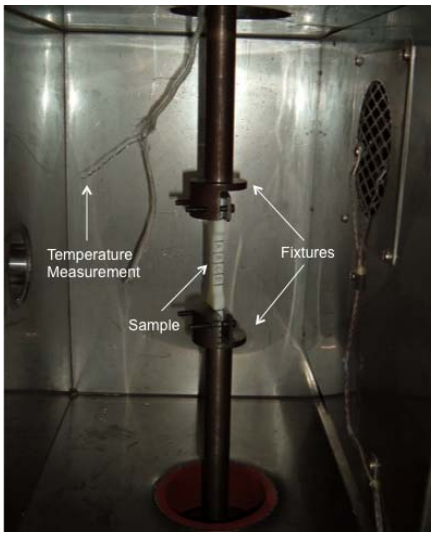

(a) Dog-bone specimen under tension programming

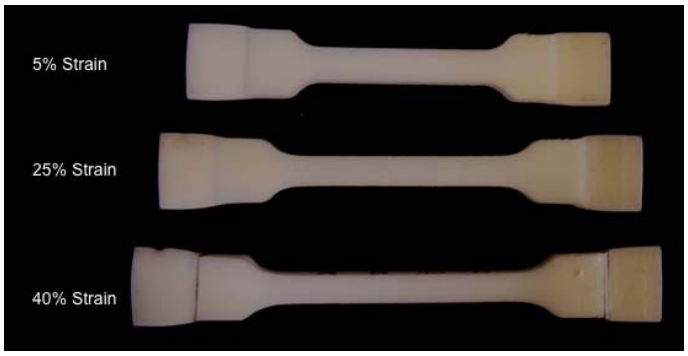

(b) Comparison of dog-bone specimens programmed to various tensile strains

(c) A specimen after tensile programming to 25% strain and compressive programming to 5% strain. Letter "C" stands for compression direction and "T" for tension direction.

Figure **15**. Specimens after the two-stage programming

In stage 2 programming, the programming was in the transverse direction (perpendicular to the tension direction) at room temperature. The tension programmed block specimens were first smoothed using sand paper on the two opposite sides to ensure parallel surfaces. The block specimens were then mounted in a compression fixture. Teflon sheets were inserted between the specimen and the steel platens of the fixture to reduce transverse shear force during uniaxial compression. A compressive load was applied at a constant rate of 1.3 mm/min until the desired compressive strain level was reached (step 1-precompression). The compressive load and axial displacement were directly recorded by the MTS machine and the data were used to calculate the engineering stress and engineering strain curves. Once the specimen was strained to 5% or 25% in the compressive direction, the strain was maintained and the specimen was held for 30 minutes with constant strain (step 2-relaxation). The load was then released (step 3-unloading). This completed the compression programming. Again, the stress and strain versus time were recorded by the machine. The specimen dimension was also recorded immediately after unloading and continuously monitored by linear variable differential transducers (LVDTs) until the dimension was stabilized after about 24 hours of unloading. Figure 15 (c) shows a specimen that has been programmed to a tensile strain of 25% and a compressive strain of 5%.

Free shape recovery test

After the second programming, free-shape recovery test was conducted as schematically shown in Fig. 14 by heating up the specimen to above T_g without any constraint. During free shape recovery, the specimens were placed into the heating chamber and two LVDTs were attached to two faces of the programmed specimens. The opposite two faces were placed against an angle steel so that the LVDTs measured the total displacement in each direction; see Fig. 16. The recovery step itself involved slowly ramping up the temperature in the heating chamber to ensure that the specimen has the same temperature as its environment. The temperature was increased incrementally at 2.8^{o}C per 5 minutes (i.e., the chamber temperature controller was controlled to increase the temperature step-wise every 5 minutes) until the programming temperature of 79.4^{o}C was reached. The reason was that this gave the specimen sufficient time to obtain temperature uniformity. The temperature of 79.4^{o}C was held for 20 minutes, which was sufficient to stabilize the recovery strain [22].

At the end of this holding time period, data recording was stopped and the recovery step was completed. The specimen was then taken out of the chamber and the specimen dimensions were recorded immediately. It is noted that the heating rate affects the recovery rate, but not the final recovery strain. A combination of higher heating rate and longer socking time is equivalent to a lower heating rate and shorter socking time as long as the recovery strain is stabilized, which has been validated by [38].

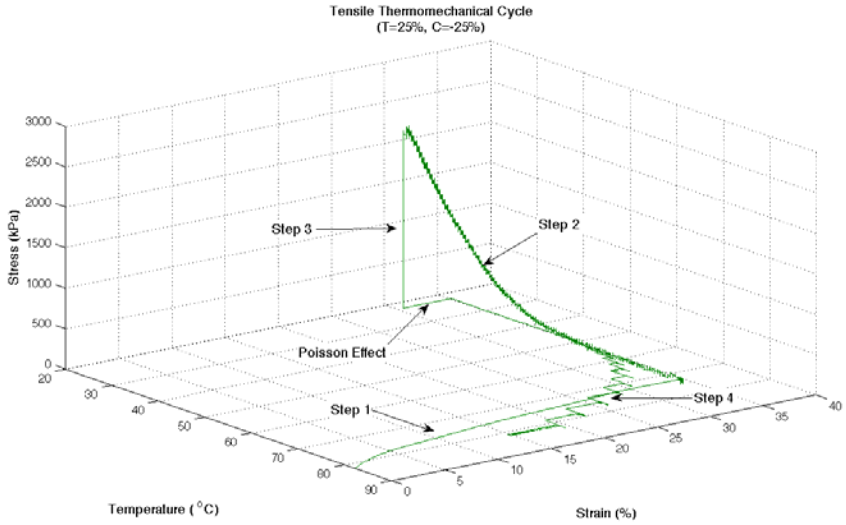

Figure **16**. Thermomechanical cycle in the tension direction for a specimen of T25C25 ((Step 1 → pretension to 25% strain at temperature above T_g, Step 2 → cooling down to room temperature while hold the prestrain constant, Step 3 → unloading, which completes the first stage of programming. The Poisson's effect is due to the second programming in the transverse direction by compression. Step 4 → free shape recovery.)

RESULTS AND DISCUSSIONS

Thermomechanical Characterization of Shape Memory Polymer Based Self-healing Syntactic Foam Sealant for Expansion Joint

Thermo-mechanical properties of biaxial specimens

Figure 17 shows the typical strain evolution during the entire thermomechanical cycle subjected to various prestress levels. Similar to previous 1-D stress controlled programming

and free shape recovery [22], each direction (compression in vertical direction and tension in horizontal direction) shows similar four-step thermomechanical behavior. From Figure 17, the thermo-mechanical cycle includes four steps: Step1 (loading), Step 2 (cooling while holding the load constant), Step 3 (unloading), and Step 4 (recovery). The small spikes are due to manual control of the testing setup.

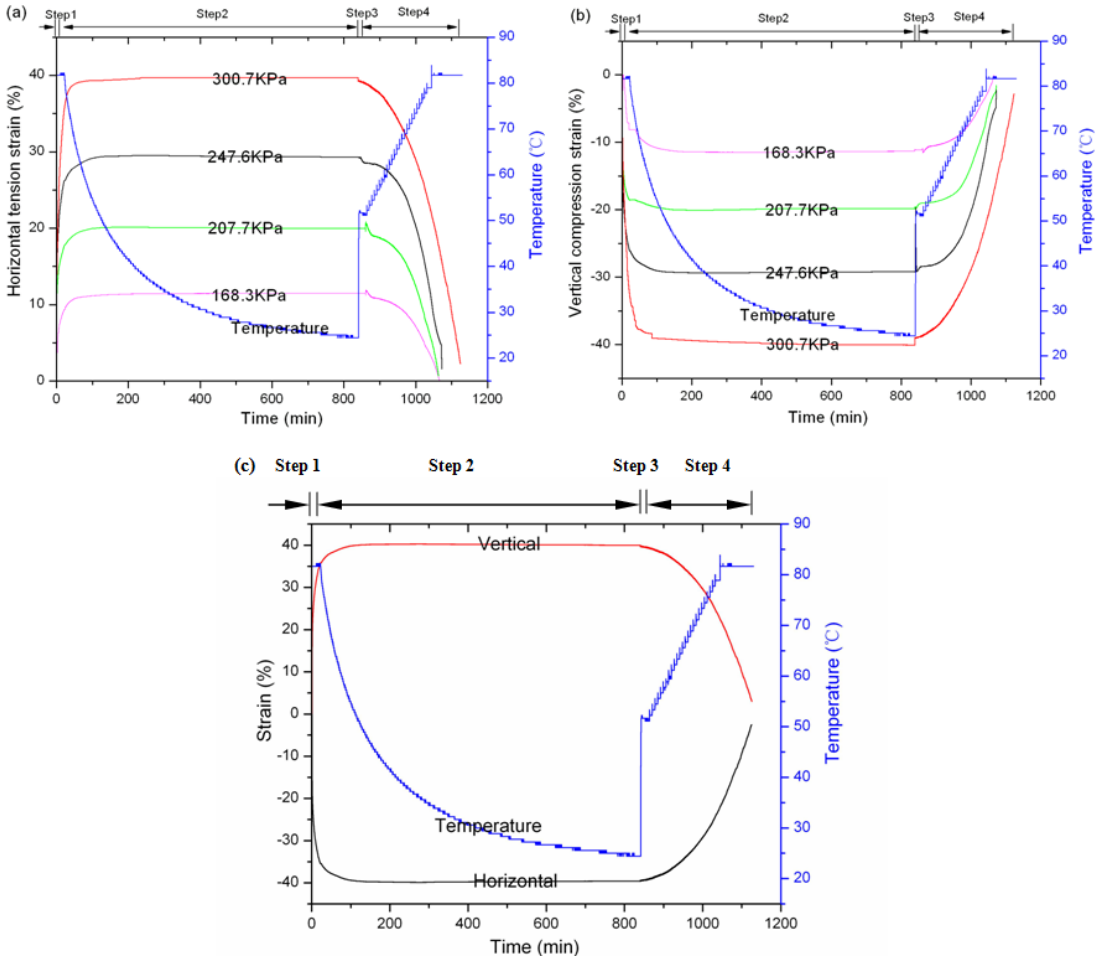

Figure **17**. (a) Horizontal and (b) vertical strain evaluation of the cruciform sealant specimens under various prestress levels during programming and recovery (Steps 1-3 represent programming and Step 4 represents free shape recovery) and (c) horizontal and vertical strain evaluation of the 10th thermomechanical cycle under the prestress level of 300.7kPa.

Based on Figure 17 (a) and (b), the shape fixity ratio and shape recovery ratio were obtained. According to [19], the shape recovery ratio is defined as the ratio of the strain at the end of step 3 over the strain at the end of step 2 during programming; the shape recovery ratio is defined as the ratio of the difference between the strain at the end of step 2 and the strain at the end of step 4 over the strain at the end of step 2 during the thermomechanical

cycle. The shape fixity ratio is 95.6%, 96.7%, 98.6%, and 99.2% for the four prestress levels (168.3kPa, 207.7kPa, 247.6kPa, and 300.7kPa), respectively. The shape recovery ratio is 97.3%, 95.4%, 94.1%, and 91.6%, respectively. It is clear that as the prestress level increases, the shape recovery ratio decreases. This is understandable because higher prestress may cause some damage to the foam (such as crushing of microspheres), which is unrecoverable during shape recovery. For the shape fixity, with the increase in the prestress, the foam sealant specimen becomes denser and stiffer, resulting in a smaller springback and higher shape fixity.

From Figure 17 (a) and (b), when the prestress level reaches 300.7kPa, the prestrain is about 40%, which is similar to the designed strain for compression test (39.6%). Therefore, for the mechanical properties tests (uniaxial compression, uniaxial tension, and double-lap shear), all the foam specimens were programmed by 300.7kPa prestress.

Additionally, as shown in Figure 17 (c), the horizontal and vertical strain after 10 thermomechanical cycles is close to the strain evolution of the first thermomechanical cycle. The shape fixity ratio is 98.5 %, and the shape recovery ratio is 88.3%. It is noted that both shape fixity ratio and shape recovery ratio are slightly lower than those in the first thermomechanical cycle (99.2% and 91.6%, respectively) under the same prestress level (300.7KPa). This is because more unrecoverable damages are accumulated during each additional thermomechanical cycle, leading to the decrease in shape recovery ratio. Also the density of the foam increases as the thermomechanical cycle increases, resulting in an increase in springback when the load is removed and the decrease in shape fixity ratio. However, this change in shape recovery ratio and shape fixity ratio is comparatively small. Therefore, the shape recovery functionality of this foam sealant is stable and sustainable.

To visualize the programming and recovery process, Figure 18 shows the original and programmed cruciform foam sealant specimen and its recovery process under various temperatures. During Step 1 and Step 2 of the programming, the 2-D stress condition causes the orientation of the macromolecular chains of the SMP matrix aligns along both vertical and horizontal directions. This leads to a decrease in entropy of the material system in the programming process [39-40]. Meanwhile, some microspheres may be bent or buckled, and the deformed microspheres or crushed debris may align in the tension orientation due to the compression in the transverse direction. Furthermore, a wrinkle-like pattern can be seen with

naked eye on the stretched specimen surface along both directions, as shown in Figure 18 (b). This reflects the 2-D stress conditions. It is believed that the central square of the cruciform foam sealant specimen is changed from isotropy to anisotropy. From Figure 18 (c-f), the recovery rates in horizontal and vertical directions are faster when the temperature is up to T_g, which is consistent with the strain evolution shown in Figure 17. Additionally, the recovery process occurs in both directions simultaneously, which is important for the sealant in expansion joints to expand in the horizontal direction and contract in the vertical direction without distortion. It is beneficial to achieve the design purpose of smart foam sealant proposed in this study.

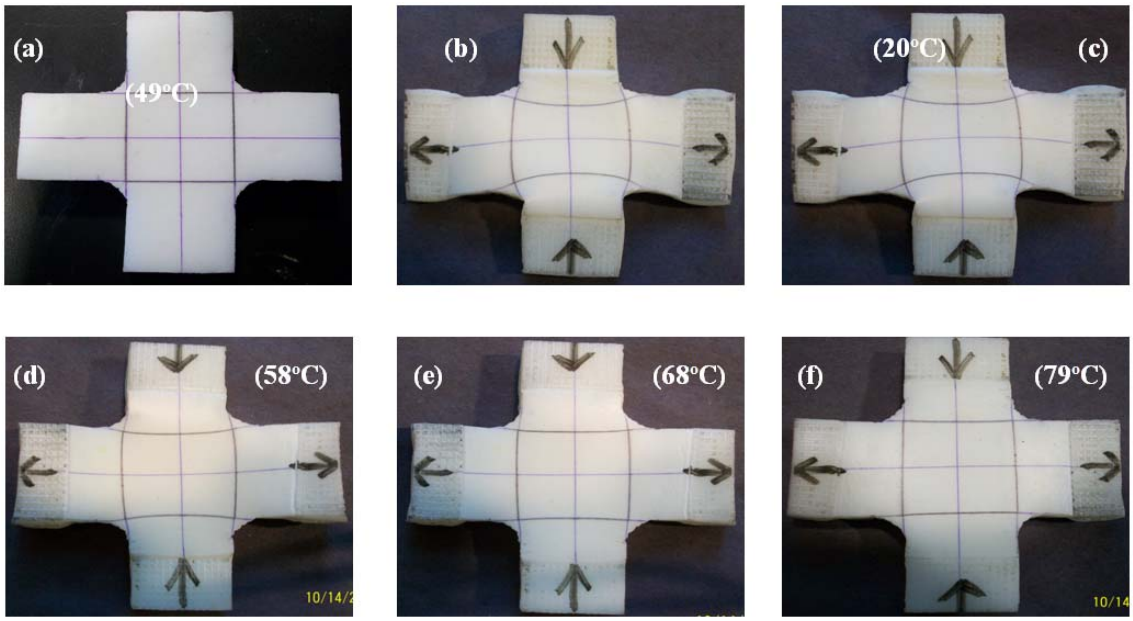

Figure **18**. (a) Original and (b) programmed cruciform foam sealant specimen and (c-f) its recovery process under various temperatures

Compression test

Stress–strain responses of the programmed foam sealant (including 0 cycle (original nonprogrammed foam), 1 and 10 programming-recovery cycles) at room temperature are shown in Figure 19.

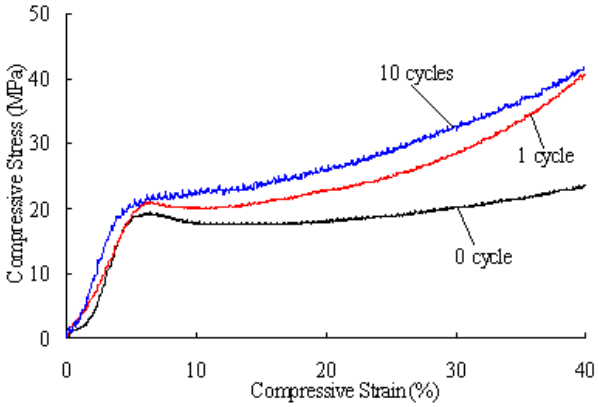

Figure **19**. Compressive stress–strain responses of the foam sealant specimen under various programming-recovery cycles

From Figure 19, for various programming-recovery cycles, the stress–strain curve can be almost characterized by three distinct regions. The first region (strain less than 5%) is characterized by an almost linear-elastic behavior of the syntactic foam. The region ends when the material starts to yield and reaches its compressive yield strength. This is due to the glassy state of the SMP matrix at room temperature. Once the yield point is reached, a slight drop in stress occurs, implying strain-softening behavior of the SMP.

The second region is characterized by an almost horizontal plateau. The horizontal plateau is attributed to the implosion of the hollow microspheres under the increasing compression strain [41]. This region is referred as densification stage.

The third region is characterized by an increase in stress again at the end of the plateau region. The steep increase is caused by a large number of microspheres being crushed and compacted, and the maximum density is being reached. The point, where this region starts, is considered to be the point of failure for the syntactic foam, as this is the point where a considerable amount of the load bearing microspheres has been crushed. This is consistent with the previous study [22].

From Figure 19, the yield strength increases and the densification region shortens as the programming-recovery cycle increases. The reason for this is that each programming-recovery cycle leads to crushing of some additional microspheres. The crushing of microspheres results in increase in the density of the foam sealant. Therefore, the repeated programming-recovery cycle leads to the continuous increase in density. The increase in density causes the increase in yield strength and shortening or disappearance of the densification region.

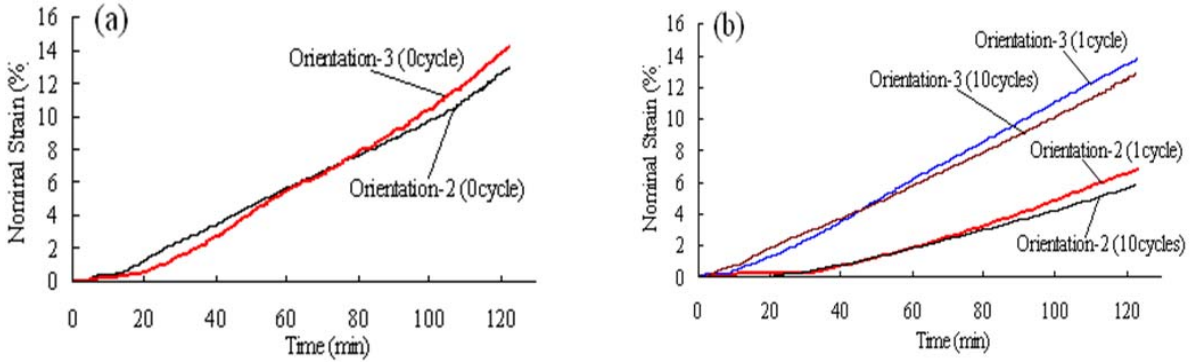

Figure **20**. Lateral strain evaluation of (a) nonprogrammed and (b) programmed specimens during compression test

Meanwhile, the nominal lateral strain-time diagrams are shown in Figure 20. From Figure 20, for the nonprogrammed foam sealant, the compression load causes the foam sealant specimen to linearly barrel outward in the two lateral directions, and the lateral strains developed along the two orientations are very close (see Figure 20 (a)). This suggests that the nonprogrammed foam sealant can be regarded as an isotropic body. However, for the programmed foam sealant (including 1 cycle and 10 cycles), within the first 30 min of loading, the lateral strain along Orientation-2 (the tension programmed direction) is close to zero or slightly negative, and then the lateral strain increases gradually. This suggests that when the compressive stress programmed face is under further compression, the tensile stress programmed face keeps undeformed. This is anticipated for a sealant in expansion joint. As shown in Figure 1 (c), when the expansion joint narrows due to the thermal expansion of the structural elements, it is desired that the deformation in the transverse direction (vertical direction) maintains zero in order to solve the squeezing-out problem. With further loading, the strain in Orinetation-2 becomes positive, suggesting that the stored energy by the tensile programming has been fully consumed. The deformation in Orientation-2 starts to be controlled by Poisson's effect. Therefore, for practical applications, the tensile programming in Orientation-2 must be carefully controlled so that its deformation maintains almost zero when uniaxial compression is applied to Orientation-1.

It is also noticed that, basically, the lateral strains of the foam sealant with 10 programming-recovery cycles is slightly higher than those with 1 programming-recovery cycle, which may be because the foam becomes more anisotropy as the thermomechanical cycle increases. However, the effect of the programming-recovery cycle is small and can be

neglected, which once again validates the functional stability of the foam sealant.

Tension test

Tensile stress–strain responses of the foam sealant under various programming-recovery cycles are shown in Figure 21.

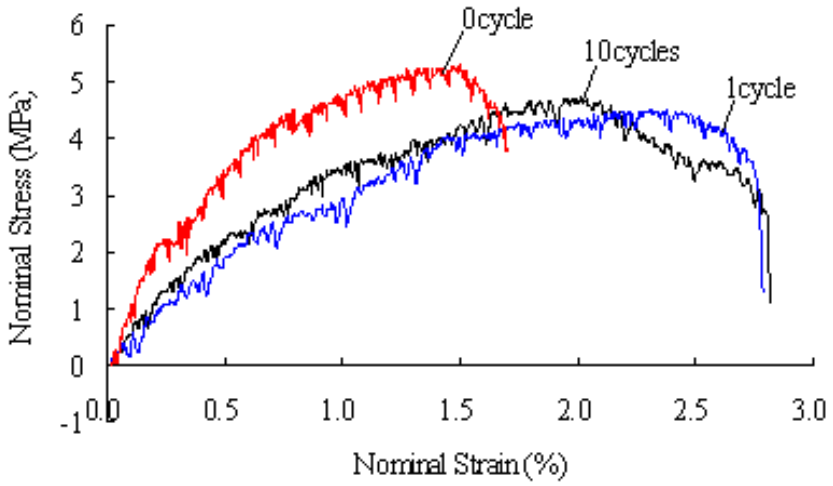

Figure **21**. Tensile stress–strain responses of foam sealant specimens under various programming-recovery cycles

For all three programming-recovery cycles, the tensile stress-strain curves tend to show non-linearity, which may be due to the viscoplastic behavior of the foam sealant and the lower loading rate used [42]. The stiffness of the original foam sealant is higher than that of the programmed sealant. The normal ultimate strain is 1.5% for the nonprogrammed foam sealant and becomes 2.5% and 2.0% for the 1-cycle and 10-cycle of programmed-recovered foam sealant. Also, the ultimate stress for the nonprogrammed foam sealant is 5.2MPa and becomes 4.4 MPa and 4.6MPa for the 1-cycle and 10-cycle programmed foam sealant. The reason for the increased ultimate strain in the programmed specimens is that some compressive pre-strain is stored in the foam sealant in the compressive direction (Orientation-1) during programming. The compressive pre-strain can consume some tensile strain by absorbing the strain energy [43]. The reason for the decreased tensile strength in the programmed specimens is that the programming caused some damage of the microspheres, which leads to reduction in tensile strength in the foam. Also, the number of thermomechanical cycles has a certain effect but is insignificant.

Shear test results

According to the compression test results of the foam sealant with 1-cycle of programming (as shown in Figure 19), the transverse compressive stresses applied to the specimens were decided, which were used to simulate the actual compressive conditions of the sealant due to joint expansion at different service temperatures. The three transverse compressive stress levels and their corresponding compressive strain as determined from Figure 19 are summarized in Table1. Shear test results are shown in Figure 22.

Table 1 Applied transverse compressive stresses and corresponding strain determined per Figure 19

Transverse stress levels	Programmed foam sealant		Nonprogrammed foam sealant	
	Stress (MPa)	Strain (%)	Stress (MPa)	Strain (%)
Larger	40.1	40.0	23.4	40.0
Smaller	6.3	2.0	3.6	2.0
zero	0	0	0	0

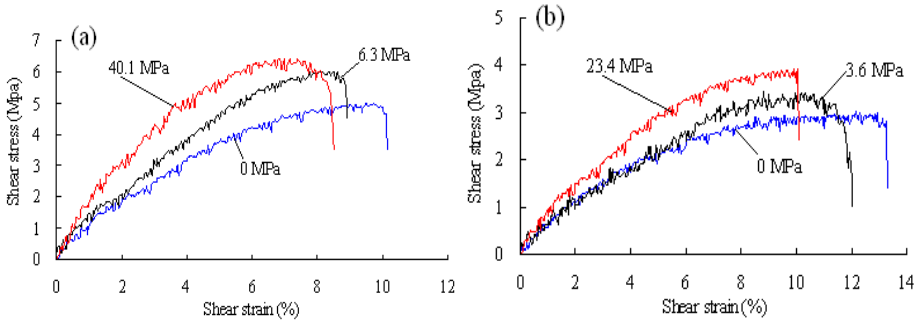

Figure **22**. Shear stress–strain responses of (a) programmed and (b) nonprogrammed foam sealant specimens under various transverse compressive stress levels

From Figure 22, it is noticed that the shear strength and stiffness of the programmed foam sealant is higher than that of the nonprogrammed foam sealant. For each type of the foam sealant, the shear strength increases as the applied transverse compressive stress increases. This may be because the applied transverse compressive force increases the

friction between the foam sealant and concrete blocks. Also, the lateral force serves to increase the density of the foam. This suggests that the programmed foam sealant possesses a higher strength and stiffness when the expansion joints narrows as the environmental temperature rises. This is beneficial for the foam sealant to enhance its serviceability, and extend its service life. The failure mode of the programmed foam sealant with the larger transverse compressive stress is shown in Figure 23. It is clear that the foam sealant fails by shear cracking.

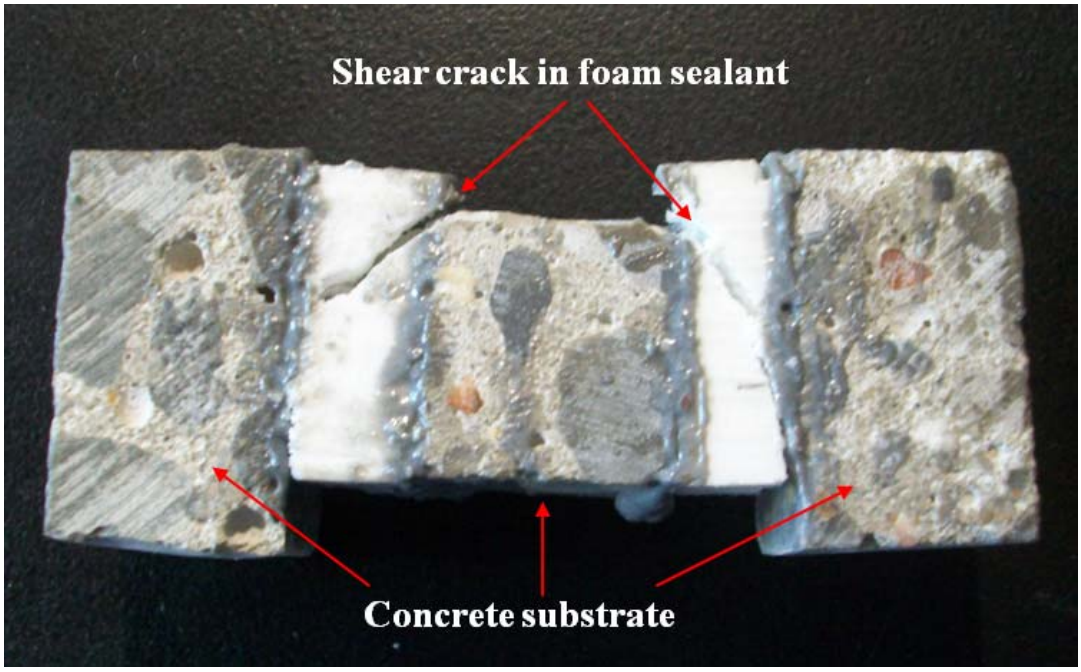

Figure **23**. Failure mode of programmed foam sealant specimen

Summary

Based on the comprehensive test results, the following conclusions are obtained:

- By the special 2-D training, it is proved that, if the SMP based syntactic foam sealant is installed at the lowest temperature the joint will experience, the foam sealant will always expand in the traffic direction and contract in the vertical direction. Therefore, it has a potential to serve as a sealant in expansion joints.
- The compressive force applied to the concrete wall is limited due to the shape (stress) memory functionality of the SMP matrix (the programming stress was 0.3MPa). Therefore, the concrete wall would not be compressed to failure.

- The 2-D programming makes the syntactic foam sealant transform from isotropy to anisotropy.
- When the expansion joint narrows by 40% during service, the foam sealant in the compression programmed direction can survive this deformation without failure.
- The shape memory functionality of the foam sealant is stable under repeated thermomechanical cycles.
- After 2-D training, the foam sealant exhibits an increase in compressive strength and stiffness, ultimate tensile strain, and shear strength. This facilitates the foam sealant to accommodate substantial shear deformation caused by traffic load in the joints, and would improve the serviceability and extend the service life of the expansion joints.

A Shape Memory Polymer Based Syntactic Foam with Negative Poisson's Ratio

XRD analysis

To better understand the mechanical properties of the original and programmed foam, it is important to analyze microstructure changes within the programmed syntactic foam. The XRD patterns are shown in Fig. 24. From Fig. 24, the glass microspheres are amorphous without any crystalline domain. For the pure SMP, it is seen that there are two very broad peaks, corresponding to diffraction angle (2θ) of 10^{o} and 19.5^{o}, respectively. Because of the wide peak, it suggests that, in general, the pure SMP is not a crystal (or crystals in very small size). It is known that the SMP used in this study is a thermosetting SMP with chemical cross-links. The wider peaks most likely correspond to the slight orientation (long range order) of the cross-linked domain (hard phase) and the amorphous domain (soft phase). When glass microspheres were added to the pure SMP, the resulting syntactic foam follows almost the same pattern as the pure SMP, a direct indication that the incorporation of glass mciroballons does not change the morphology of the SMP. After 2-D programming, it is seen that one of the peaks of the foam disappears. The reason is that the 2-D stress condition may disorient the hard phase and the soft phase. Because the hard phase usually takes higher stress, it may be disoriented more, leading to the disappearance of the corresponding peak. When the foam recovers, the pattern of the XRD follows the foam without programming, which is a piece of direct evidence that the foam has recovered its original shape, not only

macroscopically, but also microscopically in terms of microstructure and morphology.

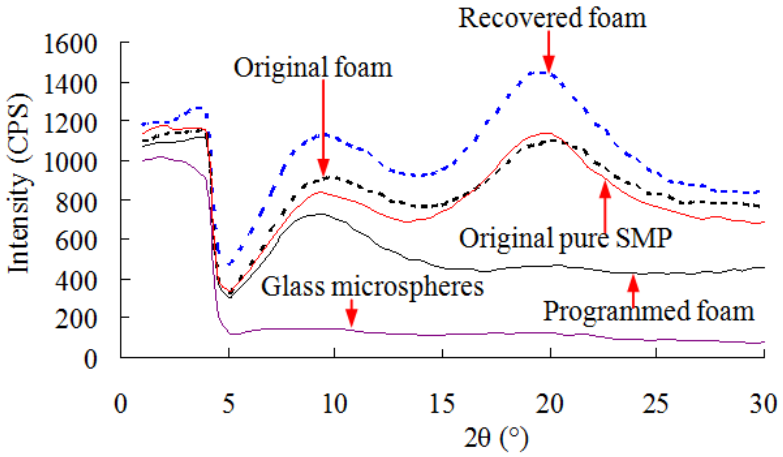

Figure **24**. XRD patterns for original, programmed, recovered foam, original pure SMP specimens, and hollow glass microspheres.

Compression tests along three orientations

The anisotropy in the programmed foam may lead one to expect differences in the mechanical properties of the foam when loaded in different directions [44]. To investigate comprehensively the effects of the aforementioned changes during programming on the compressive properties of the foam, compressive stress-strain behaviors of the foam along the three orientations (see Fig. 7) were examined. The test results are shown in Fig.25.

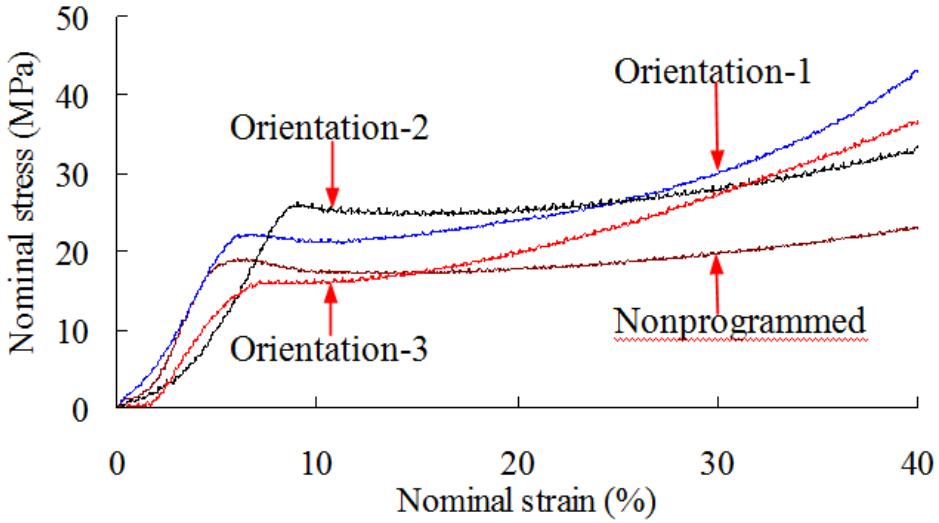

Figure **25**. Compressive stress–strain responses of nonprogrammed and programmed foam specimens along various orientations

From Fig. 25, the shapes of the compressive stress-strain curves of the programmed foam specimens are different from that obtained from non-programmed specimen. For all the foam specimens, it is seen that there are three regions in the stress-strain curves. After experiencing the initial small non-linear portion due to non-perfect contact between the specimen and the loading platens, the foams behave almost linearly elastic within which Hooke's law is obeyed. The slopes of the stress-strain curves in this linear elastic region are the modulus of elasticity.

After reaching yield point, the curves enter the second region. In this region, glass microspheres undergo rupturing or crushing. Hence hollow space within the microspheres is released, which may be occupied by crushed debris and matrix material. These lead to compaction or densification of the material. Hence the stress is almost constant with the increase in strain. Damage tolerant characteristics of the syntactic foams are attributed to this plateau region. However, it can be observed that the plateau regions are different for each type of the syntactic foams. The original foam possesses a larger plateau region than that of the programmed foam.

The third region is the solidification region. Solidification begins when the internal open space is fully occupied by crushed microspheres and surrounding matrix material and the foam behaves more like a solid. As the solidification increases, the foam becomes stiffer (strain hardening) so that the load required to compress the specimen increases with further strain. Eventually, the load reaches a maximum value when the foam is fully damaged.

From Fig. 25, it can be seen that the compressive properties of the programmed foam depend heavily on the orientation of loading. This may be due to microstructure changes of the foam in the process of programming. As compared to the nonprogrammed control specimen, the programmed specimens show increased yield strength in orientations 1 and 2, and reduced yield strength in orientation 3. This is because, under the 2-D stress condition, the molecules align more towards orientation 1 and orientation 2. Therefore, the yielding strength is higher in these two orientations than the non-programmed specimen, which has no preferred orientation. For orientations 3, the number of aligned molecules has been significantly reduced, leading to a yielding strength lower than the non-programmed foam specimen. Therefore, the programmed specimens become anisotropic, or more specifically, orthotropic.

Poisson's ratio of the programmed foam under compression along the three orientations

To evaluate the effects of the programming process on the lateral deformation of the foam, the lateral strains of the foam specimens in different orientations were measured. Based on the test results, the Poisson's ratio-longitudinal strain diagrams for the original and programmed foam are shown in Fig. 26.

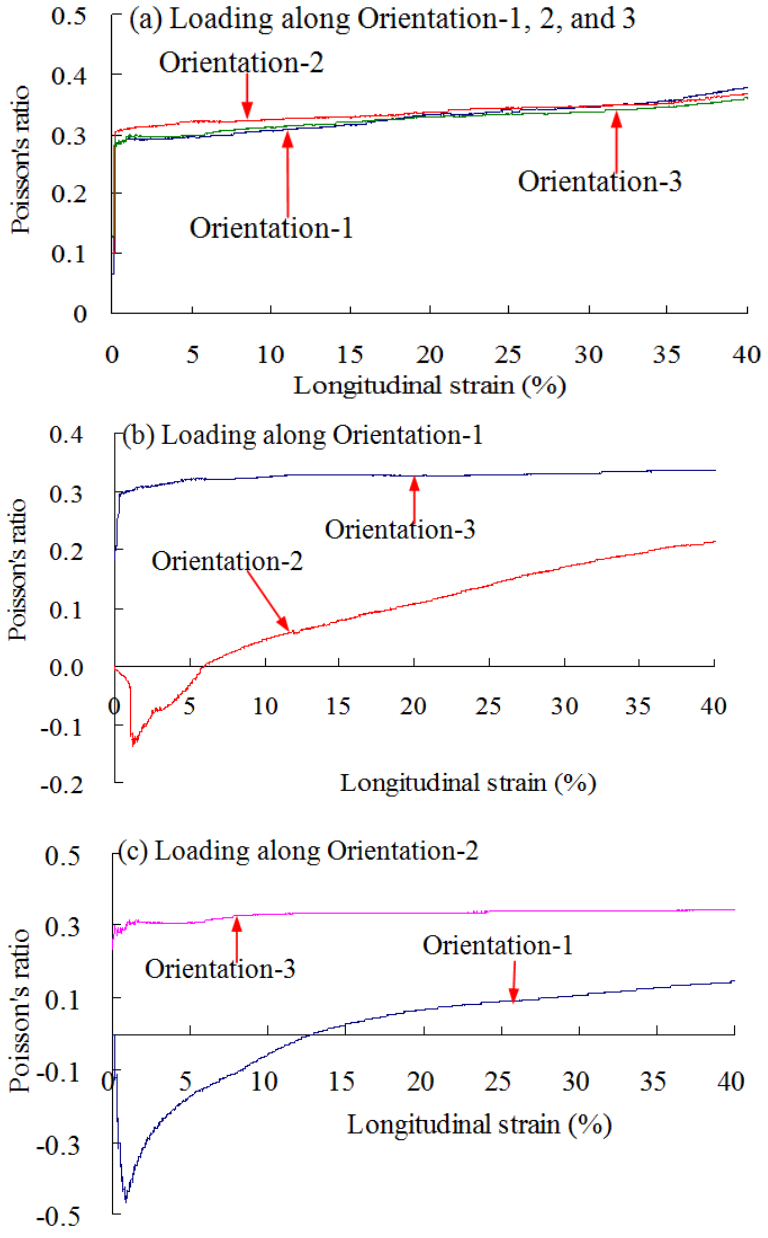

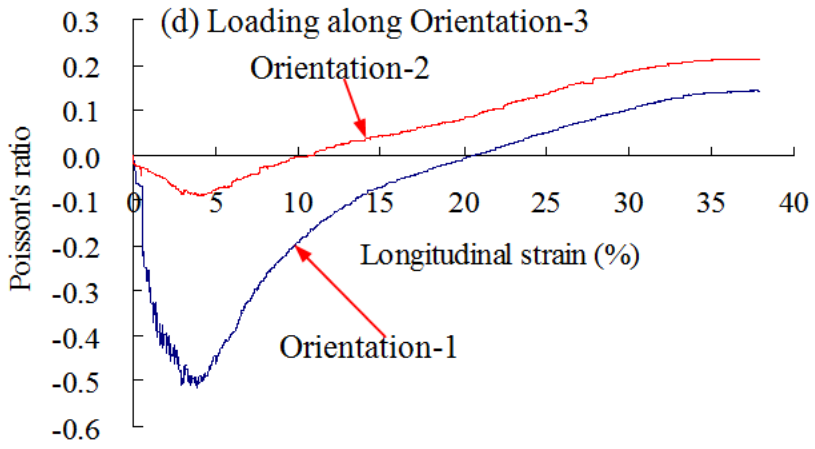

Figure **26**. Graphs of Poisson's ratio vs. longitudinal strain for (a) nonprogrammed and (b, c and d) programmed specimens during compression test

From Fig. 26 (a), for the nonprogrammed foam, it is seen that the Poisson's ratio is positive and almost constant as longitudinal strain increases. Also, the two transverse orientations have almost the same Poisson's ratio, suggesting that the nonprogrammed foam is basically an isotropic material. This is because the dispersion of the hollow glass microspheres in the foam is random or uniform and the mechanical behaviors in the three directions are much similar.

For the programmed foam, as shown in Fig. 26 (b), a small portion of negative Poisson's ratio occurs in orientation 2 when the longitudinal strain in orientation 1 is small. When the longitudinal strain is larger than 6%, the Poisson's ratio becomes positive. However, it is still smaller than that in orientation 3. The Poisson's ratio in orientation 3 (the direction free of stress during programming) is normal. This is because the foam is programmed by tension in orientation 2 and compression in orientation 1 while the foam is free of stress in orientation 3 during programming. This 2-D programming method facilitates to align SMP molecules in orientation-1 and orientation-2, and form some reentrant microstructures in the foam as shown in Fig. 27. Therefore, the programmed foam becomes anisotropy, and some tension strain was already stored in orientation 2. When compressively loaded in orientation 1, those reentrant structures bulge inwards. Hence the foam slightly shortened instead of expansion in the orientation 2. Once the reentrant structures are densificated, and the stored tension strain is consumed, the normal tendency (lateral expansion) occurs, leading to a positive Poisson's ratio.

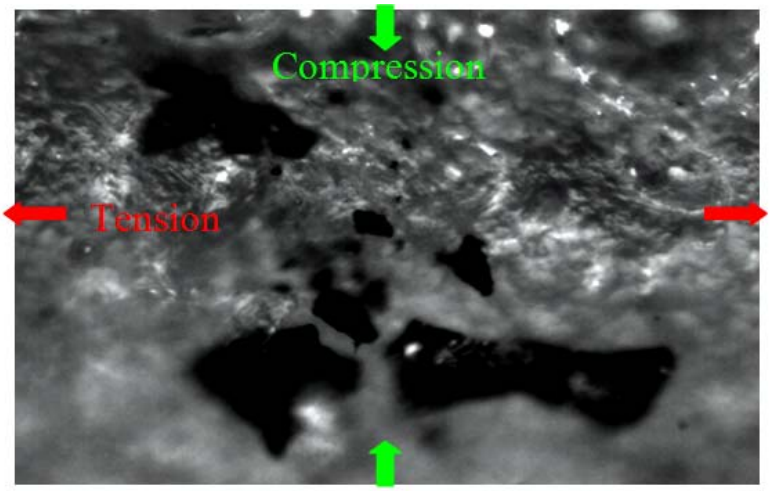

Figure **27**. SEM picture of reentrant structure in the programmed foam

Fig. 26 (c) mirrors Fig. 26 (b) because the orientation 1 and orientation 2 are exchanged. However, when loaded along orientation 3, Fig. 26 (d), negative Poisson's ratio occurs at both orientation 1 and orientation 2, and the negative Poisson's ratio in orientation 1 is larger than that in orientation 2. Also, when the longitudinal strain (orientation 3) is less than 10%, the foam is a material with negative Poisson's ratio, regardless of the directions (orientation 1 or orientation 2). The reason for this is that the orientation 3 is paralleled with the deformed microspheres, the loading in orientation 3 is applied along the erect direction of the deformed or ruptured or crushed microspheres. Therefore the re-entrant microstructures continue to collapse inwards in orientation 1 and orientation 2, leading to negative Poisson's ratio. However, this effect is not as significant in orientation 2 as in orientation 1. Consequently, the orientation 2 has smaller negative Poisson's ratio.

Uniaxial tension tests along two orientations

The tension test results are shown in Fig. 28. From Fig. 28, the 2-D programming method facilitates the anisotropy in the foam. The anisotropy causes the increase in the ultimate nominal strain and the decrease in modulus along orientation-1, compared with the nonprogrammed specimen. This is because there are some pre-strain stored in the foam in the compressive direction (orientation-1) during programming. The pre-strain can consume some tensile strain by absorbing the strain energy [45]. Additionally, under tension along orientation-1, the deformed microspheres along orientation-1 can gradually restore their

original shapes, and the bending or buckling microsphere walls are straightened under tension. This also needs to absorb a large amount of strain energy [46]. All these can delay the fracture of foam specimen.

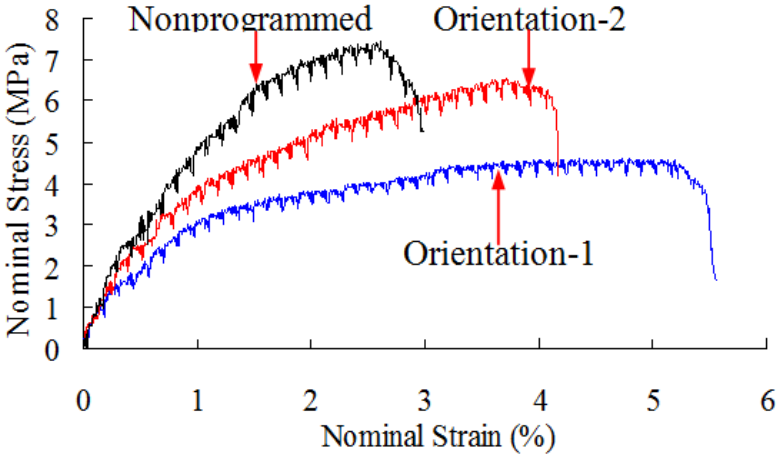

Figure **28**. Tensile stress–strain responses of nonprogrammed and programmed foam along various orientations

By contrast, when loaded along orientataion-2, an increase in nominal strength and modulus and a decrease in nominal ultimate strain are observed in Fig. 28, compared with that in orientation-1. The orientation of the SMP macromolecular chains along orientation-2 during programming is more responsible for the increase in strength. Under a tensile load along orientation-2, the oriented chains in the programmed foam are more difficult to further stretch at room temperature than that along orientation-1. Therefore, the foam exhibits a decrease in ultimate nominal strain in orientation-2.

Poisson's ratio of the programmed foam under tension along two orientations

Similarly, graphs of tensile Poisson's ratio vs. longitudinal strain for nonprogrammed and programmed foam are shown in Fig. 29. From Fig. 29 (a), the Poisson's ratio of the nonporgrammed foam is positive and almost the same for the two lateral directions, suggesting isotropic behavior of the non-programmed foam.

In Fig. 29 (b), the Poisson's ratio of the programmed foam in orientation-3 is normal when loaded in orientation-1. However, the foam shows a small portion of negative Poisson's ratio in orientation-2 when the longitudinal strain is within 1.0%. After that, the Poisson's ratio becomes positive and gradually increases as the longitudinal strain increases.

This is because the programming process produces some molecule alignments and re-entrant microstructures by forcing the hollow glass microspheres walls to buckle, rupture or crush along the orientation-1 in the foam. Under tension, these deformed microspheres walls restore their original shapes or re-entrant microstructures unfold along orientation-2, leading to the lateral strain expansion at lower stain (less than 10%). Furthermore, the oriented SMP molecule segments along orientation-2 in the programmed foam restrict the specimen to contract laterally during tension [47].

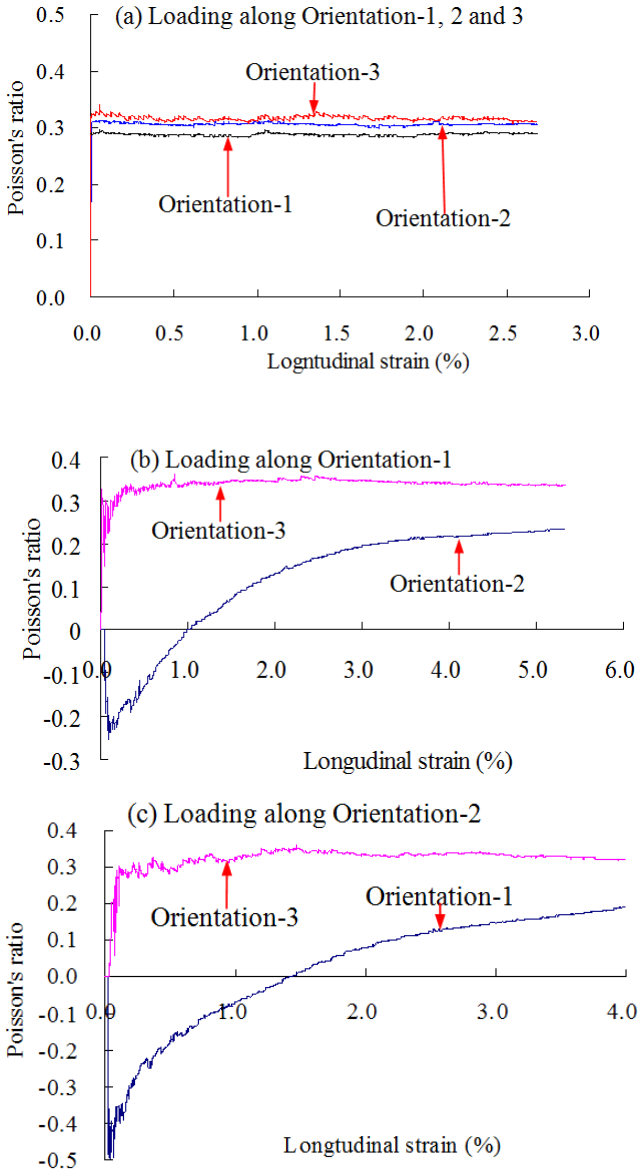

Figure **29**. Graphs of tensile Poisson's ratio vs. longitudinal strain for nonprogrammed (a) and programmed (b and c) foam

Similarly, when loaded along orientation-2, negative Poisson's ratio occurs in orientation 1 at lower strain level (less than 15%) as shown in Fig. 29(c). The reason for this may be the re-entrant microsphere walls unfold along orientation-1 under tension when the programming compressive load along orientation-1 is removed, giving rise to the negative Poisson's ratio. Again, the nonprogrammed orientation 3 behaves normal.

It is noted that negative Poisson's ratio may have some potential applications in structures, for instance as a sealant in expansion joint in bridge deck or concrete pavement. For compression sealed joint, it is required that the sealant has a negative Poisson's ratio in the vertical direction so that when the concrete wall narrows due to thermal expansion, the sealant will not be squeezed out of the channel or groove.

Summary

Based on the comprehensive tests and analysis, the following conclusions are obtained:

- The 2-D programming changes the molecular orientations of the SMP, leading the foam towards anisotropy from original isotropy. And when reheated above its T_g, the microstructure and morphology of the foam recover, together with the recovery of the macroscopic shape.
- The microstructure anisotropy leads to differences in mechanical properties when loaded in different directions. Compressive and tensile properties of the programmed foam specimen depend heavily on the orientations of loading during programming.
- In the two programmed directions, the programmed foam exhibits negative Poisson's ratio, regardless of the loading directions during the compression or tension testing of the programmed foam.
- The foam with negative Poisson's ratio may have a potential to be used as a sealant for expansion joint in bridge decks or concrete pavements.

Effects of Ultraviolet Radiation on Morphology and Thermo-mechanical Properties of Shape Memory Polymer Based Syntactic Foam

Morphology

The degradation of the foam usually starts at the outer surface and penetrates gradually into the bulk of the material [48]. Foam specimens exposed to UV underwent yellowing on the exposed surface as shown in Fig. 30.

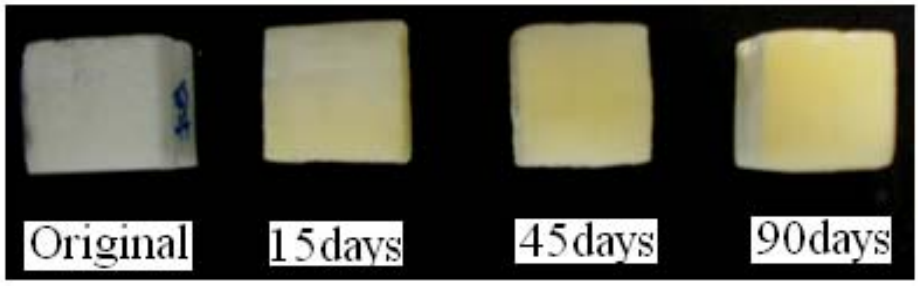

Figure **30**. Yellowing changes with duration of exposure to UV

From Fig. 30, the yellowing on the exposed surfaces of the foam increased approximately linearly with the duration of exposure. This is because the SMP used in this study is a polystyrene (PS) based polymer. As a result of phenyl groups, PS shows strong absorption of UV light [49]. PS obtained through radical polymerization in the presence of oxygen contains peroxide groups. By the breaking of the weak O-O bonds (40-50 kcal/mol) in SMP by UV irradiation or heating, the PS macromolecular chains are transformed in alkoxy chain-end radicals [49]. The decomposition of tertiary hydro-peroxides is considered the most probable cause for the observed PS chain scissions. It is attributed to conjugated polyenes, various oxygenated species, or products of ring-opening reactions [50]. Therefore, a basically linear increase in yellowness is observed with the time of exposure for general-purpose polystyrene exposed to UV. This is consistent with Davis and Sims' report [51]. Additionally, most organic polymers undergo chemical modification upon irradiation with UV light because they or their impurities or additives possess chromophoric groups, and the early stages of photo initiation must involve the absorption of photons by chromophoric groups or impurities [52].

Furthermore, a field emission scanning electron microscopy (SEM) (Model Quanta 3D FEG, FEI Company, USA) was used to characterize micro-length scale characteristics of the programmed and original foam surface (see Fig. 31). Fig. 31 (a) and (c) show that no

cracks are observed on the surface of the programmed and original foam specimen before exposure to UV. However, from Fig. 31 (b), some inclined cracks with respect to the compression direction are seen on the surface of the programmed foam after exposure to UV for 90 days. It is noted that the cracks are not observed on the original foam surface after exposure to the same UV (Fig. 31(d)). This is because the pre-stress is stored in the programmed foam specimen along the tension and compression direction during programming. The stored pre-stress accelerates polymer chain-scission near the surface [53]. Thus, cracks occur on the programmed foam surface.

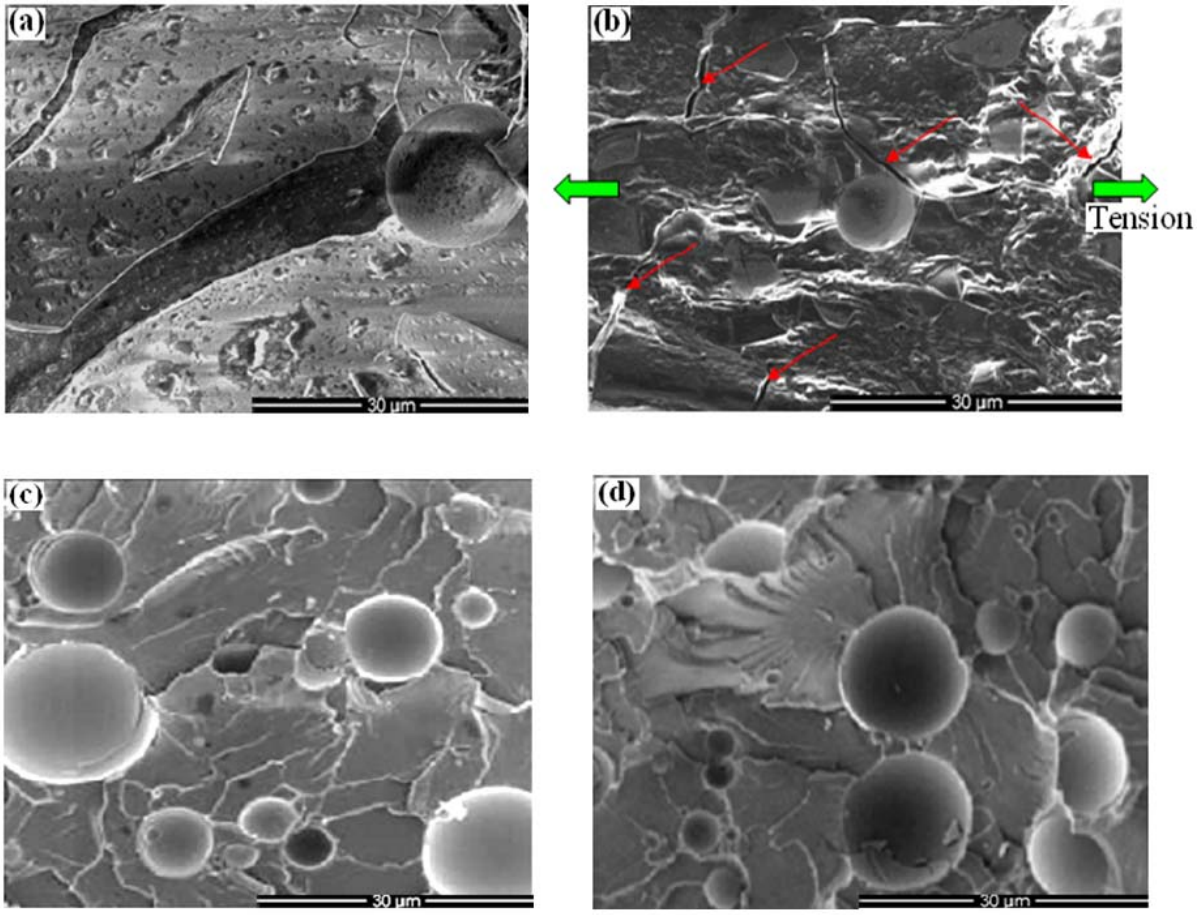

Figure **31**. Surface morphology of programmed (a, b) and original (c, d) foam ((a) and (c) before and (b) and (d) after exposure to UV for 90days)

Compression test results

It is important to evaluate the deterioration of mechanical properties in any assessment of the material resistance to their working environment. To study effects of UV on mechanical properties, mechanical tests were conducted. The compression test results are

shown in Fig. 32.

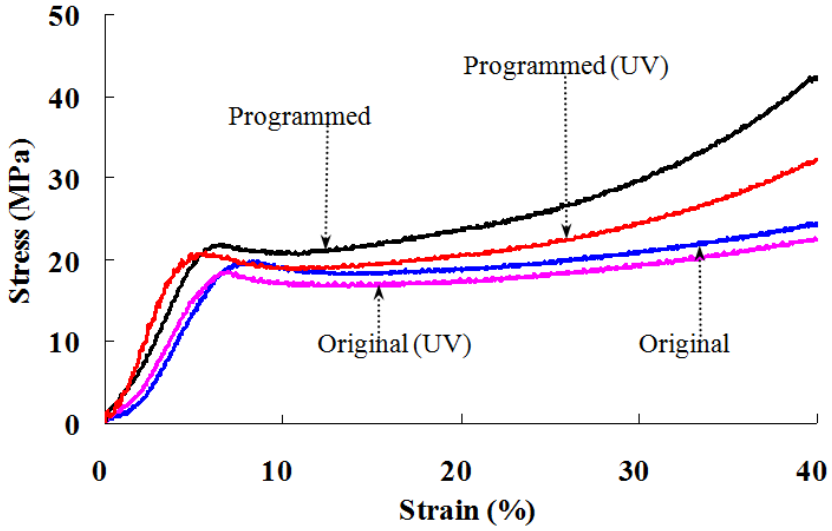

Figure **32**. Compression stress-strain response of original and programmed foam before and after exposed to UV

From Fig. 32, as compared to the original foam, the foam exposed to UV exhibits a decrease in compressive yield strength by 13.7% and 10.6%, and a reduction in yield strain by 7.2% and 4.6% for original and programmed foam, respectively, However, the exposure to UV causes an increase in modulus by 6.2% and 7.7% for original and programmed foam, respectively. This indicates that the exposure to UV seems to make the foam less ductile. All these are because polymer molecules in the foam break (chain-scission), cross-link, or suffer substitution reactions in an aggressive environment [54]. The decrease in compressive yield strength and strain is due mainly to photolysis and photo-oxidation, while the increase in stiffness is attributed to cross-linking of polymer network [55]. When the polymer in the foam absorbs UV rays, energy transfer occurs to produce an excited state of the oxygen molecule, singlet oxygen [49].

Furthermore, the absorbed UV light energy causes the dissociation of bonds in the molecules of the SMP constituents to produce free radicals as the primary photochemical products [48]. Subsequently, this event can lead to one or more of the following chemical changes: chain-scission, cross-linking, separation of small molecules, formation of double bonds in the main chain, depolymerization, and photohydrolysis (photolysis), etc [48].

Meanwhile, the polymer reaction rate is faster under mechanical stress state [56]. This is undesirable for the programmed foam because the pre-stress was stored in the foam during

programming. On the other hand, the polymer morphology has effects on the UV ageing. Degradation reactions of polymer occur almost exclusively in the amorphous phase since it takes up oxygen much more readily than the crystalline phase [57]. The diffusion rate of oxygen is lower in the programmed foam than that in the original foam, causing the former to be more resistant to degradation. Therefore, this leads to a slight decrease in compressive strength and stiffness for programmed foam specimen.

Tension test results

Changes in tensile properties of the foam with duration of outdoor exposure are also an important consideration, particularly ultimate extension. The tension test results are shown in Fig. 33.

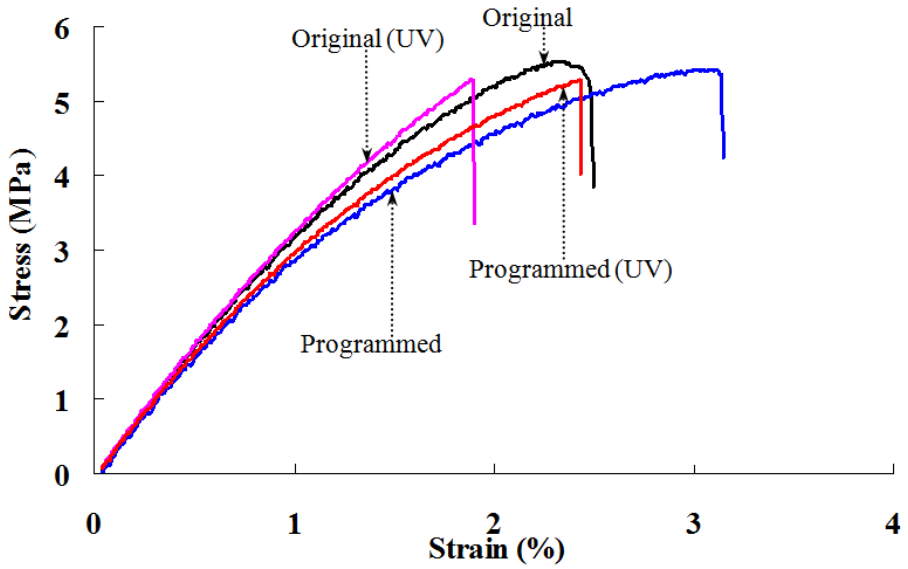

Figure **33**. Tensile stress-strain response of original and programmed foam exposed to UV

As shown in Fig. 33, the aged foam has a lower tensile strength and extension at break than that of control foam specimens. The exposure to UV causes a decrease in tensile strength by 4.6% and 7.3%, as well as a decrease in extension at break by 11.4% and 15.1% for original and programmed foam, respectively. But the exposure also leads to an increase in modulus by 7.6% and 9.2% for original and programmed foam, respectively. At the same time, the ultimate strain of programmed foam is larger than that of original foam. The reason for this is that some compressive pre-strain was stored in the programmed foam in the compressive direction during programming. The pre-strain can consume some tensile strain by absorbing the strain energy [58]. This can delay the tensile fracture of foam specimen at a

larger tensile strain.

For the foam exposed to UV, the ageing is produced by oxygen and UV radiation, referred to as photo-oxidation. Foams subjected to oxygen are degraded much faster in the presence of radiation than in its absence. The low diffusion coefficient of oxygen in foam results in a gradient of oxidation from the surface to the bulk [56]. Furthermore, the chemical reactions are accelerated by elevated temperatures caused by the warming effect from the UV lamp (since UV lamp was placed 33cm above the foam), leading to an increase in temperature on the specimen by about 20-23^{o}C.

As we know that the SMP used in this work is a polystyrene based polymer matrix. It has been generally accepted that UV photons interact with polystyrene, resulting in carbon-carbon scissions. This generates a variety of oxygen-containing functionalities at the specimen surface, such as C-O, C=O, COOH, etc [59]. This causes both cross-linking and chain-scission to occur concurrently as a result of ageing exposure to UV in the presence of air [60].

On the other hand, the programmed foam shows a larger decrease in strength and extension than the original foam. This is because the chemical reactions are accelerated by the presence of internal stress that was stored during programming [53]. Another reason for this is polymer molecule chains are stretched during programming which is prone to cause chain-scission on the foam surface [53]. Comparatively, it is noted that cracks in the programmed foam have a less effect on tensile strength than that on compressive strength, but have more influence on extensibility.

Combined effects of UV and water

The degradation of foam in the outdoor environment involves a very complex reaction. Oxidation can occur in conjunction with UV in air alone. But foam often undergoes combined effects of UV and water in its actual working conditions.

To evaluate synergetic effects of UV and water on the ageing of the foam, compression and tension tests were conducted on original and programmed foams immersed in rainwater and saturated saltwater and synchronously exposed to UV. The compression and tension test results are shown in Fig. 34 and Fig. 35, respectively.

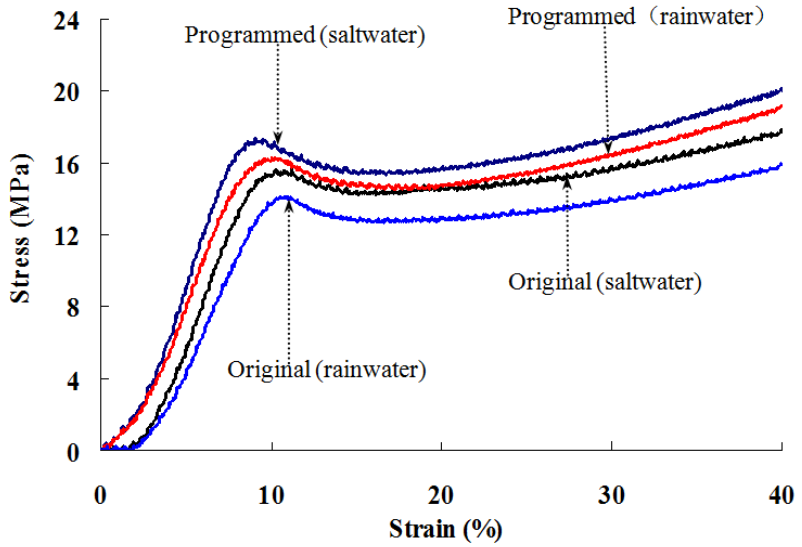

Figure **34**. Compressive stress-strain response of original and programmed foams immersed in water and synchronously exposed to UV

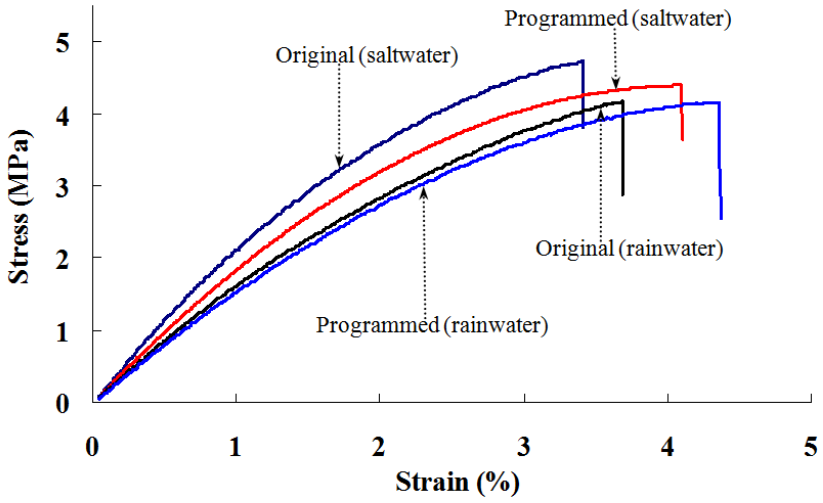

Figure **35**. Tensile stress-strain response of original and programmed foams immersed in water and synchronously exposed to UV

From Fig. 34 and Fig. 35, combined effects of UV and water cause a larger decrease in compressive and tensile strength than that of UV ageing alone regardless of original and programmed foams. Also, it is observed that the decrease for foams immersed in saltwater is less than that in rainwater. This is attributed to absorption of UV energy which raises some bonds to a higher energy level. The elevated energy in bonds exceeds their stability, and thus initiating their breakdown, involving in photo oxidation and hydrolysis as well. This causes extensive chain scission in SMP matrix [61]. Additionally, the chemical composition of

saltwater and rainwater includes major inorganic ions (Cl^-, SO_4^{2-}, F^-, NH_4^+, etc.) and organic species (CH_3COO^-, $HCOO^-$, $CH_2(COO)_2^{2-}$, $C_2O_4^{2-}$, etc.) [62]. The water impingement causes mechanical erosion, since some polymers undergo hydrolysis reactions and are swollen by water. This also causes chain scissions, leading to a decrease in strength [61]. Another reason for this is some aggressive ions in water. Those ions not only hydrate the polymeric matrix but also possibly hydrated the interfaces and the glass material [63]. And such degradation phenomena occur in immersed syntactic foams at any ageing temperature [64]. Subsequently, the hydrolytic attack can also cause chain scission in polymer film.

The hydrolytic reaction in foam can occur at room temperature in the absence of UV light. However, when the immersed foam specimen is exposed to UV, the most common effects result from the combined action of hydrolysis and photo-degradation. This is because it combines the photo-physical and photo-chemical effects of UV radiation photons, oxidative effects of the oxygen, and hydrolytic effects of water [56]. Therefore, the foam in water might undergo a faster degradation than that in air. This is consistent with the previous observation [65].

Moreover, polymer based foams are more susceptible to hydrolytic at elevated temperature owing to the UV lamp. Although water can cool the temperature of foam specimens, heat effects from the light source cause an temperature increase on the foam surface by an average of 12.7℃. This accelerates the photo oxidation and hydrolysis in SMP film around microspheres. Hence, it is seen that synergetic effects of UV and water dramatically accelerate the deterioration process of foam specimens. All these lead inevitably to deterioration in strength.

However, Fig. 34 and Fig. 35 also show that the combined effects of UV and water cause an increase in extensibility compared with that of UV ageing alone. And the increase for foams immersed in saltwater is less than that in rainwater. This is mainly due to the hydrolysis of foams in water. When the polymer film around microspheres is immersed in saltwater and rainwater, ion species in the water have a plasticizing effect on the polymer first, followed by chemical interaction or physical swelling effects [66]. This indicates that the water makes polymer softer and more flexible at ambient temperature, known as plasticizers. As a result, the extensibility of immersed foams increases compared with that of UV ageing alone.

Recovery stress test

Recovery stress-strain-temperature responses of programmed foam exposed to UV alone and simultaneously immersed in saltwater and rainwater under fully confined condition are shown in Fig. 36.

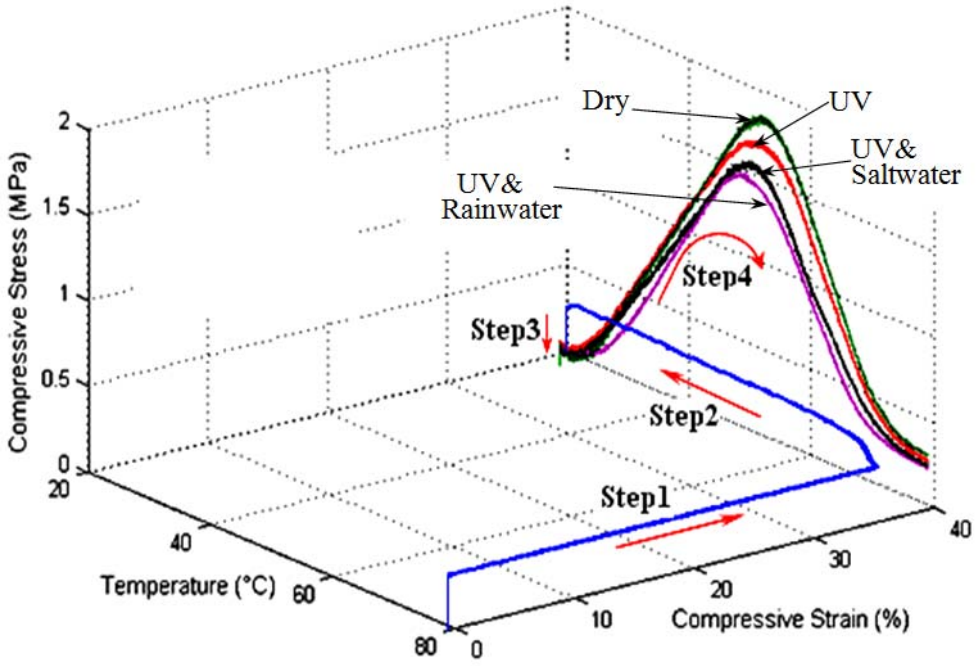

Figure **36**. Programming (Step1: loading→Step2: cooling→Step3: unloading) for the foam and recovery stress-temperature response (Step4) under fully confined condition for the programmed foams exposed to UV alone and simultaneously immersed in saltwater and rainwater

As shown in Fig. 36, the stress comes from two parts during recovery: thermal expansion stress and entropically stored stress. When the temperature is below the T_g, the modulus is high, and the recovery stress increases gradually as the temperature rises. When the temperature reaches the start of the glass transition region, the stress shows a peak. While the coefficient of thermal expansion still increase within the glass transition zone, and yet the modulus decreases sharply, leading to a continuous decrease in stress [22]. Once the temperature approaches the programming temperature (79^{o}C), the recovery stress shows some relaxation initially due to large-scale segmental motion.

Under various ageing conditions, the programmed foams show different decrease in peak recovery stress. From Fig. 36, the programmed foams exposed to UV alone show a decrease in peak recovery stress by 8.6%. But the immersed programmed foams exposed to UV show a larger reduction in peak recovery stress by 15.7 and 19.5% for saltwater and

rainwater, respectively. Also, the temperature of UV aged programmed foam corresponding to the peak stress is basically unchanged, while the temperature for specimens immersed in saltwater and rainwater is lowered by 3.1□ and 4.8□, respectively, as compared to the dry programmed foam. This indicates that the T_g becomes lower after immersion in saltwater and rainwater at room temperature for 90 days [67]. As shown in Fig. 36, it is observed that the final average recovery stress of the dry programmed foam is 295.5kPa, which is slightly less than the programming stress of 300.7kPa. And the final average recovery stresses of immersed programmed foams are lower than that of the dry programmed foam.

All these are because the absorbed water in the SMP film weakens the hydrogen bonding between N–H and C=O groups, which lowers the T_g of the foam [67]. Therefore, the temperature of the immersed foams corresponding to the peak stress is lowered. In addition, low molecular weight molecules in saltwater and rainwater diffuse into the SMP film which works as a plasticizer, leading to the irreversible ageing [68]. All these make the foam more ductile, lowering the immersed foam modulus. Therefore, the peak recovery stress of hydrolytic foams is lower than that of the dry programmed foam. Meanwhile, UV exposure of foam in water results in a faster decrease in peak recovery stress than that for exposure in air. The exposure results in UV absorbance and chain scission of the macromolecules on foams surface, causing loss in recovery stress.

Summary

Based on the above experiments and analysis, the following conclusions are obtained:

- UV exposure results in discoloration on the exposed surface of the foam in air. And the yellowing increases with duration of exposure. UV exposure results in cracks on the foam surface along the compression direction.
- UV radiation causes a decrease in mechanical strength and ductility, and an increase in modulus. Cracks in the foam have a less effect on tensile strength than that on compressive strength, but have a greater influence on ductility.
- Combined effects of UV and water lead to a larger decrease in strength and ductility than that of UV alone. And the decrease for foams immersed in saltwater is less than that in rainwater. Water immersion also causes a reduction in T_g of the foam.
- The peak recovery stress is much higher than the programming stress, facilitating

self-healing of the smart foam. The combined environmental attacks induce a larger decrease in peak and final recovery stress than that of the dry programmed foam.

- Although the accelerated ageing of UV or/and water leads to a decrease in strength, ductility and shape recovery functionality, the decrease listed above do not cause serious degradation of the engineering properties in the foam. It is concluded that the foam possesses the shape recovery functionality after 2-D programming and environmental attacks.

Cyclic Stress–Strain Behavior of Shape Memory Polymer Based Syntactic Foam Programmed by 2-D Stress Condition

2-D programming results

The horizontal and vertical strain evolution for a typical foam specimen during the 2-D programming is shown in Fig. 37. It is observed that the strain evolution during the 2-D programming includes three steps: step 1 (loading), step 2 (cooling while holding the load constant), and step 3 (unloading). The strain evolutions in compression or vertical direction and tension or horizontal direction are similar due to the symmetry of the truss fixture and the specimen. The final strains in vertical and horizontal direction are 39.63% and 39.48%, respectively, and the corresponding shape fixity ratios are 99.1% and 98.7% for the preload levels in the two directions.

The high shape fixity ratio is understandable because the preload causes the foam specimen to become denser and stiffer, leading to a smaller spring-back and thus higher shape fixity at the end of step 3. To visualize the programming results, Fig. 38 shows the nonprogrammed and programmed cruciform foam specimens.

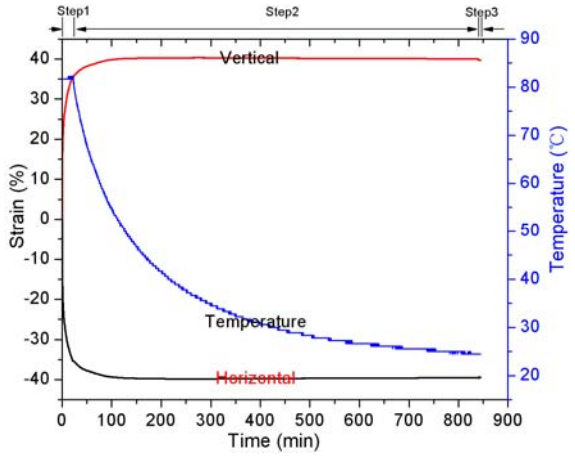

Figure **37**. Horizontal and vertical strain evolution during the 2-D programming (step 1: loading → step 2: cooling → step 3: unloading)

Cyclic stress-strain behavior of the foam

To clearly compare the stress–strain responses under cyclic loading at room temperature, representative hysteresis loops for typical nonprogrammed and programmed foam specimens are shown in Fig. 39. And Fig. 40 presents the effects of cyclic loading on characteristic parameters such as average peak stress, dynamic modulus, and stiffness. Standard deviation is also give in Fig. 40. To facilitate the interpretation of the results, numbers 1, 2, 3, etc. is marked on the stress-strain curves as described in Fig. 39, denoting the number of cycles experienced.

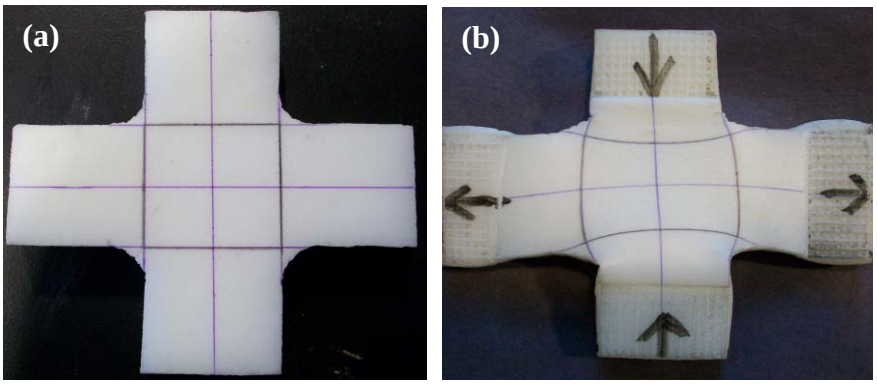

Figure **38**. (a) Nonprogrammed and (b) programmed cruciform foam specimen

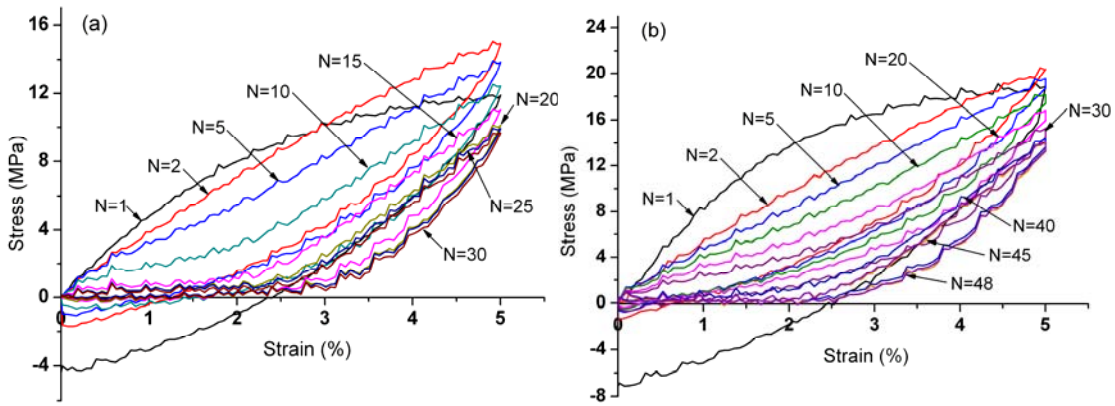

Figure **39**. Stress–strain response under cyclic loading for (a) nonprogrammed and (b) programmed foam at room temperature

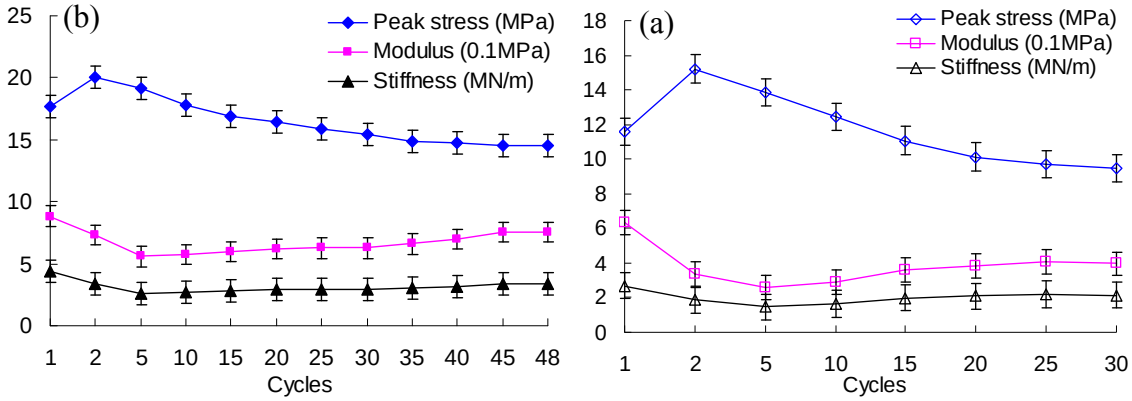

Figure **40**. Effects of cyclic loading on characteristic parameters of (a) nonprogrammed and (b) programmed foams at room temperature

From Fig. 39, the general trend of the hysteresis loops, from the second cycle to the last cycle, exhibits a gradual drop in peak stress (cyclic softening) for both the non-programmed and programmed foam, respectively. When the foam specimens are compressed to 5% strain and then reversed to zero strain by tension, a lower loading is required for the same strain in subsequent cycles. Further cyclic loading leads to a continued softening, but at a progressively slower rate, regardless of compression or tension stage (Fig. 39). During the subsequent cycles, more microspheres are fractured and these newly broken microspheres are crushed and compacted, which causes the foam to more densify [69]. The densification results in a smaller reduction in cyclic softening and residual strain [70]. It is noted that the degree of cyclic softening is smaller for the programmed foam than that for the nonprogrammed one. Comparing the peak compressive stress of the last cycle to that of the

second cycle, the nonprogrammed foam has a reduction by 37.7% (or 37.7% / 29 cycles = 1.30% per cycle), while the programmed foam has a reduction by 27.0% (or 27.0% / 47 cycles = 0.57% per cycle). The smaller decrease in cyclic softening for the programmed foam is related to the initial densification due to the 2-D programming (see Fig. 41), since the shape of the hysteresis loop largely depends on the state of material microstructure [71]. The cyclic loading may also cause molecular rearrangements and change its viscoplastic properties [70]. In addition, part of the dissipated energy may cause some heating and additional viscoplastic changes. This behavior is typical of strain induced softening of polymeric materials [72].

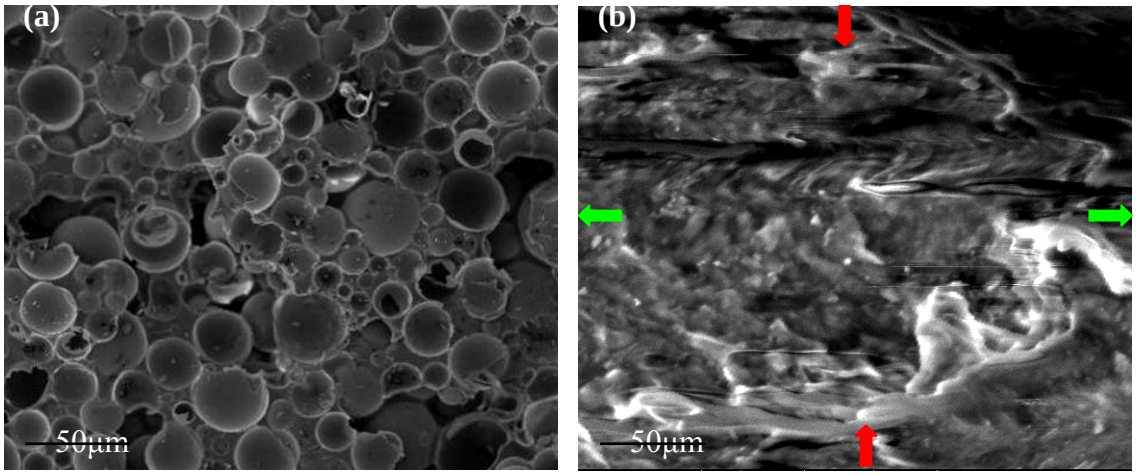

Figure **41**. SEM pictures of (a) nonprogrammed and (b) programmed foam

From Fig. 39, the hysteresis loops tends to shrink and approach asymptotically to a steady state after 26 and 42 cycles for the nonprogrammed and programmed foam, respectively. After the steady stage, further cyclic loading may cause structural damage in the foam, such as SMP matrix fracture, leading to fatigue failure (30 cycles for the nonprogrammed foam and 48 cycles for the programmed foam).

As shown in Fig. 39, the first cycle is highly nonlinear and much different from the subsequent hysteresis loops. The compressive stress is initially higher in the compression stage, but the peak stress corresponding to the 5% strain is lower (Fig. 40) than that of the second loading cycle by 31.1% and 13.3% for the nonprogrammed and programmed foam, respectively. For the nonprogrammed foam, this is because glass hollow microspheres are

very close to each other due to the high volume fraction (40%) of microspheres in the foam. At the beginning in the first cycle, the intact microspheres can provide a higher capacity to undertake the loading, showing a higher stress. As the compression strain increases, a large number of microspheres are crushed and fragmented into pieces, leading to the decrease in peak stress [22]. This is also consistent with the result in [73], although the materials tested are different. However, for the programmed foam, it has been considerably densified during the 2-D programming. Therefore, the difference between the first cycle and the second cycle is not as large as that for the nonprogrammed foam.

Meanwhile, the strain at zero stress point during tension stage shows a decrease for cyclically deformed foams as the cyclic number increases. The reason is that in the first cycle, the compression stage leads to considerable plastic strain due to the crushing and solidification of the microspheres. Therefore, some tensile stress is needed in order to bringing the specimen back to its zero strain status. As the cycle increases, the foam tends to become a viscoelastic or elastic material (no more microspheres are available for crushing and solidification). Therefore, the compression-tension cycles become similar to compression loading-unloading process. No tensile stress develops before the strain becomes zero.

Additionally, Fig. 40 also presents the response trend of dynamic modulus and stiffness versus loading cycles. The trend of dynamic modulus exhibits a sharp drop in the first few cycles for both the nonprogrammed foam and programmed foam, respectively, and then followed by a slight increase process. However, the programmed foam shows a slower increase in dynamic modulus as the cycle number increases. This is because the programmed foam itself has a higher modulus than that of the nonprogrammed foam. Similarly, the stiffness also shows a drop in the first few cycles for the nonprogrammed foam and programmed foam, respectively, but followed by an almost plateau. This indicates that the stiffness becomes steady after the first few cyclic loadings. Once the foam is densified after the first few cycles, the foam preserves its integrity and the loss in stiffness shows little sensitivity to the increasing number of loading cycles.

Cyclic stress-strain response of the pure SMP

In order to identify the underlying principles controlling the cyclic behavior of the SMP based syntactic foam, understanding of the cyclic behavior of the pure SMP is essential.

The cyclic stress-strain responses of typical nonprogrammed and programmed pure SMP specimens are shown in Fig. 42. Similar to the foam, the change of the characteristic parameters for the pure SMP under cyclic loading are presented in Fig. 43.

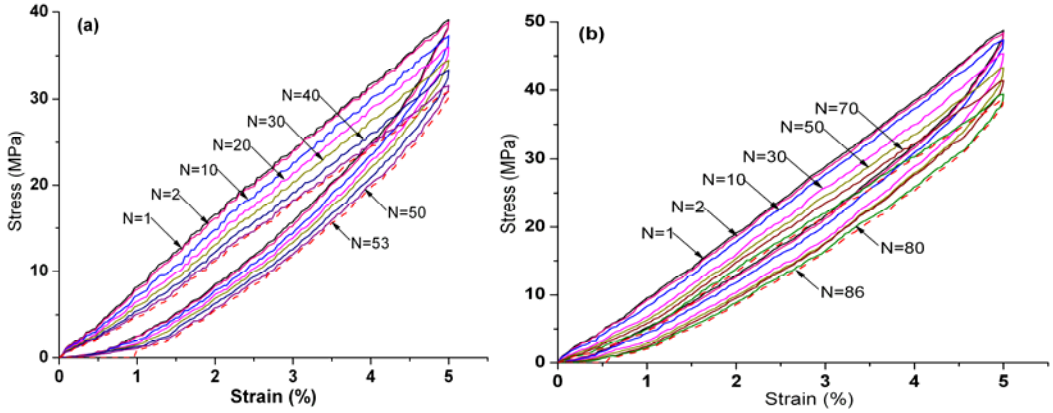

Figure **42**. Stress–strain response under cyclic loading for (a) nonprogrammed and (b) programmed pure SMP at room temperature

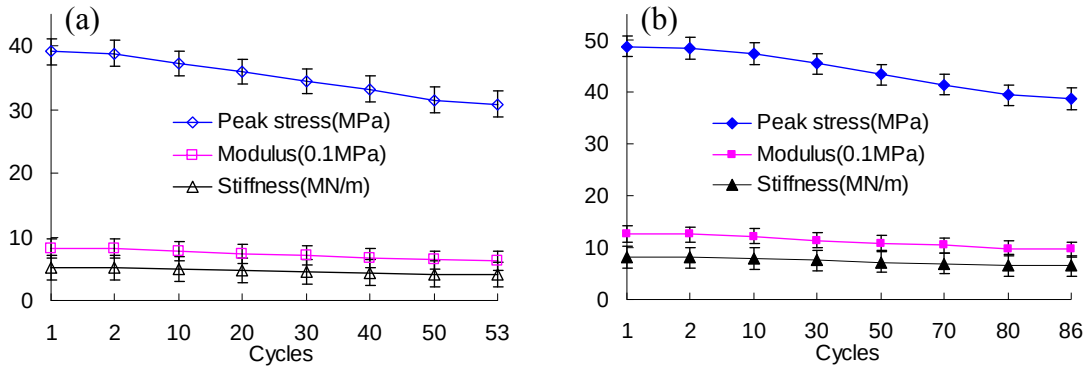

Figure **43**. Effects of cyclic loading on characteristic parameters of (a) nonprogrammed and (b) programmed pure SMP at room temperature

As compared to the cyclic behavior of the foam (Fig. 39), it is clear that the effect of programming on the cyclic behavior of the pure SMP is similar to that on the foam: (1) increase in the number of cycles to fatigue failure (from 53 cycles for the nonprogrammed SMP to 86 cycles for the programmed SMP) and (2) increase in compressive yield strength. The reason is that programming changed the molecular orientations of the SMP and reduced the entropy of the system [39]. The SMP molecules or segments aligned along the loading direction during programming, changing the SMP from isotropy to anisotropy [37]. Therefore, when cyclically loaded in orientation 1 (Fig. 44), the aligned molecules or segments led to higher compressive yield strength as compared to the nonprogrammed

material. Also because of the molecular alignment in the loading direction, the programmed SMP shows higher fatigue life during cyclic loading, similar to uniaxial fiber reinforced composites.

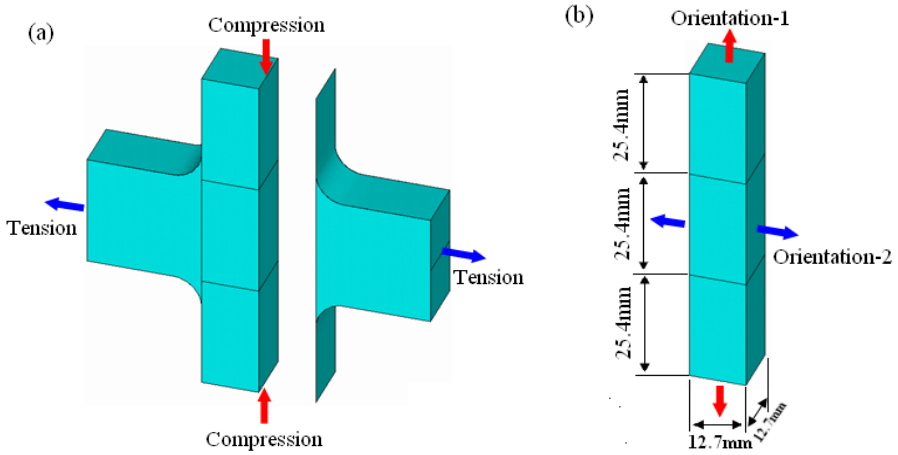

Fig. **44**. A schematic diagram of (a) the programmed specimen and (b) the preparation for cyclic loading test specimen with cyclic loading along orientation-1(compression direction during programming)

Comparing Fig. 42 and Fig. 39, it is clear that both the pure SMP and the foam show cyclic softening and shrinking of hysteresis loops. Cyclic softening is mainly attributed to accumulation of microscopic damage such as molecule scission as well as stiffness reduction due to slight temperature rising by viscoelastic energy dissipation [74]. As for the shrinking of the hysteresis loops, it is believed that it is due to the gradual loss of the ability for the SMP molecules to dissipate energy in terms of viscoelastic deformation [75]. This is because the gradually damaged polymer chains cannot effectively dissipate energy through viscoelastic deformation. Because the matrix (continuous phase) of the foam is SMP, its cyclic behavior is similar to the pure SMP.

Next, our focus is on the difference between the foam and the pure SMP. Comparing Fig. 39 with Fig. 42, the first difference is the stress-strain behavior in the first cycle. Obviously, the foam behaves highly nonlinear and yet the pure SMP behaves almost linear during the compression stage, regardless of the programmed or nonprogrammed specimens. This is due to the significant fracture, crushing, and solidification of the microspheres in the foam in the first loading cycle. Also because of this, the foam shows hardening in the second cycle before subsequent softening, while the pure SMP shows monotonic softening with cycles. Second, the foam shows cyclic softening in the tension stage, while tensile stress

disappears in the pure SMP. The compression-tension process is similar to a compression loading-unloading process for the pure SMP. Clearly, this is because the pure SMP is basically a linear elastic material under 5% maximum compressive strain. For the foam, the SMP matrix only occupies 60% by volume; hence, the 5% maximum compressive strain consists of both elastic strain and plastic strain due to microsphere damage. While the elastic strain can be fully recovered by unloading, plastic deformation cannot be recovered and additional tensile stress is needed to bring the total strain to zero.

Based on the above analyses, it is clear that the similar behavior between the pure SMP and the foam is due to the SMP matrix. In other words, the SMP controls the cyclic behavior of the foam. The foam and the pure SMP also have some differences, particularly for the first few cycles. The difference is due to the incorporation of the 40% by volume of microspheres in the foam and their gradual crushing and densification during the first few loading cycles.

Energy dissipation under cyclic loading

A useful quantity for the estimation of the fatigue behavior of specimens is the accumulated dissipated energy, since this characteristic is nearly independent of the test conditions and yet sensitive enough to structural influences [76]. The stress–strain behavior observed upon deformation typically includes a significant strain energy contribution and the area enclosed by the hysteresis loop corresponds to the dissipated energy for each cycle. For any given cycle (n), the dissipated energy is given by:

$$\Delta E(n) = \oint \sigma d\varepsilon = \int_0^{\varepsilon_{\max}} (\sigma_{ld}(n,\varepsilon) - \sigma_{ul}(n,\varepsilon)) d\varepsilon$$

where $\varepsilon_{\max}$ is the maximum strain; σ_{ld} and σ_{ul} are the stress during loading and unloading, respectively. With the above equation, the dissipated energy is obtained for each specific cycle as shown in Fig. 45 (a).

The accumulation of dissipated energy over a given number of cycles (n) can be described by:

$$W_{cum} = \sum_{i=1}^{n} \Delta E(n)$$

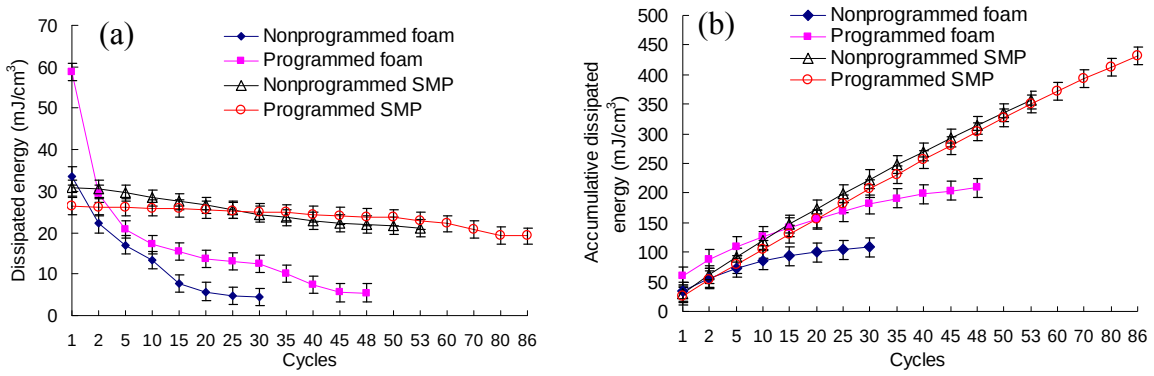

Figure **45**. (a) Dissipated energy in each cycle and (b) accumulative dissipated energy of the foam and pure SMP versus the number of loading cycles

Fig. 45 (b) shows the accumulative dissipated energy at the specific number of cycles. As shown in Fig. 45 (a), the dissipated energy in each cycle decreases with increasing the number of cycles, in particular for the first few cycles. This decrease trend is a direct representation of the shrinking hysteresis loops of the foams (see Fig. 39) and the pure SMP (Fig. 42). Part of the dissipated energy heats up the material because of the internal friction during cyclic loading test. Another part of this dissipated energy leads to disintegration of the composite material, such as resin failures, debonding, microsphere crushing, etc. By the destruction of the microstructure, the viscoelastic behavior of the composite changes [77]. It is believed that the viscoelasticity of the foams plays an important role in absorbing and dissipating energy, especially during dynamic loading [74]. All these may be reasons to cause the foams and the pure SMP to soften as aforementioned.

The initial large and rapid decrease in energy dissipation in the foam is explained by microsphere crushing in the first few cycles, allowing the foams to more densify. During the subsequent cycles, dissipated energy shows a slower decrease behavior. The reason for this is that, as the cycles increase, the available microspheres for crushing reduce. Therefore, the energy dissipated through microsphere crushing becomes smaller and smaller. Once this microsphere crushing mechanism is fully consumed, the energy dissipation becomes stabilized and the behavior is mainly controlled by the viscoelastic behavior of the SMP matrix [69].

Compared to the foam, the pure SMP shows larger energy dissipation in each cycle (except for the first cycle, Fig. 45 (a)) and the decrease with loading cycles is slower. The reason is that the energy dissipation comes from two parts: (1) viscoelastic energy dissipation

of the SMP matrix and (2) damage of the microspheres. For the damage mechanism, it is irreversible [72], while the viscoelastic energy dissipation mechanism is partially reversible. Therefore, viscoelastic energy consumption is more effective in energy dissipation than damage. For the pure SMP, the energy dissipation is through viscoelestic consumption only; for the foam, it consists of both mechanisms. However, the foam only consists of 60% by volume of SMP. Therefore, its energy dissipation is not as effective as the pure SMP, which consists of 100% SMP. The exception in the first cycle is due to the large amount of energy consumed by microsphere damage. Because the microsphere damage is irreversible, the pure SMP consistently dissipates more energy than the foam starting from the second cycle.

From both Fig. 45 (a) and (b), it is seen that the programming enhances the energy dissipation capability of the foam. This result suggests that the programmed foams possess better fatigue resistance at the same strain level. However, the effect of programming on the pure SMP is not as significant as that on the foam. The reason is again due to the inclusion of microspheres in the foam and their partial crushing and densification during programming. In other words, the difference between the foam and the pure SMP is primarily due to the microspheres and their damages.

Stress-strain response under one thermo-mechanical cyclic loading

Stress-strain responses of the nonprogrammed foam and programmed foam under one thermo-mechanical cyclic loading are shown in Fig. 46. From Fig. 46 (a), the thermo-mechanical cycle of the programmed foam, for instance, includes four stages: stage1 (compression stress increase while heating), stage 2 (compression stress decrease while heating), stage 3 (compression stress decrease while cooling), and stage 4 (tension stress increase while cooling).

In stage 1, it is clear that there is a quicker increase in compression stress for the programmed foam than that for the nonprogrammed foam. This is understandable because the 2-D programming process may cause some damage to the foam (such as crushing of microspheres), which causes the programmed foam to be more compacted (see Fig. 41); it may also form some special reentrant microstructures in the foam, which increase the compressive stiffness and thus compressive stress of the programmed foam [75]. The compressive stress of the foam specimen comes from two aspects when the temperature is

below T_g: external compressive loading and thermal expansion stress. However, the applied compressive stress is much larger than the thermal stress. Therefore, the behavior of the foam is mainly controlled by the applied compressive stress when the temperature is below T_g. Hence, when the compressive strain is about 5% for the programmed foam and about 10% for the nonprogrammed foam, compressive yielding occurs and the compressive stress crests. This is the end of stage 1. The programmed foam yields at smaller compressive strain due to the compressive prestrain stored during programming.

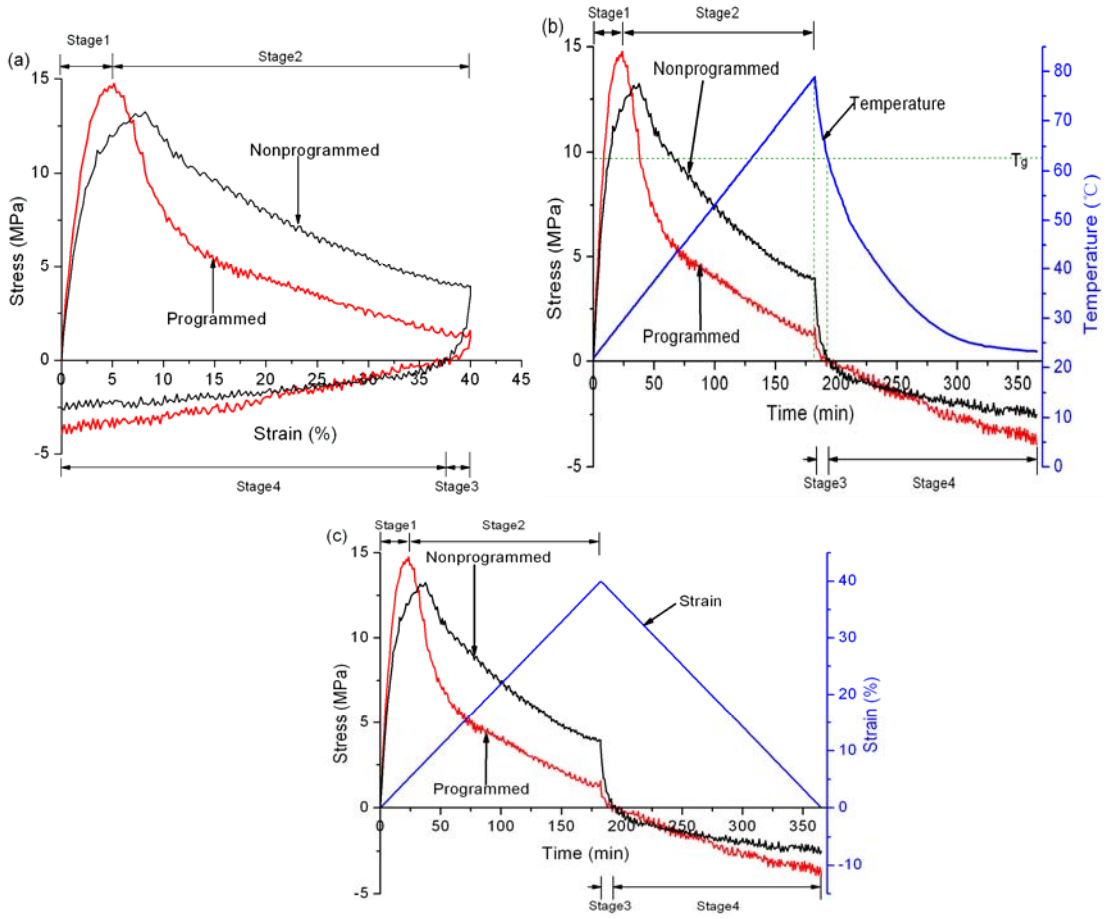

Figure **46**. Responses of (a) stress vs. strain, (b) stress and temperature vs. time, and (c) stress and strain vs. time for one-cyclic loading tests of nonprogrammed and programmed foams under changing temperature

In stage 2, as the temperature further rises, the foam modulus continues to decrease, leading to a continuous strain softening. It is seen that the nonprogrammed foam experiences a slower decrease in stress compared with that of the programmed one. The reason for this is that the compressive loading is mainly undertaken by the yielded SMP matrix in the

programmed foam due to microsphere crushing during programming. Deformational resistance of the SMP is deemed to be lower than that of microspheres at high temperature. However, intact microspheres in the nonprogrammed foam can form some skeleton structure and carry the compressive loading (see Fig. 41), although the SMP becomes very soft at high temperature. This retards the decrease in compression stress for the nonprogrammed foam.

In stage 3, once the temperature reached the programming temperature (79^oC), the heating was first stopped, and then the chamber started to naturally cool back to room temperature. Meanwhile, the compression was reversed to tension at the same loading (strain) rate (see Fig. 46 (c)). It is interesting to note that once the original compression is reversed to tension at 40% strain, the compression stress quickly reaches zero. This is because the foam modulus is much smaller at the beginning of this tension stage, and the compression stress developed during the compression stage is easy to be reversed to zero by tension. Furthermore, at 79^oC, the recovery stress in the programmed foam shows some relaxation due to large-scale segmental motion, hence, the programmed foam shows a quicker drop in stress.

In stage 4, when the temperature is slightly below the T_g (Fig. 46 (b)), and the foam modulus slowly becomes higher, the tensile stress starts to develop gradually. Here, there is little difference between the stress curves for the nonprogrammed and programmed foam, indicating that the foam properties are similar at this temperature range. However, when the temperature is much below the T_g, there is a faster increase in tensile stress for the programmed foam, because the programmed foam modulus is higher than the nonprogrammed foam. Additionally, the thermal contraction during cooling also results in the increase in tensile stress until the temperature reaches room temperature.

Stress-strain response under one-cyclic loading at room temperature

One-cyclic loading test results for nonprogrammed and programmed foams under 40% strain at room temperature are shown in Fig. 47.

From Fig. 47 (a), the shape of the hysteresis loops of the programmed foam is similar to that of nonprogrammed one, but with higher compressive yield strength (35.6% higher than that of the nonprogrammed foam). In the compression stage, it can be characterized by three distinct regions. The first region (less than around 5% strain) is characterized by an

almost linear-elastic behavior of the syntactic foam. The region ends when the material starts to yield and reaches its compressive yield strength. Then a slight drop in stress occurs, implying the strain softening behavior of the material. The second region is an almost horizontal plateau. The horizontal plateau is attributed to the implosion of the hollow microspheres under the increasing compression strain [78]. This region is referred to as densification stage [22]. The third region exhibits a slight increase in stress again at the end of the plateau region. The increase is caused by a large number of microspheres being crushed and compacted.

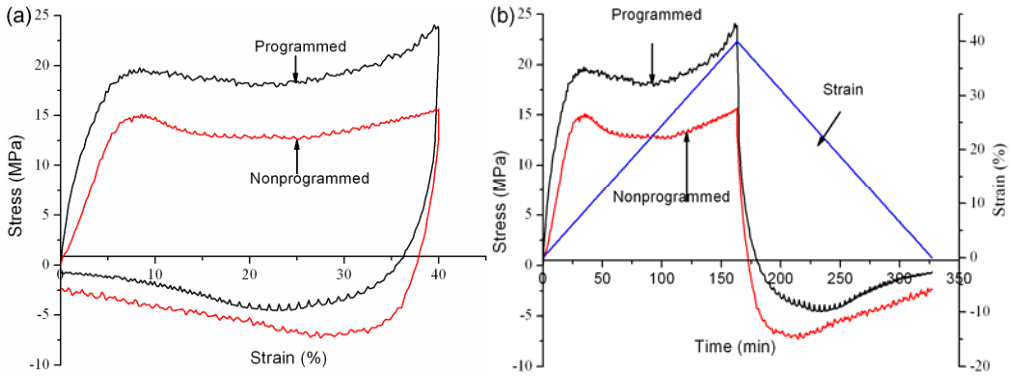

Figure **47**. Responses of (a) stress-strain and (b) stress-time and strain-time under one-cyclic loading tests for nonprogrammed and programmed foam at room temperature

In the tension stage, first there is a sharp stress drop when the loading is reversed from compression to tension at 40% strain, leading to a higher tangential slope just after strain reversal (Fig. 47 (b)). Once the compressive stress reaches zero, the tensile stress develops, first increases and then decreases gradually with increase in strain.

The trend of tensile stress-strain curves shows strong non-linearity due to the viscoplastic behavior of the foam and the lower loading rate used [79]. For the nonprogrammed foam, the residual tensile stress (at zero strain) is larger than that of the programmed foam in this stage. The reason for this is that some compressive pre-strain is stored in the programmed foam in the compressive direction (orientation-1 in Fig. 44) during the 2-D programming. The pre-compression can consume more tensile strain by absorbing the strain energy [58]. This is consistent with the tension test result in [38].

From the point of view of dissipated energy, the programmed and nonprogrammed foam absorb 804.67mJ/cm^3 and 683.05 mJ/cm^3 of energy during this one loading cycle,

respectively. This indicates that the programmed foam can better accommodate the external loading change.

Summary

Based on the above experiments and analyses, the following conclusions are obtained:

- The 2-D programming leads to longer fatigue life, higher compressive yield strength, and higher energy dissipation, regardless of the foam or the pure SMP.
- Cyclic loading leads to cyclic softening and shrinking of hysteresis loops, again regardless of the foam or the pure SMP. The similar behavior between the foam and the pure SMP under cyclic loading is controlled by the SMP matrix.
- The major difference between the pure SMP and the foam is in the first few cycles of compression-tension loading. The underlying principle is due to the fracture, crushing, and densification of the microspheres in the first few loading cycles.
- The energy dissipation is due to the viscoelastic energy dissipation of the SMP matrix and the irreversible energy consumption by the crushing microspheres. The pure SMP dissipates more energy than the foam in each cycle except for the first cycle.
- With one compression-tension cycle and a compression strain as high as 40%, the programmed foam exhibits higher compressive yield strength and lower residual tensile stress; Coupled with temperature change, the programmed foam still has higher compressive yield strength, but with larger residual tensile stress.
- The fast drop in compressive stress in the glass transition zone and the decrease in residual tensile stress at room temperature, together with the improved fatigue resistance, suggest that the programmed foam has a good potential to be used as a compression sealant in expansion joints.

Behavior of Thermoset Shape Memory Polymer Based Syntactic Foam Sealant Trained by Hybrid Two-stage Programming

Thermomechanical behavior

A typical thermomechanical cycle for T25C25 specimen in both tension direction and compression direction is shown in Figs. 16 and 48, respectively. Because of the hybrid two-stage biaxial programming, the thermomechancial behavior is very complex. The complexity in thermomechanical behavior first comes from the coupling between the prestrain and Poisson's ratio effect during programming. Based on Xu and Li [80], the same SMP based syntactic foam has a Poisson's ratio about 0.3; two-dimensional programming transformed the foam from isotropic to orthotropic; also, the foam exhibits negative Poisson's ratio after the 2-D programming when the strain was in a certain range. During the first programming in tension in the longitudinal direction, there is contraction in the two transverse directions (compression direction and free direction) due to Poisson's ratio effect, which can be treated as prestrain in the transverse direction before the second room temperature programming in the compression direction.

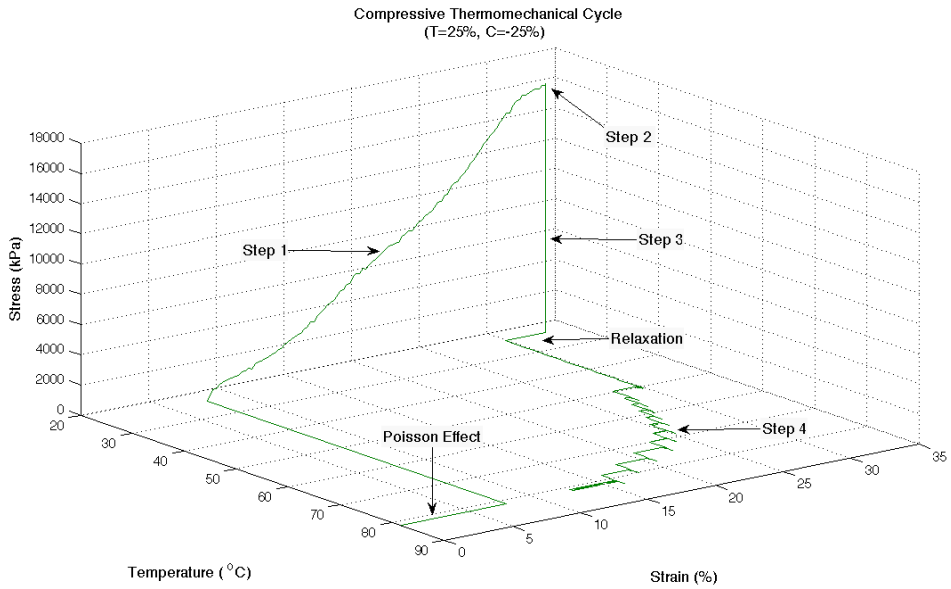

Figure **48**. Thermomechanical cycle in the compression direction for a specimen of T25C25 (the deformation history starts with Poisson's effect due to first tension programming at temperature above T_g, followed by cooling down to room temperature, then second programming starts: Step 1 → compression to 25% additional strain, Step 2 → hold the strain for 20 minutes, and Step 3 → unloading. After unloading, relaxation (viscoelastic rebound) occurs and after 24 hours, it is stabilized, completing the second programming. Step 4: → free shape recovery)

As a result, while the first programming behaves similar to traditional one-stage programming at temperature above T_g, see Fig. 16, the second programming looks considerably different from the first programming, see Fig. 48. Another feature which is not usually seen in traditional high temperature programming is the viscoelastic rebound or relaxation after the second programming. Usually, this rebound reduces as the prestrain level or relaxation time increases [81]. It is noted that the second programming also has Poisson's effect on the tension direction, which makes the length in tension direction further increase.

Because Fig. 48 is a stress-strain-temperature plot, the Step 2 (30 minutes of holding or relaxation) during programming cannot be visualized. To have a better understanding of the stress-strain evolution with time, typical thermomechanical cycle in terms of stress-strain-time for the four groups of specimens is shown in Fig. 49 (a) – (d), respectively. In order to have both tension and compression direction in the same quadrant, the compression stress and compression strain are also treated as positive.

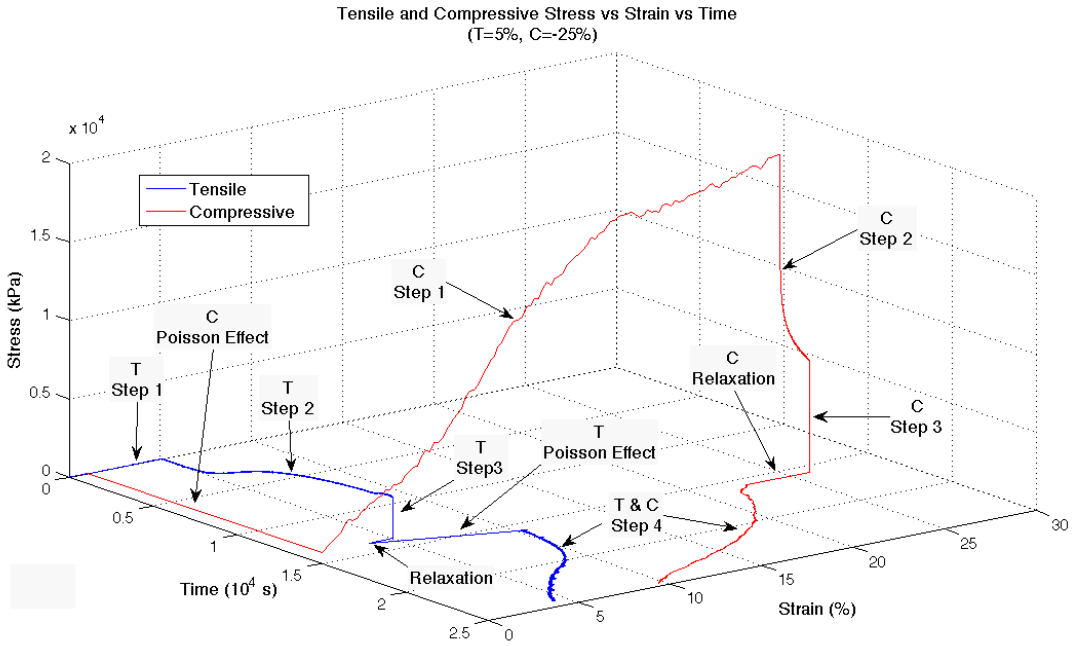

(a) Thermomechanical cycle for a specimen from group T5C25

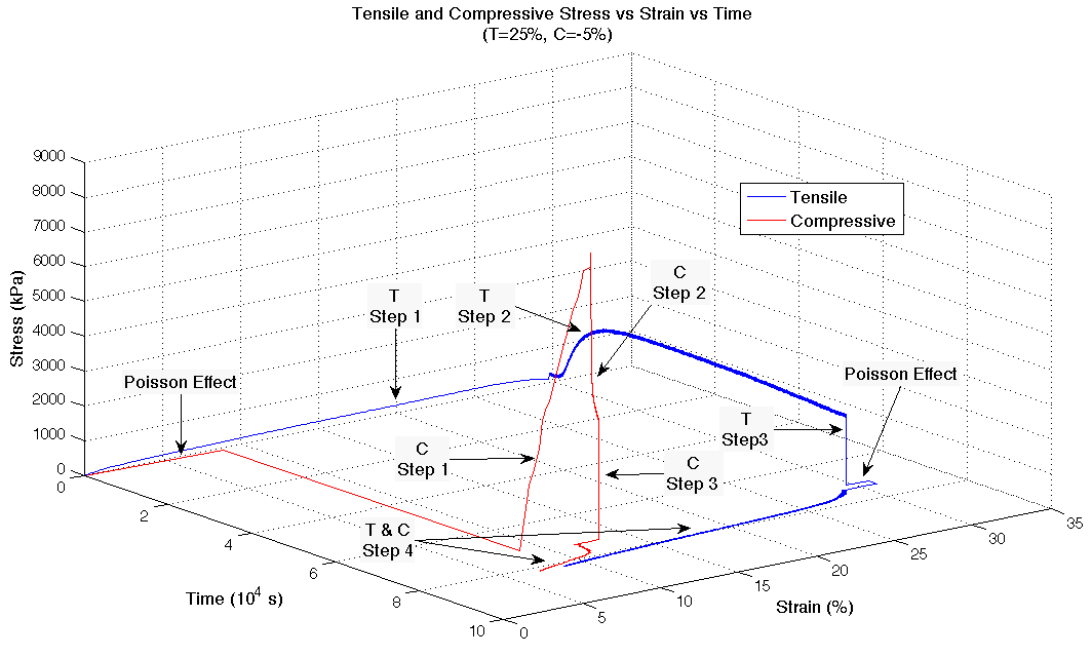

(b) Thermomechanical cycle for a specimen from group T25C5

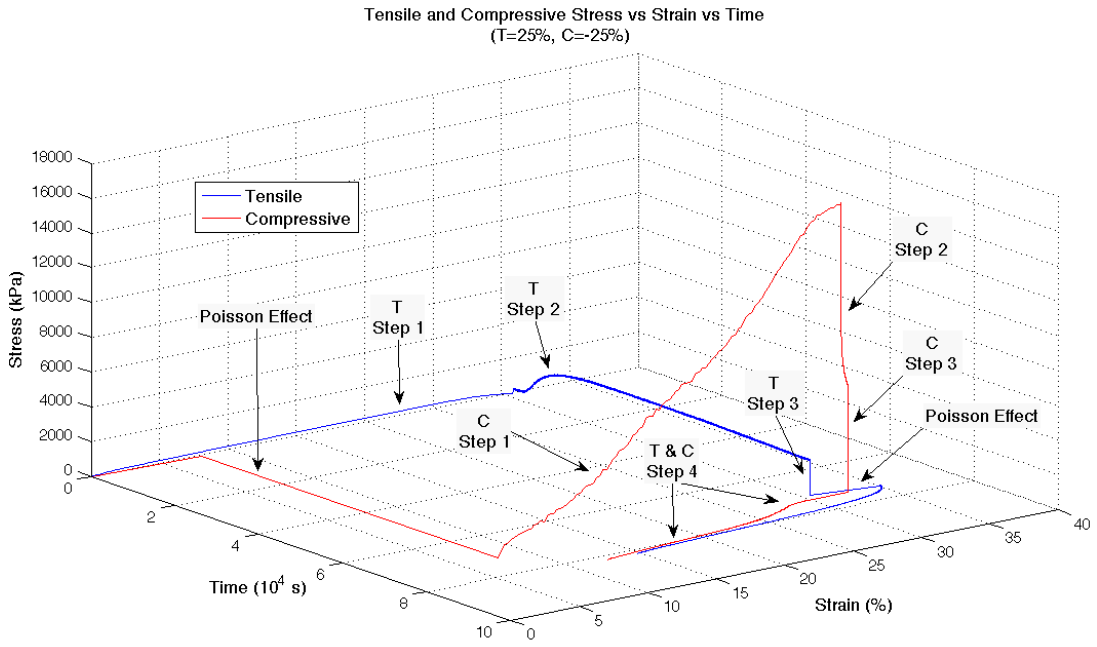

(c) Thermomechanical cycle for a specimen from group T25C25

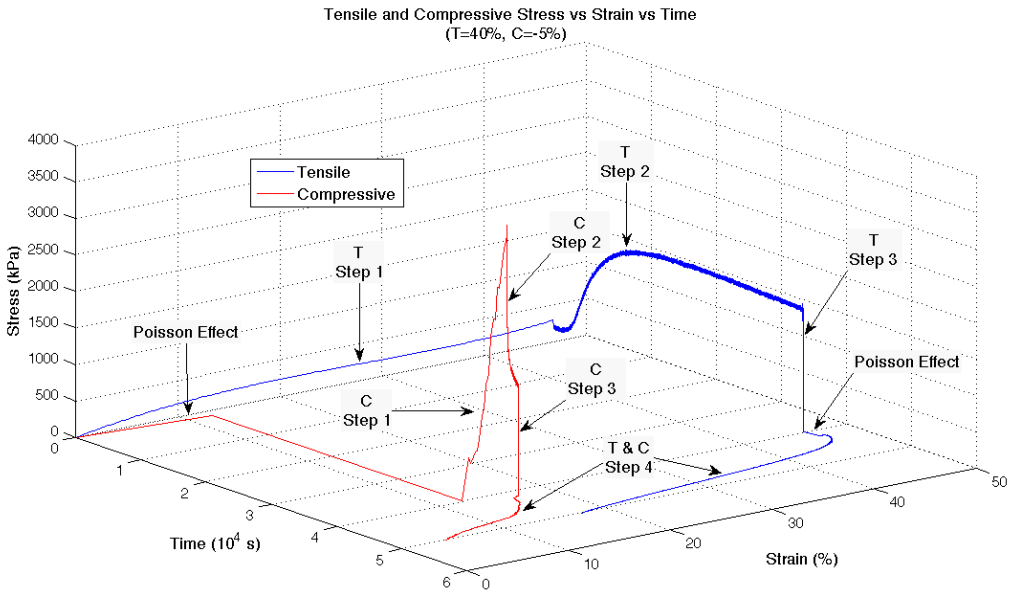

(d) Thermomechanical cycle for a specimen from group T40C5

Figure **49**. Entire thermomechancial cycles in both tension direction and compression direction for each group of specimens in terms of stress-strain-time scale (in the figures, letter "T" represents tension, letter "C" stands for compression, and letters "T&C" represent coupled tension and compression, respectively)

From Fig. 49, while each group of specimens behaves similarly, the effect of prestrain levels on the thermomechanical cycle is significant. The effect can be evaluated by the shape fixity and shape recovery ratios. In this study, the shape fixity and shape recovery ratios are determined per the following equations:

$$\text{Shape fixity ratio} = \frac{(u_0 - u_3)}{(u_0 - u_1)} \times 100\%$$

$$\text{Shape recovery ratio} = \frac{(u_3 - u_4)}{(u_3 - u_0)} \times 100\%$$

Depending on the direction, the meaning of each term in the shape fixity and shape recovery ratios is as follows: in tension direction, u_0, u_1, u_2, u_3, and u_4, are respectively the initial length, length after prestrain imposed in step 1, length after step 2, length after step 3, and length after Poisson's ratio effect and step 4; in the compression direction, they are respectively the initial length, length after Poisson's ratio effect and prestrain in step 1, length after step 2, length after step 3, and length after step 4. All the lengths were measured at the face center of the specimens. The shape fixity and shape recovery ratios are summarized in

Table 2.

Table 2 Shape fixity and shape recovery ratios in each direction

Group	Tension direction		Compression direction		Free direction
	Shape fixity ratio (%)	Shape recovery ratio (%)	Shape fixity ratio (%)	Shape recovery ratio (%)	Shape recovery ratio (%)
T5C5	72.9 ±2.1	77.1 ± 10.3	87.9 ± 6.8	31.0 ± 1.7	70.9 ± 7.8
T5C25		81.4 ± 4.0	86.9 ± 2.1	42.1 ± 5.7	85.9 ± 6.1
T25C5	81.2 ±6.7	83.5 ± 2.2	88.4 ± 3.8	65.2 ± 4.2	68.2 ± 6.7
T25C25		74.9 ± 3.3	93.1 ± 1.6	48.5 ± 3.2	72.9 ± 6.8
T40C5	90.0 ±2.5	83.0 ± 2.7	97.4 ± 1.3	66.0 ± 4.7	47.5 ± 5.8
T40C25		88.4± 1.0	94.4 ± 0.7	54.7 ± 3.3	26.9 ± 1.9

Upon recovery, the tensile direction is expected to contract while the compressive direction should expand. For the free direction, it depends on the stored strain due to the two programmings. Figure 50 (a) shows a specimen after the two-stage programming and Figure 50 (b) and (c) shows the specimen after free shape recovery. Generally, shape recovery is a reverse process of the programming. The recovered shape should be the same as the original permanent shape if the shape recovery ratio is 100%. However, the recovered shape is distorted for several reasons. One reason is that the shape recovery ratio is not perfect due to the damage of microballoons during the cold-compression programming [82]; see Table 2. Therefore, the specimen does not restore its prismatic shape. Another reason is the coupling between the shape memory and Poisson's ratio effect. The shape memory (shortening) in the tension direction causes expansion in the compression direction due to Poisson's ratio effect. This expansion is then coupled with the shape memory (expansion) in the compression direction. As a result, the compression direction expands more than pure shape memory. Similarly, the tension direction shortens more than pure shape memory, i.e., the two effects enhance each other in each direction. However, based on Xu and Li [80], the foam after programming has different Poisson's ratios in the tension and compression directions, which suggests the contribution by the Poisson's ratio to shape recovery is not the same in the two

directions and thus leads to distorted recovery shape. The third reason is the different constraints at the center and edge of each face. At the center of the face, the specimen is freer to move because it is away from the constraint by the boundary (the four edges on each programmed face). At the edge, the constraint is the strongest. One direction tends to expand and the other tends to contract. This physical discontinuity leads to distortion of the recovered specimen.

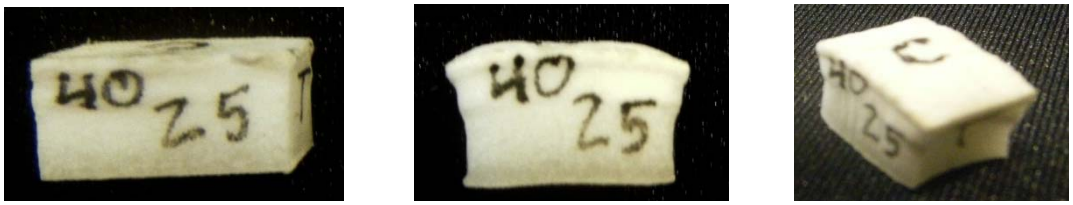

(a) **(b)** **(c)**

Figure **50**. Comparison of (a) programmed specimen and (b) recovered specimen (side view) and (c) recovered specimen (isometric view) (the face marked "T" is perpendicular to the tension direction, the face marked "C" is perpendicular to the compression direction, and the face marked "40/25" is the free direction subjected to the Poisson's effects only)

Comparing the three directions, it is clear that the tension direction sees the largest recovery ratio, followed by the free direction, and the least by the compression direction. The reason is that the compression programming needs very large stress (about 10 times of that for the tension programming), which may cause microballoon crushing [82] or molecular level damage, so that it cannot be fully recovered. Also, the compression programming pushed some molecular segments, which have rotated towards the tension direction in the first programming, align more towards tension direction. Consequently, the recovery in tension direction is more significant.

The effect of prestrain levels on the shape fixity is clear. In the compression direction, the shape fixity increases as the pretension increases. It is noted that in a previous study, uniaxial compression programming by a precompression of 5% did not fix a temporary shape because 5% was lower than the yielding strain of about 7% [81]. In the current study, 5% "nominal" precompression leads to considerable shape fixity. The reason is that pretension serves as a precompression in the compression direction, due to the Poisson's ratio effect. The total compression prestrain is greater than the yielding strain, resulting in the shape fixity. In the tension direction, the shape fixity was calculated once the first stage

programming was completed. Therefore, the effect of the second stage programming (Poisson's ratio effect) was not considered. As a result, the shape fixity is the same for the same pretension, regardless of the second programming. Similar to the shape fixity in the compression direction, the shape fixity increases as the pretension increases.

As given in Table 2, the shape recovery ratios in the tension direction are slightly smaller than those programmed by the one-stage 2-D stress condition, which is between 91% and 96% depending on the prestress levels [38]. The slight reduction is due to the damage during the cold-compression programming. Because tension direction is the direction that has the squeezing-out problem for sealant in expansion joints, the similar shape recovery ratios in tension direction suggests that the two-stage 1-D programming may be a viable alternative for the one-stage 2-D programming.

Recovery sequence

To have a better view of the free-shape recovery in the three directions (tension, compression, and free), Figure 51 (a) – (d) shows typical recovery strain versus temperature results for groups T25C5, T5C25, T40C5, and T25C25, respectively. It is noted that the seemly stepped recovery curve is due to the stepped heating profile used during shape recovery test.

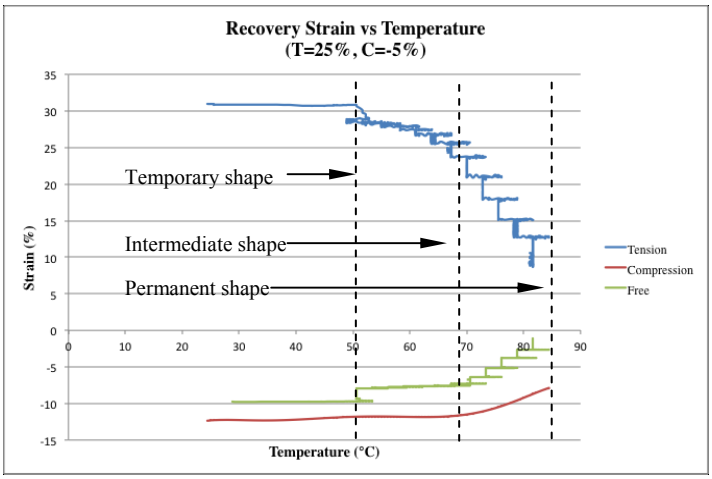

(a) Free shape recovery for a specimen from group T25C5

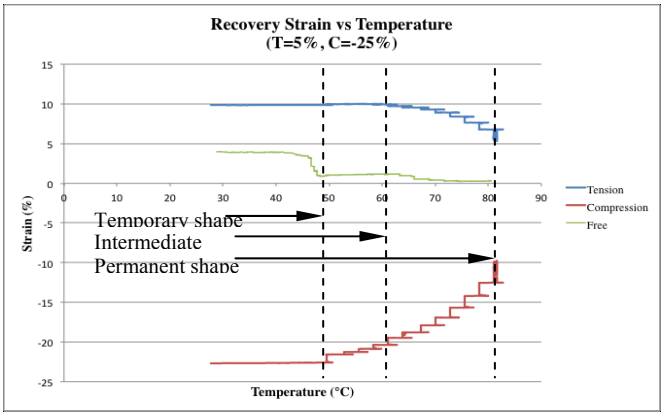

(b) Free shape recovery for a specimen from group T5C25

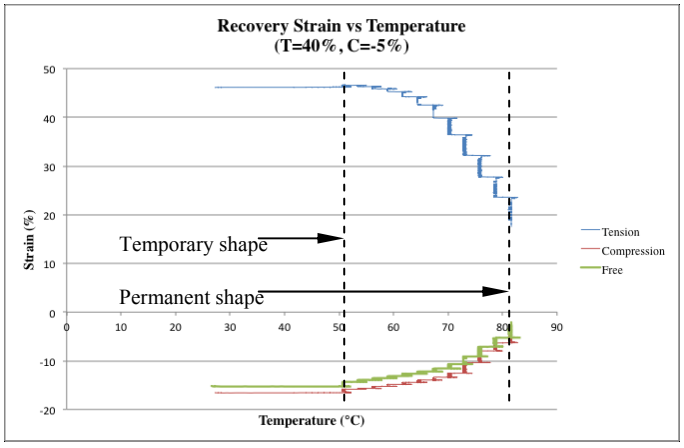

(c) Free shape recovery for a specimen from group T40C5

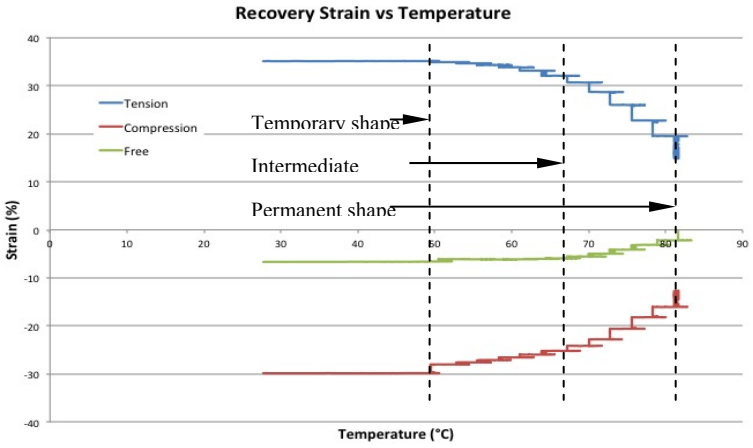

(d) Free shape recovery for a specimen from group T25C25

Figure **51**. Free shape recovery with temperature for three groups of specimens in each direction

From Fig. 51 (a), the foam shows a sequential shape recovery. The tension direction starts to recover at temperature around 50^{o}C. However, the recovery for the compression direction and free direction does not occur until the temperature is about 70^{o}C. From Fig. 51 (b), it is seen that the sequence of shape recovery is reversed. The compression direction starts to recover at about 50^{o}C. The tension direction and free direction does not recovery until about 60^{o}C. It is noted that the sudden recovery at about 50^{o}C for the free direction is most likely due to equipment error. Obviously, the difference in the recovery sequence between Fig. 51 (a) and Fig. 51 (b) is due to the reverse in the prestrain levels.

Based on Sun and Huang [85], if SMPs are continuously programmed in the glass transition region, the SMPs will recover their original shapes following the exact order of the previous predeformation but in an inverse fashion. Clearly, the result in Fig. 51 (b) followed this pattern but Fig. 51 (a) did not. From this result, it is inferred that the recovery sequence depends on the effort during programming, not the sequence of programming. As is well known, the driving force for shape recovery is due to the conformational entropy. Programming leads to alignment of molecular segments towards loading direction or reduction in entropy. During the two-stage 1-D programming, the first programming aligns some molecular segments along the tension direction. In the subsequent compression direction training, some molecular segments align along the compression direction. It also pushes some already aligned segments in the tension direction further aligning along this direction; see a schematic in Fig. 52. Depending on the degree of alignment (or degree of departure from equilibrium configuration or degree of reduction in entropy), shape recovery first occurs along the direction that has the largest number of aligned molecular segments (least entropy), regardless of the programming sequence.

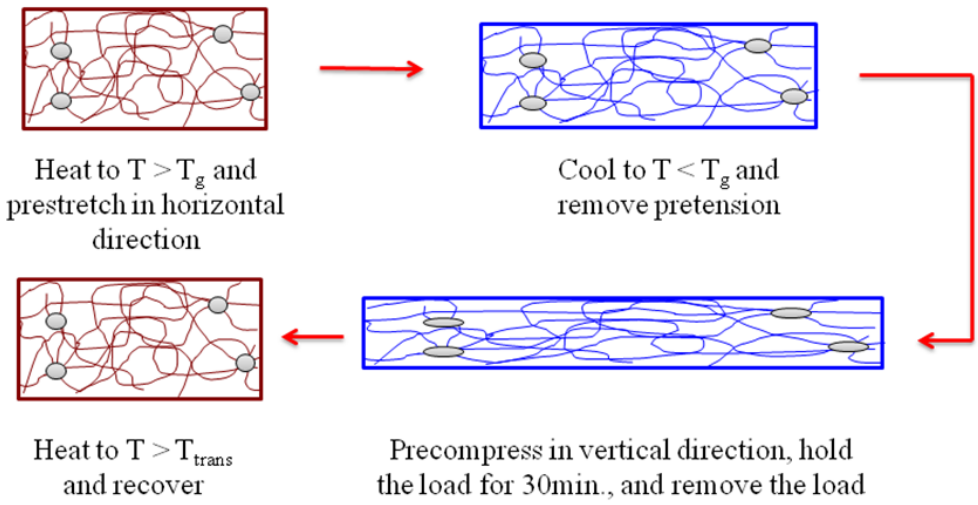

Figure **52**. Schematic showing the shape memory mechanism involved in the two-stage, biaxial programming and recovery (Note the contribution of the compression programming to the further segmental alignment along the tension direction)

For the group T25C5, the molecular segments predominately align along the tension direction. Therefore, the recovery occurs in the tension direction first (Fig. 51 (a)). For the group T5C25, the molecular segments predominately align along the compression direction. Therefore, the recovery occurs first in the compression direction (Fig. 51 (b)). However, because the compression programming in T5C25 also further aligns some segments towards tension direction, the temperature range between the first and second recovery narrows to 50-60^{o}C, instead of 50-70^{o}C for the group T25C5.

For both Fig. 51 (a) and (b), it is clear that the foam recovers in two stages. Obviously, for these cases, the two-stage 1-D programming leads to behavior different from the one-stage 2-D programming, which shows recovery in both directions simultaneously [38]. In other words, for these two cases, the one-stage 2-D programming as required for sealant application cannot be replaced by the two-stage 1-D programming.

With absolute predominance of segmental alignment in one direction, such as T40C5 in Fig. 51 (c), the recovery seems simultaneously in all directions. In other words, the foam becomes a routine dual-shape. The reason is that there are very few segments aligned along the compression direction for T40C5. The absolute majority of the segments align along the tension direction. The two-stage 1-D programming is thus similar to a one-stage 2-D programming. The foam recovers all the way to its permanent shape, similar to dual-shape SMPs.

This entropy driven shape recovery can be further validated by Fig. 51 (d). The prestrain level in both tension direction and compression direction is the same (25%). Therefore, it is expected that the two directions will recover simultaneously. This is exactly the case. From Fig. 51 (d), both directions start to recover at temperature about 50^{o}C. For the free direction, it is mainly affected by the Poisson's effect up to the temperature about 68^{o}C. After that, this direction also recovers to its permanent shape. Overall, this case suggests that the one-stage 2-D programming can be replaced by the two-stage 1-D programming.
In practical applications, assuming the maximum compression in the programmed sealant along the traffic direction is 20% (for small span bridge or concrete pavement), the vertical strain due to Poisson's ratio effect will be about 2%, which is determined based on the test result of Poisson's ratio about 0.1 [80]. Obviously, the ratio of the strains (20% and 2%) in the two perpendicular directions is 10, which is similar to the case in Fig. 51 (c), where the ratio of the prestrains (40% and 5%) is 8. Based on the above discussions in Fig. 51 (c), it is expected that the foam sealant will recover simultaneously. In other words, the one-stage 2-D programming can be replaced by the two-stage 1-D programming in practice.

For field level applications, as discussed in [38], the programmed sealant slab needs to be installed at the lowest temperature that the joint will experience, which ensures that the sealant will always apply a compressive force to the concrete wall so that debonding can be avoided. Also, the sealant may have healing capabilities per the confined shape recovery mechanism as proposed by Li and Uppu [24]. As shown in Fig. 53, assuming that the concrete wall provides full constraint at the temperature close to or above the glass transition temperature of the sealant, we can calculate the prestrain level required to close the crack due to constrained shape recovery of the sealant:

$$\varepsilon = \frac{t}{Rw}$$

where ε is the required prestrain to close the crack, t is the crack width, w is the joint width, and R is the shape recovery ratio in the traffic direction (compression). As an example, if the crack width is t = 1mm, the joint width is w = 20mm, and the shape recovery ratio of the sealant is R = 50%, the prestrain level required to close the crack is ε = 10%.

It is noted that the functional stability of this foam sealant under UV radiation, water immersion, cyclic loading, and cyclic temperature change has been validated previously [83,

84]. This further ensures the potential applicability of the smart sealant in short span bridge decks and concrete pavements.

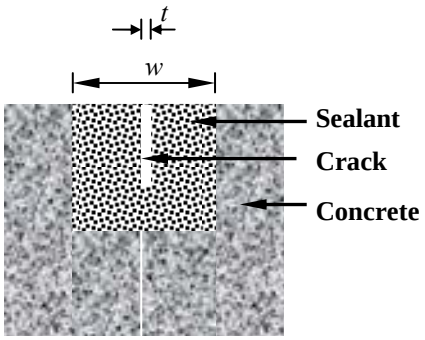

Figure **53**. Schematic of the sealant with a crack to be closed by constrained shape recovery

Summary

Based on test results and analysis, the following conclusions are obtained:

- The two-stage hybrid 1-D programming can replace the one-stage 2-D programming as long as (1) the prestrain level in one direction is much larger than that in the transverse direction (for instance 8 times higher) or (2) the prestrain levels in both directions are similar.
- Because 1-D uniaxial programming is much easier to be implemented in practice, this study provides an alternative training approach for the proposed foam to serve as sealant in expansion joint.
- As against some common belief that the recovery sequence reverses the sequence of programming, this study shows that the prestrain level takes a leading role, regardless of the programming sequence.

FIELD-LEVEL INSTALLATION

Specimen Preparation and Experimental Set-up

Raw materials

The shape memory polymer was synthesized by using poly (tetrahydrofuran) glycol-250 and poly (tetrahydrofuran) glycol-650 (Sigma-aldrich) as the soft segments. Methylenebis (phenyl isocyanate) (Sigma-aldrich) and Butanediol (Sigma-aldrich) was used as the hard segments. All the chemicals were dried before use. The synthesis was conducted by bulk polymerization. Dibutyltin dilaurate was used as the catalyst. The switching transition of the shape memory polymer was tailored by varying the soft segment length and hard segment content. The hard segment contents were 50.29% and 73.16%. The NCO/OH value was 1.05%.

Specimen preparation

The poly (tetrahydrofuran) glycol first reacted with the Methylenebis (phenyl isocyanate) for 20 minutes. Then the prepolymer was reacted with the chain extender. After about 30 seconds of mixing, the mixture was cast into a mold covered with polytetrafluoroethylene for further reaction. The cast polyurethanes were cured for 12 hours at 110^{o}C by using heating blanket, as shown in Fig. 54. The temperature range of the heating blanket was from 25^{o}C to 450^{o}C. After fully cured, the SMP sealant was demolded from the aluminum mold and ready for programming, as shown in Fig. 55.

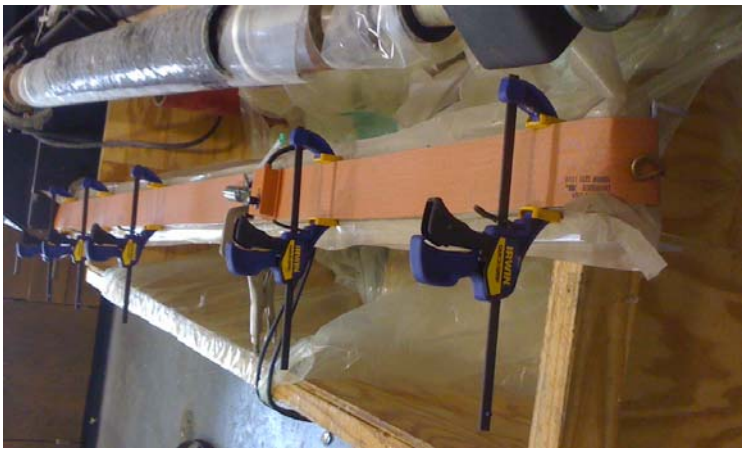

Figure **54**. SMP sealant during the curing process.

Based on the glass transition temperature and programming method, three types of

SMP sealants (1S-T-38, 1S-T-29, and 2S-T-29) were fabricated. Here 1S-T-38 and 1S-T-29 suggest that the designed glass transition temperature is 38^{o}C and 29^{o}C, respectively, and they are programmed by one-stage compression programming. 2S-T-29 suggests that the designed glass transition temperature is 29^{o}C and its programming is by the two-stage 1D stress condition.

Figure **55**. Fabricated SMP joint after curing and demoulding.

Programming process

One-stage compression programming. The fully cured SMP slab was inserted between two square steel tubes and covered by the heating blanket at 90^{o}C, as shown in Fig. 56. Axial compression loading was added on to the steel tubes by using the MTS 810 machine.

Figure **56**. 1-D programming test setup.

The loading force data "P" and the displacement data were collected and the loading rate was 0.6 mm/min in order to ensure quasistatic loading conditions. When the compression strain reached 45%, the strain was hold and the heating blanket was turned off, as shown in Fig. 57. It was observed that the compression stress for 1S-T-38 and 1S-T-29 were 38.12 MPa and 14.98 MPa at 45% strain, respectively. After temperature dropped to the room temperature, the slab was removed from the steel tubes and ready to be used.

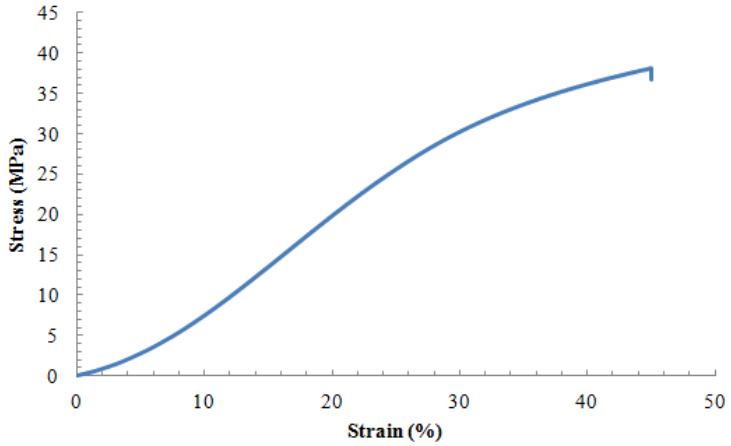

(a)

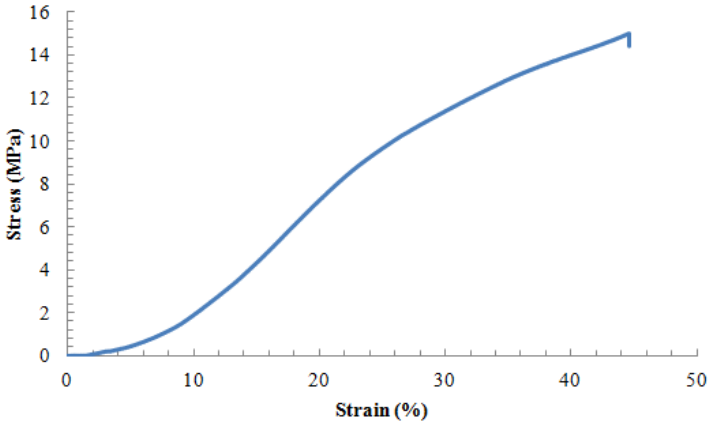

(b)

Figure **57**. 1D programming of stress-strain curve for (a) 1S-T-38, (b) 1S-T-29

Two-stage hybrid programming. The 2-stage programming was conducted by heated tensile programming and cold compression programming. The fully cured SMP slab was clamped by the home-made fixture, as shown Fig. 58 (a). The heating blanket was wrapped round the fixture and covered the entire SMP slab, as shown in Fig. 58 (b). After the temperature reached 100^{o}C and held for 30 minutes, tensile load was added by using the MTS 810 machine.

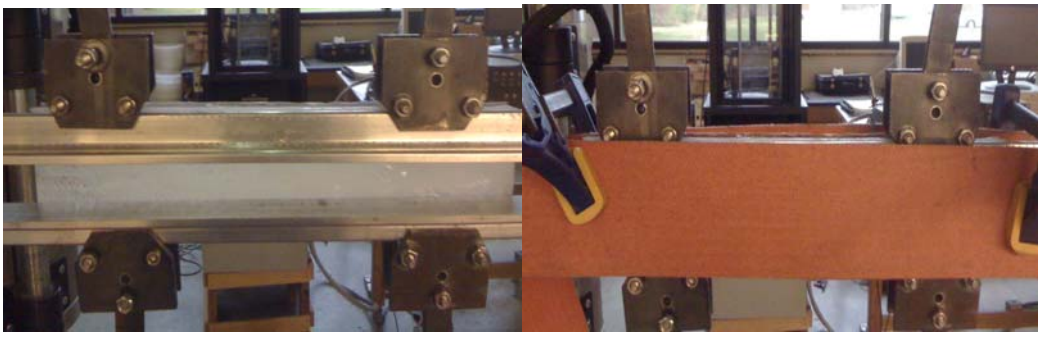

(a) (b)

Figure **58**. Two-stage programming test setup: (a) slab in the home-made fixture, (b) fixture covered by heating blanket

The loading force data "P" and the displacement data were collected and the loading rate was 0.6 mm/min in order to ensure quasistatic loading conditions. When the tensile strain reached 12%, the strain was maintained and the heating blanket was turned off. The tensile stress was 1.5 MPa when the strain reached 12%. The stress-strain curve by tensile programming is presented in Fig. 59.

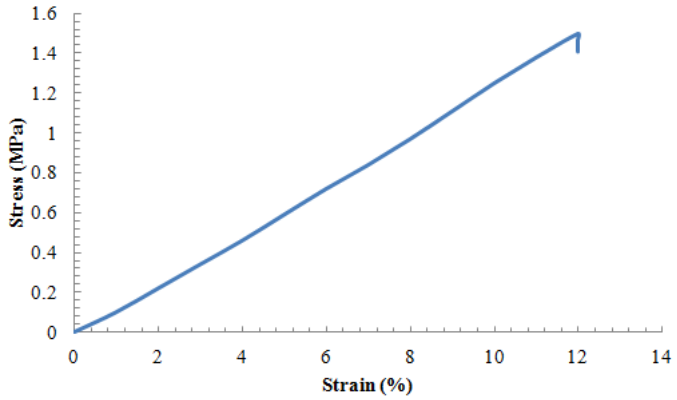

Figure **59**. Tensile stress-strain curve for 2S-T-29 slab during tension programming

Once the temperature dropped to the room temperature, the slab was removed from the fixture and put into a hydraulic compressor (with a maximum of 50t load) to start the cold compression programming. The compression strain was measured by using LVDT. When the compression strain reached 40%, the strain was maintained for about 3 hours at room temperature. The compression stress was 32.1 MPa when the strain reached 40%.The stress-strain curve by the cold compression programming is presented in Fig. 60.

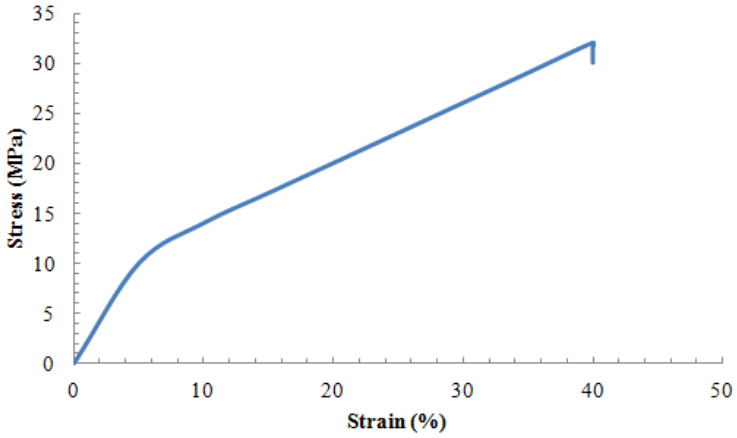

Figure **60**. Compression stress-strain curve for 2S-T-29 slab during cold-compression programming

Thermal and moisture analysis

In order to monitor the temperature change during service, two thermal couples were glued to the bottom (location 1) and middle (location 2) of the SMP slab, as shown in Fig. 61. Temperature at the top surface (location 3) was measured with infrared thermometer. Monitoring of moisture change in the SMP slab during service was measured with Pinless deep sensing moisture meter.

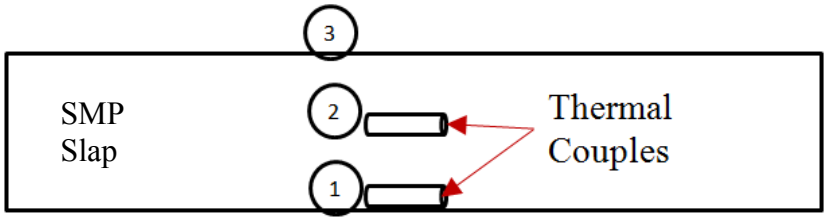

Figure **61**. SMP slab attached with thermal couples.

Dynamic mechanical analysis

In order to determine the glass transition temperature and the viscoelastic properties of the adhesive layer, dynamic mechanical analysis (DMA) test was conducted on a RSA III tester from TA Instruments. A rectangular bar with dimensions of 15 mm × 8 mm × 1 mm was placed into the DMA tensile grips. A small dynamic load at 1 Hz was applied to the beam and the temperature was ramped from room temperature to 80 °C at a rate of 3 °C/min. The amplitude was set to 15 μm. The glass transition temperature T_g was determined from the loss modulus.

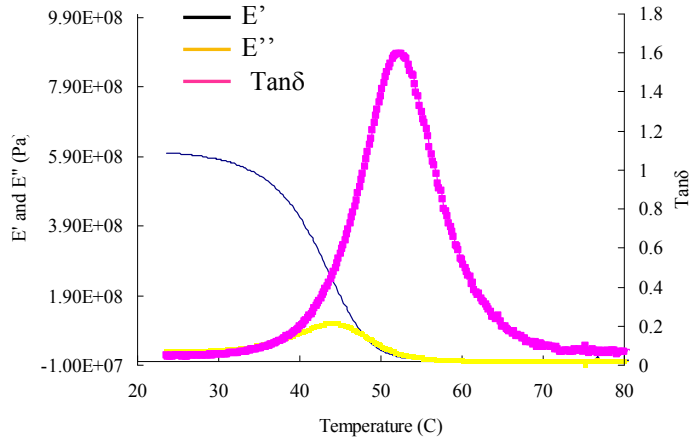

(a)

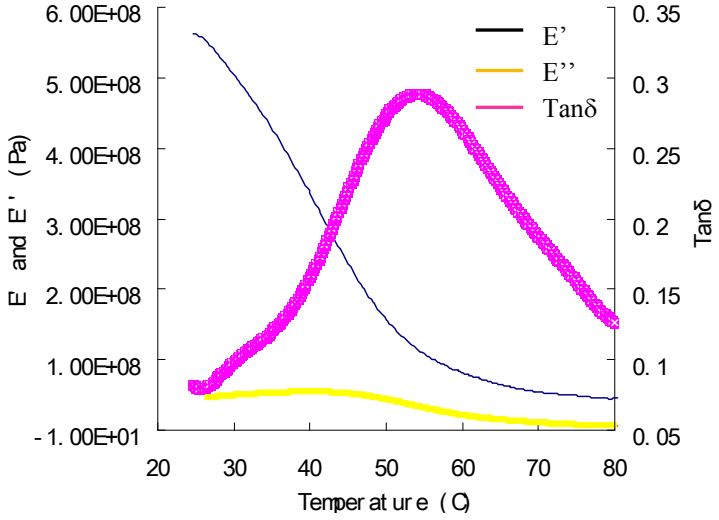

(b)

Figure **62**. DMA test results of SMP materials (a) 1S-T-38 (b) 1S-T-29

The storage modulus, loss modulus and tan δ were shown in Fig. 62. The peak in the loss modulus (E") represents the middle temperature at which the material is undergoing the maximum change in polymer mobility, which corresponds to the chemical definition of the glass transition temperature (T_g). The loss tangent (tanδ) peak describes the damping characteristics of a material and also has historical significance, since it was the first DMA property quantified and many of the DMA T_g reference data were based on the tanδ peak temperature. It was found form the peak of the loss modulus that the 1S-T-38 and 1S-T-29 specimen had an obvious single T_g at 45°C and 40°C, respectively. This result was not the same as the design because DMA usually shows higher T_g as compared to DSC test results.

Further investigation was conducted by DSC test.

DSC analysis

Differential scanning calorimetry (TA Instruments, Q100) test was performed in order to investigate the glass transition temperature of the SMP. The sample size was 5 mg and the test was conducted from 0 °C to 200 °C at a ramping rate of 5 °C/min. Three effective specimens were tested to obtain an average glass transition temperature value.

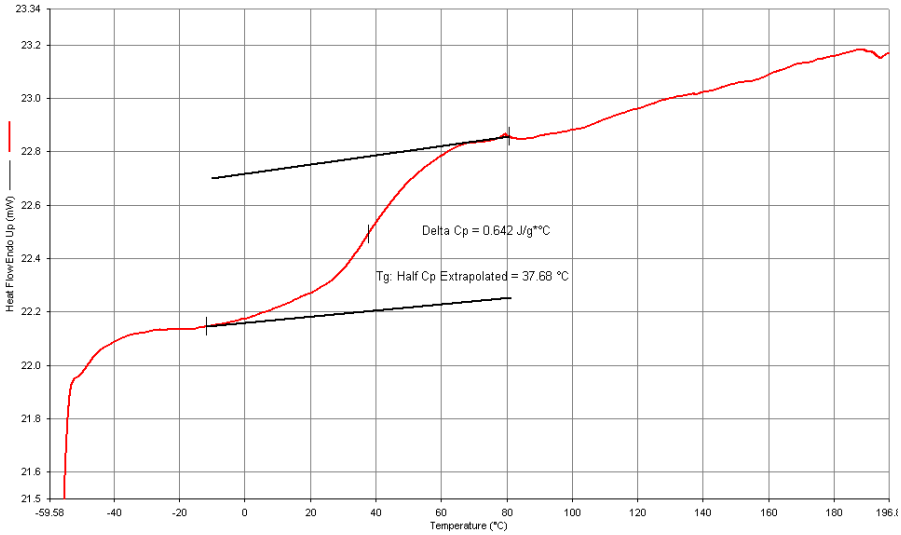

(a)

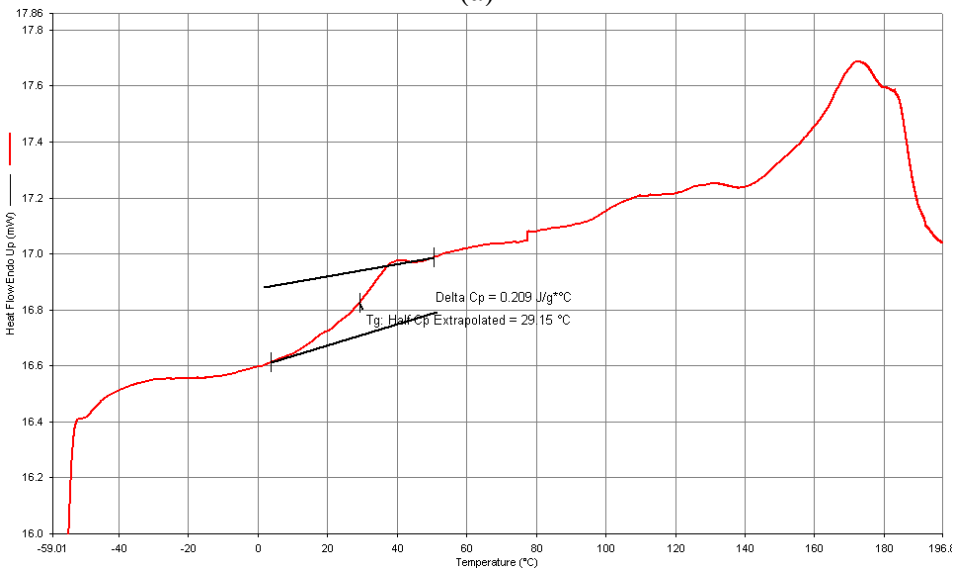

(b)

Figure **63**. DSC test result of SMP joints (a) 1S-T-38, (b) 1S-T-29.

The DSC test results of the SMPs were shown in Fig. 63. From Fig. 63 (a) and (b), there is a change of slope at about 37.68°C in Fig. 63 (a) and 29.15°C in Fig. 63(b). This

suggests that the glass transition temperature of the 1S-T-38 and 1S-T-29 are around 37.68°C and 29.15°C. These results are close to the designed properties of the SMP slabs.

Thermomechanical test

Typical three-step stress-controlled cold-compression programming at strain level of 40%, for both the 1S-T-38 and 1S-T-29, are respectively shown in Fig. 64 (a) and Fig. 64 (b). The programming consists of a room temperature loading, followed by holding during which time the strain was held constant and unloading at room temperature. During free shape recovery test, the programmed 1S-T-38 and 1S-T-29 specimens were heated up to 55°C and 90°C, respectively, and was soaked for about 30 min; see Fig. 65.

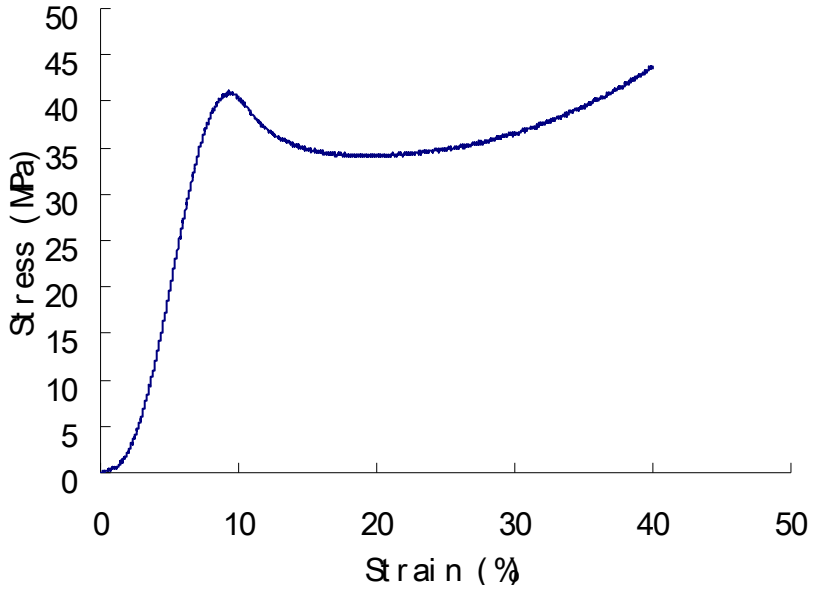

(a)

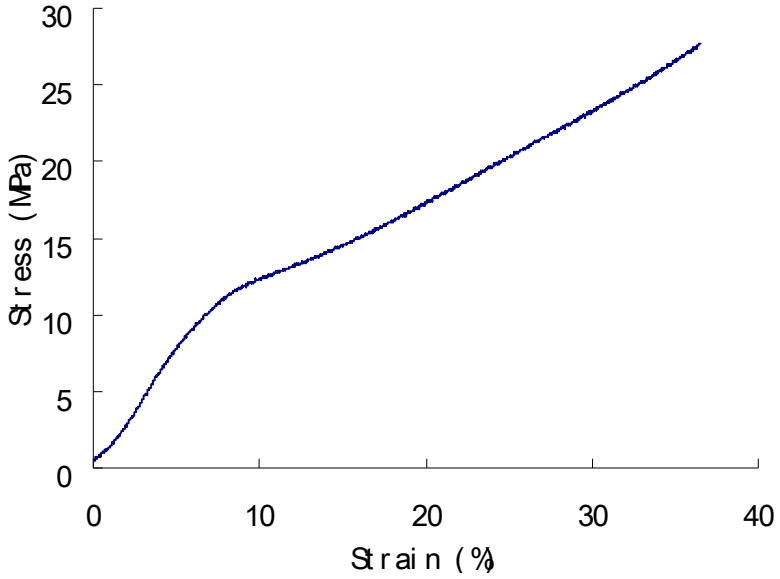

(b)

Figure **64**. Cold-compression programming (a) 1S-T-38, (b) 1S-T-29.

The shape recovery ratios of the 1S-T-38 and 1S-T-29 are presented in Fig. 65 (a) and (b), respectively. Shape recovery ratio is defined as the recovered stain during free shape recovery over the prestrain during programming. From Fig. 65 (a) and (b), it is observed that the strain recovery occurred once the temperature reached the start of the glass transition zone when the switching phase was activated. The majority of strain recovery occurred between 40°C and 50°C for the 1S-T-38 and between 40°C and 60°C for 1S-T-29, respectively. This suggests that the SMP slab during service would start to release the stored strain once the pavement surface temperature reaches 40°C in the summer.

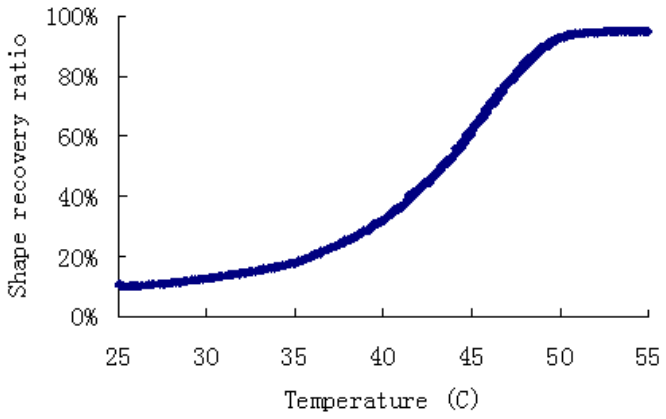

(a)

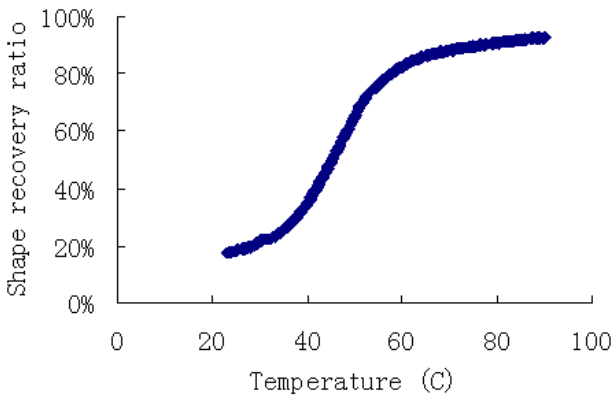

(b)

Figure **65**. Free-shape recovery of the SMP slabs (a) 1S-T-38, (b) 1S-T-29.

SMP Slab Installation and Monitoring

SMP slab installation

A concrete pavement was constructed on the CEBA lane at Louisiana State University campus in January 2012. The geometry of the concrete pavement slab and dimension are presented in Fig. 66. The left-hand side of the concrete slab was connected with asphalt concrete pavement and the concrete slab on the right-hand side was connected with another concrete slab, which formed two expansion joints.

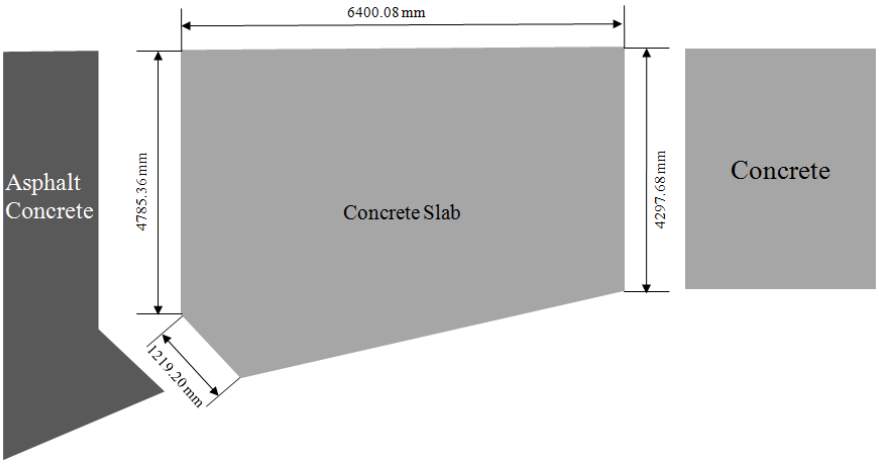

Figure **66**. Schematic of concrete slab and two expansion joints

On the left-hand side, two types of one-stage programmed SMP slabs (1S-T-38 and 1S-T-29) were installed. On the right-hand side, two types of one-stage and one type of two-

stage programmed SMP slabs (1S-T-38, 1S-T-29, and 2S-T-29) were installed, as shown in Fig. 67.

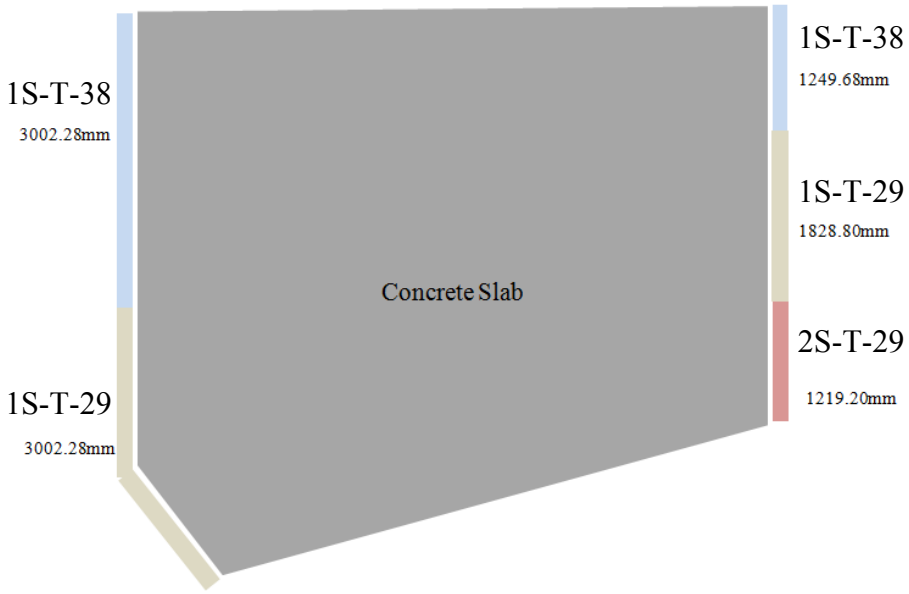

Figure **67**. Schematic of SMP joint installation

During the concrete pavement construction, plywood slab was inserted into the fresh concrete to create the expansion joint, as shown in Fig. 68. Due to the shrinkage and exothermic reaction during the concrete curing process, the SMP slab was not inserted into the fresh concrete directly. Once the concrete slab was fully cured, the plywood slab was removed, and then the SMP slab was installed. After removing the plywood slab, the channel left behind was 82.35mm deep and 25.05mm wide.

Figure **68**. Plywood slab was inserted in fresh concrete to create the joint channel

The SMP slabs were installed on January 12, 2012. The weather was sunny and the temperature was 3^{o}C during the installation. The channel was first cleaned by high power

blower and brush. And then, various programmed SMP slabs of 80.01mm deep and 19.05mm wide were inserted into the channel. Finally, the Urethane PL Premium Liquid Adhesive was poured into the channel to seal the gap between the SMP slab and the concrete wall, as shown in Fig. 69.

(a) (b)

Figure **69**. SMP slab installation: (a) slab in concrete-concrete channel, (b) slab in concrete-asphalt concrete channel.

SMP joint observation

After two days curing of the Urethane PL premium liquid adhesive, the CEBA lane was opened to traffic, as shown in Fig. 70. It was observed that the SMP joints had no macro and micro cracks on the surface and at the interface.

Figure **70**. Road test by passing school bus

Since the SMP slabs were installed, the data of joint geometry, temperatures at three locations, and moisture were measured and collected every week. The protrusion (vertical deformation) and width of the SMP slabs are given in Table 3. The moisture and temperature

data are summarized in Table 4. Fig. 71 shows the surface moisture test and moisture within the SMP slab test after raining.

Table 3 Protrusion and width data

Date	1S-T-38		1S-T-29		2S-T-29	
	Protrusion (mm)	Width (mm)	Protrusion (mm)	Width (mm)	Protrusion (mm)	Width (mm)
Jan. 12th	-2.34	19.05	-2.34	19.05	-2.34	19.05
Jan. 14th	-2.34	19.05	-2.34	19.05	-2.34	19.05
Jan. 21th	-2.34	19.05	-2.34	19.05	-2.34	19.05
Jan. 28th	-2.34	19.05	-2.34	19.05	-2.34	19.05
Feb. 4th	-2.34	19.05	-2.34	19.05	-2.34	19.05
Feb. 11th	-2.34	19.05	-2.34	19.05	-2.34	19.05
Feb. 18th	-2.34	19.05	-2.36	19.15	-2.41	19.13
Feb. 25th	-2.34	19.05	-2.45	19.72	-2.55	19.65
Mar. 3th	-2.45	19.85	-2.53	20.21	-2.62	20.16
Mar. 10th	-2.51	20.78	-2.55	20.28	-2.65	20.22

Table 4 Moisture and temperature data

Date	Temperature (^{o}C)			Moisture (%)	
	Location 1	Location 2	Location 3	Surface	Bottom
Jan. 12th	0	1.1	3.3	2.3	22.5
Jan. 14th	0	1.2	2.1	2.4	22.3
Jan. 21th	3.5	5.7	12.8	3.3	22.5
Jan. 28th	4.5	6.6	14.2	2.8	22.4
Feb. 4th	6.3	8.1	16.8	2.7	22.6
Feb. 11th	8.3	12.4	28.7	3.2	22.8
Feb. 18th	9.7	14.1	30.2	3.1	22.7
Feb. 25th	11.2	16.5	34.6	2.5	22.4
Mar. 3th	13.5	18.2	39.8	2.3	22.3
Mar. 10th	12.5	17.1	38.5	2.6	22.2

From Table 3, it is seen that the dimensions of the SMP slabs are becoming larger as temperature rises. This is a direct indication of thermal expansion. It is believed that the width will further grow and the protrusion will reduce when the temperature is within the glass transition zone, such as in the summer, which will trigger the shape memory effect.

According to the test data, it is believed that the SMP slabs would not be squeezed out of the channel due to the negative poison ratio and shape recovery in vertical direction.

The SMP slab will shrink in the vertical direction as the SMP slab expands in the horizontal direction in the summer. Therefore, the two major functions of the SMP sealant (seal the joint and stay within the channel) can be achieved.

(a) (b)

Figure **71**. (a) Surface moisture test and (b) moisture within the SMP slab test.

The moisture test result was also compared with the regular asphalt sealant in neighboring joints after raining. It was observed that the asphalt sealant did not seal the channel tightly and water was easily seeped into the channel after raining, as shown in Fig. 72 (a). The moisture test result of the asphalt sealant was still 99.9% two days after raining, as shown in Fig. 72 (b), which means the water still exists at the bottom of the asphalt sealant.

(a) (b)

Figure **72**. (a) Asphalt sealant after raining, (b) moisture within the asphalt sealant after raining.

Raw materials cost

Raw materials cost and manufacturing cost are the primary components for the cost of SMP. Because the installed SMP slabs were fabricated in lab scale, it is difficult to figure out the manufacturing, transportation, and installation cost for large scale manufacturing and

construction. Therefore, only raw materials cost is given below.

The shape memory polymers were made of five main chemicals. The prices of the raw materials were obtained on-line. The minimal order for the raw materials is 1 Metric Ton except for additives. The raw materials cost for T-38 and T-29 slabs are tabulated in Table 5. The price may vary because the quotations were from one source only.

Table 5 Raw materials cost of the shape memory polymer slabs

Raw materials cost	USD/m^3	USD/$inch^3$	USD/ton	USD/pound
T-38	2277.98	0.037	1998.23	0.91
T-29	2791.54	0.046	2448.72	1.11

Summary

- Two expansion joints have been installed in a concrete pavement and they are currently under monitoring. It is found that installation is simple and the performance so far is satisfactory.
- Raw materials cost is analyzed for the installed slabs.

CONCLUSIONS

The research presented herein describes the development of a novel shape memory polymer based sealant for expansion joint in short-span bridge deck or concrete pavement. A systematic lab-scale study including programming, performance evaluation under both static and cyclic loading, and functional stability under environmental conditioning was conducted. The feasibility of replacing one-stage 2D programming by hybrid two-stage 1D programming was evaluated. Field-level installation was also completed and it is currently under monitoring. Some important conclusions are obtained:

- The lab-scale testing shows that shape memory polymer, after 2-D programming, has a potential to solve two critical problems for compression-sealed sealant in expansion joints – accumulation of excessive compressive stress and squeezing-out-of the channel of sealant when the concrete wall expands in the summer.
- Lab scale testing shows that the sealant has sufficient strength and stiffness under simulated traffic loading, thermal stress, and cyclic loading.
- The sealant is proved to be functionally stable, i.e., maintaining its shape memory functionality subjected to various combinations of environmental attacks.
- The sealant shows negative Poisson's ratio at normal working temperature, which facilitates integrity of the sealant.
- It is proved that the ideal one-step 2-D programming can be replaced by a two-step 1-D programming. Also, it is proved that thermosetting shape memory polymer can be cold-compression programmed. These findings lay a foundation for implementation of the smart sealant in practice.
- Two expansion joints in a concrete pavement were prepared and installed with SMP slabs. Monitoring of these two joints is underway.

RECOMMENDATIONS

In this study, a novel shape memory polymer based smart sealant is proposed and validated through a systematic experimental program. The results from this study show that this new sealant may potentially solve the two most critical problems facing compression-sealed joints: accumulation of excessive compressive and sealant squeezing-out-of the channel when the concrete wall expands in the summer. The mechanical behavior and functional stability further validate that this smart sealant has a potential to be used in small-span bridges or concrete pavement. The validation that the one-step 2-D programming can be replaced by two-step 1-D programming makes implementation of this sealant feasible. Field-level installation of this sealant proves that construction technology is straightforward. However, the scope of this study was limited. More detailed studies are needed before its large-scale applications. The following further studies are recommended:

- Systematic study of polyurethane based smart sealant;
- Installation in a small-span bridge;
- Theoretical or numerical modeling of the sealant coupled with actual structures.
- Long-term monitoring of the installed joints;
- Life-cycle cost-benefit analysis;
- Optimization of sealant design;
- More field testing of various shapes under real traffic conditions;
- Larger scale lab testing of various sizes matching those of actual expansion joints;
- Field-installation at multiple temperature ranges.

ACRONYMS, ABBREVIATIONS & SYMBOLS

SMP: Shape memory polymer

XRD: X-ray diffraction

CTE: Coefficient of thermal expansion

PS: Polystyrene

DMA: Dynamic mechanical analysis

DSC: Differential scanning calorimetry

T_g: Glass transition temperature

τ: Shear stress

γ: Shaer strain

F: Applied load

A: Sealant cross-sectional area

T: Sealant thickness

δ: Vertical displacement.

m_s: Moisture content

w_0: Mass before immersion

w': Mass after immersion

ε_{max}: Maximum strain

σ_{ld}: Stress during loading

σ_{ul}: Stress during unloading

n: Number of cycles

t: Crack width

w: Joint width

R: Shape recovery ratio

ε: Required prestrain to close the crack

REFERENCES

[1] Al-Qadi, I.L., and Abo-Quadis, S.A. (1995). Joint width and freeze/thaw effects on joint sealant performance. *ASCE Journal of Transportation Engineering*, 121: 262–266.

[2] Biel, T.D., and Lee, H. (1997). Performance study of Portland cement concrete pavement joint sealants. *ASCE Journal of Transportation Engineering*, 123: 398–404.

[3] Lima J.M. and de Brito J. (2009). Inspection survey of 150 expansion joints in road bridges. *Engineering Structures*, 31: 1077-1084.

[4] Fincher H.E. (1983). *Evaluation of rubber expansion joints for bridges*. Report No. FHWA/IN/RTC-83/1, Washington, D.C., 15–16.

[5] Price A.R. (1984). *The performance in service of bridge expansion joints*. TRRL Report LR 1104, Transport and Road Research Laboratory, Crowthorne, U.K., 4–10.

[6] Lee D.J. (1994). *Bridge bearings and expansion joints*. Alden Press, Oxford, U.K.

[7] Wallbank E.J. (1989). *The performance of concrete in bridges: a survey of 200 highway bridges*. Department of Transport, HMSO, London.

[8] Chang L.M. and Lee Y.J. (2002). Evaluation of performance of bridge deck expansion joints. *ASCE Journal of Perforamce of Constructed Facilities*, 16: 3–9.

[9] NCHRP Synthesis Report #319 Project: *NCHRP 20-05*(2003).Washington, D.C.

[10] Odum-Ewuakye B. and Attoh-Okine N. (2006). Sealing system selection for jointed concrete pavements – a review. *Construction and Building Materials*, 20:591–602.

[11] Lima J.M. and de Brito J. (2009). Inspection survey of 150 expansion joints in road bridges. *Engineering Structures*, 31: 1077-1084.

[12] Malla R.B., Shrestha M.R., Shaw M.T., and Brijmohan S.B. (2011). Temperature aging, compression recovery, creep, and weathering of a foam silicone sealant for bridge expansion joints. *ASCE Journal of Materials in Civil Engineering*, 23:287-297.

[13] Malla R.B., Shaw M.T., Shrestha M.R., and Brijmohan S.B. (2007). Development and laboratory analysis of silicone foam sealant for bridge expansion joints. *ASCE Journal of Bridge Engineering*, 12: 438–448.

[14] Koerner H., Price G., Pearce N.A., Alexander M., and Vaia R.A. (2004). Remotely actuated polymer nanocomposites- stress-recovery of carbon-nanotube-filled thermoplastic elastomers. *Nature Materials*, 3: 115–120.

[15] Lendlein A., Jiang H., Jünger O., and Langer R. (2005). Light-induced shape-memory polymers. *Nature*, 434: 879–882.

[16] Mohr R., Kratz K., and Weigel T. (2006). Initiation of shape-memory effect by inductive heating of magnetic nanoparticles in thermoplastic polymers. *Proceedings of the National Academy of Sciences of the United States of America*, 103:3540–3545.

[17] Behl M. and Lendlein A. (2007). Shape-memory polymers. *Materials Today*, 20: 20-28.

[18] Lendlein A., Jiang H., Jünger O., and Langer R. (2005). Light-induced shape-memory polymers. *Nature*, 434: 879–882.

[19] Li G.Q. and John M. (2008). A self-healing smart syntactic foam under multiple impacts. *Composites Science and Technology*, 68: 3337–3343.

[20] John M. and Li G.Q. (2010). Self-Healing of Sandwich Structures with Grid Stiffened

Shape Memory Polymer Syntactic Foam Core. *Smart Materials and Structures*, 19: paper No. 075013 (12 pages).
[21] Nji J. and Li G.Q. (2010). A self-healing 3D woven fabric reinforced shape memory polymer composite for impact mitigation. *Smart Materials and Structures*, 19: paper No. 035007 (9 pages).
[22] Li G.Q. and Nettles D. (2010). Thermomechanical characterization of a shape memory polymer based self-repairing syntactic foam. *Polymer*, 51: 755–762.
[23] Xu W. and Li G.Q. (2010). Constitutive modeling of shape memory polymer based self-healing syntactic foam. *International Journal of Solids and Structures*, 47: 1306–1316.
[24] Li G.Q. and Uppu N. (2010). Shape memory polymer based self-healing syntactic foam: 3-D confined thermomechanical characterization. *Composites Science and Technology*, 70: 1419–1427.
[25] Nji J. and Li G.Q. (2010). A biomimic shape memory polymer based self-healing particulate composite. *Polymer*, 51: 6021-6029.
[26] Ratna D and Karger-Kocsis J. (2008). Recent advances in shape memory polymers and composites: a review. *Journal of Materials Science*, 43:254–269.
[27] Hickenboth CR, Moore JS, White SR, Sottos NR, Baudry J, and Wilson SR. (2007). Biasing reaction pathways with mechanical force. *Nature*, 446:423-427.
[28] Koerner H, Price G, Pearce NA, Alexander M, Vaia RA. (2004). Remotely actuated polymer nanocomposites - stress-recovery of carbon-nanotube-filled thermoplastic elastomers. *Nature Materials*, 3: 115-120.
[29] Tobushi H, Hara H, Yamada E, and Hayashi S. (1996).Thermomechanical properties in a thin film of shape memory polymer of polyurethane series. *Smart Materials and Structures*, 5: 483–491.
[30] Irie M. *Shape memory polymers*. Cambridge University Press, Cambridge, UK, (1998).
[31] Monkman GJ. (2000). Advances in shape memory polymer actuation. *Mechatronics*, 10: 489–498.
[32] Li F, Qi L,Yang J, Xu M, Luo X, and Ma D. (2000). Polyurethane/conducting carbon black composites: structure, electrical conductivity, strain recovery behaviour and their relationships. *Journal of Applied Polymer Science,* 75: 68–77.
[33] Jeong HM, Ahn BK, and Kim BK. (2001). Miscibility and shape memory effect of thermoplastic polyurethane blends with phenoxy resin. *European Polymer Journal*, 37: 2245–2252.
[34] Lendlein A and Langer R. (2002). Biodegradable, elastic shape-memory polymers for potential biomedical applications. *Science*, 296:1673–1676.
[35] Miaudet P., Derré A., and Maugey M. (2007). Shape and temperature memory of nanocomposites with broadened glass transition. *Science*, 318:1294–1296.
[36] Avanzini A. (2008). Mechanical characterization and finite element modelling of cyclic stress–strain behaviour of ultra high molecular weight polyethylene. *Materials & Design*, 29: 330–343.
[37] Xu T, Li G. (2011). A Shape Memory Polymer Based Syntactic Foam with Negative Poisson's Ratio. *Materials Science and Engineering A*, 528: 6804–6811.
[38] Li G, Xu T. (2011). Thermomechanical characterization of shape memory polymer

based self-healing syntactic foam sealant for expansion joint. *ASCE Journal of Transportation Engineering*, 137: 805-814.

[39] Khonakdar, H. A., Jafari, S. H., Rasouli, S., Morshedian, J. and Abedini, H. (2007). Investigation and Modeling of Temperature Dependence Recovery Behavior of Shape-Memory Crosslinked Polyethylene. *Macromolecular Theory and Simulations*, 16: 43–52.

[40] Morshedian, J., Khonakdar, H. A. and Rasouli, S. (2005). Modeling of Shape Memory Induction and Recovery in Heat-Shrinkable Polymers. *Macromolecular Theory and Simulations*, 14: 428–434.

[41] Wouterson E. M., Boey F.Y.C., Hu X., and Wong S.C. (2005). Specific properties and fracture toughness of syntactic foam: Effect of foam microstructures. *Composite Science and Technology*, 65: 1840–1850.

[42] Boyce M.C., Parks D.M., and Argon A.S. (1988). Large inelastic deformation of glassy polymers: Rate dependent constitutive model. *Mechanics of Materials*, 7: 15–33.

[43] Patankar S.N.and Kranov Y.A. (2010). Hollow glass microsphere HDPE composites for low energy sustainability. *Material Science Engineering A*, 527: 1361–1366.

[44] Chan N., Evans K.E. (1999). The mechanical properties of conventional and auxetic foams. Part I: Compression and tension. *Journal of Cellular Plastics*, 35:130–165.

[45] S.N. Patankar, Y.A. Kranov, (2010). Hollow glass microsphere HDPE composites for low energy sustainability. *Material Science Engineering A*, 527: 1361–1366.

[46] Liu Y., Hu H. (2010). A review on auxetic structures and polymeric materials. *Scientific Research and Essays*, 5:1052–1063.

[47] Wang M., Zhang L. (1999). Recovery as a Measure of Oriented Crystalline Structure in Poly(ether ester)s Based on Poly(ethylene oxide) and Poly(ethylene terephthalate) Used as Shape Memory Polymers. *Journal of Polymer Science Part B*, 37:101–112.

[48] Blaga A. (1980). Durability of Building Materials and Compounds, *ASTM STP*, 691:827–37.

[49] Ranby B. (1993). Basic reactions in the photodegradation of some important polymers. *Journal of Macromolecular Science Part A*, A30: 583–94.

[50] Gugumus F. (1987). Plastics Additives (2nd Edition), Hanser, Munich, 97–185.

[51] Davis A. and Sims D. (1983). *Weathering of Polymers*. Applied Science Publishers, Essex, England, 208.

[52] Wypych G, Faulkner T. (1999). *Weathering of Plastics, Plastics Design Library*. Norwich, NewYork, 1–15.

[53] Shychuk AV, Stavychna DY, White J R. (2001). Effect of tensile stress on chain scission and crosslinking during photo-oxidation of polypropylene. *Polymer Degradation and Stability*, 72: 279–85.

[54] Grassie N, Scott G. (1988). *Polymer Degradatien and Stabilisation*. Cambridge University Press, Cambridge.

[55] Torikai A, Murata T, Fueki K. (1984). Radiation-induced degradation of polycarbonate - electron-spin resonance and molecular-weight measurements. *Polymer Degradation and Stability*, 7: 55–64.

[56] Feldman D. (2002). Polymer Weathering: Photo-Oxidation. *Journal of Polymers and the Environment*, 10: 163–73.

[57] Komitov P, Kostov G, Stanchev S. (1989). Aging of ldpe - structural-changes.

Polymer Degradation and Stability, 24: 303–12.
[58] Patankar SN, Kranov YA. (2012). Hollow glass microsphere HDPE composites for low energy sustainability. *Materials Science and Engineering A*, 527: 1361–66.
[59] Zhang D, Dougal SM, Yeganeh MS. (2000). Effects of UV Irradiation and Plasma Treatment on a Polystyrene Surface Studied by IR-Visible Sum Frequency Generation Spectroscopy. *Langmuir*, 16: 4528–32.
[60] Nakatsuka S, Andrady A. (1994). Studies on Enhanced Degradable Plastics. III. The Effect of Weathering of Polyethylene and (Ethylene-Carbon Monoxide) Copolymers on Moisture and Carbon Dioxide Permeability. *Journal of Environmental Polymer Degradation*, 2: 161–7.
[61] Ghaffar A, Scott GA, Scott G. (1976). The chemical and physical changes occurring during U.V. degradation of high impact polystyrene, *European Polymer Journal*, 11: 271–5.
[62] Song F, Gao Y. (2009). Chemical characteristics of precipitation at metropolitan Newark in the US East Coast. *Atmospheric Environment*, 43: 4903–13.
[63] Kochetkov VA, Maksimov RD. (1996). Water absorption and swelling of glass/epoxy syntactic foams. *Mechanics*, 32: 61–70.
[64] Sauvant-moynot V. Gimenez N, Sautereau H. (2006). Hydrolytic ageing of syntactic foams for thermal insulation in deep water: degradation mechanisms and water uptake model. *Journal of Materials Science*, 41:4047–54.
[65] Andrady AL, Pecram JE. (1991). Weathering of Polystyrene Foam on Exposure in Air and in Seawater. *Journal of Applied Polymer Science*, 42:1589–96.
[66] Leng JS, Lv HB, Liu YJ, Du SY. (2008). Comment on "Water-driven programable polyurethane shape memory polymer: Demonstration and mechanism. *Applied Physics Letter*, 86: paper No. 114105.". *Applied Physics Letter*, 92: paper No. 206105.
[67] Huang WM, Yang B. (2005). Water-driven programmable polyurethane shape memory polymer: Demonstration and mechanism. *Applied Physics Lett*er, 86: paper No. 114105.
[68] Behl M, Lendlein A**.** (2007). Shape-memory polymers. Materials Today, 10: 20–8.
[69] Adrien J, Maire E, Gimenez N, Sauvant-Moynot V. (2007). Experimental study of the compression behaviour of syntactic foams by in situ X-ray tomography. *Acta Materila*, 55: 1667–1679.
[70] Avanzini A. (2008). Mechanical characterization and finite element modelling of cyclic stress–strain behaviour of ultra high molecular weight polyethylene. *Materials & Design*, 29: 330–343.
[71] Sivaprasad S, Paul SK, Narasaiah N, Tarafder S. (2010). Experimental investigation on cyclic deformation behaviour of primary heat transport piping materials: Masing analysis of hysteresis loops. *Transactions of the Indian Institute of Metals*, 63: 559–563.
[72] Shen Y, Golnaraghi F, Plumtree A. (2001). Modelling compressive cyclic stress–strain behaviour of structural foam. *International Journal of Fatigue*, 23: 491–497.
[73] Kitagawa M, Qui J, Nishida K, Yoneyama T. (1992). Cyclic stress-strain curves at finite strains under high pressures in crystalline polymers. *Journal of Materials Science*, 27: 1449–1456.
[74] Khonakdar HA, Jafari SH, Rasouli S, Morshedian J, Abedini H. (2007). Investigation

and Modeling of Temperature Dependence Recovery Behavior of Shape-Memory Crosslinked Polyethylene. *Macromolecular Theory and Simulation*, 16: 43–52.

[75] Kanny K, Muhfuz H, Carlsson LA, Thomas T, Jeelani S. (2002). Dynamic mechanical analyses and flexural fatigue of PVC foams. *Composite Structures*, 58: 175–183.

[76] Bezazi A, Scarpa F. (2007). Mechanical behaviour of conventional and negative Poisson's ratio thermoplastic polyurethane foams under compressive cyclic loading. *International Journal of Fatigue*, 29: 922–930.

[77] Bledzki AK, Gassan J, Kurek K. (1997). The Accumulated Dissipated Energy of Composites under Cyclic-dynamic Stress. *Experimental Mechanics*, 37: 324–327.

[78] Wouterson EM, Boey FYC, Hu X, Wong SC. (2005). Specific properties and fracture toughness of syntactic foam: Effect of foam microstructures. *Composites Science and Technology*, 65: 1840–1850.

[79] Boyce MC, Parks DM, Argon AS. (1988). Large inelastic deformation of glassy polymers: Rate dependent constitutive model, *Mechanics of Materials*, 7: 15–33.

[80] Xu T. and Li G. (2011). A shape memory polymer based syntactic foam with negative Poisson's ratio. *Materials Science and Engineering A*, 528: 6804-6811.

[81] Li G. and Xu W. (2011). Thermomechanical behavior of thermoset shape memory polymer programmed by cold-compression: testing and constitutive modeling. *Journal of the Mechanics and Physics of Solids*, 59: 1231–1250.

[82] Xu W. and Li G. (2011). Thermoviscoplastic modeling and testing of shape memory polymer based self-healing syntactic foam programmed at glassy temperature. *ASME Journal of Applied Mechanics*, 78: paper number 061017 (14 pages).

[83] Xu T. and Li G. (2011). Cyclic stress–strain behavior of shape memory polymer based syntactic foam programmed by 2-D stress condition. *Polymer*, 52: 4571-4580.

[84] Xu T. and Li G. (2011). Durability of shape memory polymer based syntactic foam under accelerated hydrolytic ageing. *Materials Science and Engineering A*, 528: 7444-7450.

[85] Sun L. and Huang W.M. (2010). Mechanisms of the multi-shape memory effect and temperature memory effect in shape memory polymer. *Soft Matter*, 6, 4403–4406.